# Bifurcation analysis and parameter estimation in low-dimensional models of global human-nature coevolution

Masterarbeit in Physik

Angefertigt am
Potsdam-Institut für Klimafolgenforschung


Vorgelegt der
Fakultät für Physik
der Georg-August-Universität Göttingen


von

Jan Nitzbon

Potsdam
Juni 2016

Erstgutachter: Prof. Dr. Ulrich Parlitz
Zweitgutachter: Dr. Jobst Heitzig

**Kurzfassung**

**Bifurkationsanalyse und Parameterschätzung von niedrigdimensionalen Modellen globaler Mensch-Natur Koevolution**

Die vorliegende Arbeit hat zum Ziel die koevolutionäre Dynamik von Menschen und Natur in der Epoche des Holozäns und des Anthropozäns zu untersuchen. Dazu wird ein niedrigdimensionales deterministisches Model verwendet, welches die zeitliche Entwicklung von global aggregierten Hauptobservablen des Erdsystems beschreibt. Während die natürliche Komponente des Erdsystems durch den globalen Kohlenstoffkreislauf repräsentiert wird, ist die sozio-ökonomische Dynamik durch eine Kombination eines etablierten Wachstumsmodells mit der Nutzung verschiedener Energieformen sowie die menschliche Populationsdynamik gegeben. Die gleichmäßige Gewichtung der natürlichen und menschlichen Sphären sowie die geringe dimensionale Komplexität, die ein qualitatives Verständnis ermöglicht, unterscheiden das Modell von anderen Ansätzen der Erdsystemmodellierung. Die Formulierung des Modells als dynamisches System ermöglicht zudem die Anwendung mathematischer Standardmethoden wie zum Beispiel der Bifurkationsanalyse.

Diverse Untermodelle wurden hergeleitet, welche verschiedene sozio-kulturelle Zeitalter der Menschheitsgeschichte widerspiegeln, wie zum Beispiel Jäger-Sammler-, Agrar- oder Industriegesellschaften. Für jedes dieser Szenarien wurde das qualitative asymptotische Verhalten des Systems charakterisiert, indem mögliche Gleichgewichtszustände und Attraktoren identifiziert wurden und der qualitative Einfluss verschiedener Parameter mittels Bifurkationsanalyse untersucht wurde. Für das Agrar- und Industrieszenario hat sich die generelle Unterscheidung zwischen einem nachhaltigen und einem kollabierenden Regime herausgestellt, was ein verbreitetes Merkmal sozio-ökologischer System darstellt. Ein weiteres dynamisches Regime, welche stabile Oszillationen aufweist, wurde für das Agrarszenario identifiziert.

Die meisten der Modellparameter konnten anhand verfügbarer empirischer Daten abgeschätzt werden, wodurch der relevante Parameterbereich eingeschränkt werden konnte und zudem charakteristische Größen mit unabhängigen Kalkulationen verglichen werden konnten. Somit konnte die planetare Belastungskapazität für landwirtschaftliche Bevölkerungen abgeschätzt werden und mit tatsächlichen Bevölkerungszahlen der Vergangenheit verglichen werden. Diese und weitere Vergleichen mit unabhängigen Daten dienen dazu Teile des Modells zu validieren und gleichzeitig weniger genaue Teile zu identifizieren, die in zukünftigen Modellversionen verbessert werden könnten.

Letztlich tragen die durch den koevolutionären Modellierungsansatz erzielten Ergebnisse zu einem besseren Verständnis der gesamten Erdsystemdynamik im Holozän und Anthropozän bei.

**Abstract**

**Bifurcation analysis and parameter estimation in low-dimensional models of global human-nature coevolution**

The intent of the present thesis is to investigate the coevolutionary dynamics of humans and nature during the Holocene and Anthropocene epochs. For this purpose a low-dimensional deterministic model is employed which describes the temporal evolution of globally aggregated key observables of the Earth system. While the natural component of the Earth system is represented via the global carbon cycle, the socio-economic dynamics are described by an established economic growth model combined with the use of different energy forms and human population dynamics. The balanced representation of the natural and human spheres and the low dimensional complexity which enables a qualitative understanding, distinguish the model from other Earth system modeling approaches. The formulation of the model as a dynamical system in addition allows the application of established mathematical methods such as bifurcation analysis.

Several sub-models have been derived which correspond to different socio-cultural eras of human history such as hunter-gatherer, agricultural or industrial societies. For each of these scenarios the asymptotic behavior of the dynamics was characterized by identifying the possible equilibrium states and attractors and investigating the influence of the model parameters through bifurcation analyses. For the agricultural and industrial model versions a general distinction between a sustainable and a collapse regime emerged which is a common feature of social-ecological systems. Another dynamic regime which features stable oscillations, was found for the agricultural scenario.

Most of the model parameters have been estimated on the basis of available real-world data in order to curtail the relevant parameter regime and to be able to compare characteristic quantities of the system to estimates gained by different means. Hence, the planetary carrying capacity of agricultural populations could be estimated and compared to actual population levels of the past. This and other comparisons to independent quantitative estimates were used to validate parts of the model and to identify less accurate parts which might be improved in further model versions.

Ultimately the results gained by the coevolutionary modeling approach contribute to a better understanding of the dynamics of the whole Earth system in the Holocene and the Anthropocene.

## Erklärung der Selbstständigkeit

Hiermit versichere ich, die vorliegende Arbeit selbstständig verfasst und keine anderen als die angegebenen Quellen und Hilfsmittel benutzt sowie die Zitate deutlich kenntlich gemacht zu haben.

Darüber hinaus erkläre ich, dass diese Abschlussarbeit nicht, auch nicht in Auszügen, im Rahmen einer nicht bestandenen Prüfung an dieser oder einer anderen Hochschule eingereicht wurde.

Potsdam, den 20. Juni 2016 Jan Nitzbon

# Contents


**1 Introduction** **1**

1.1 Modeling natural Earth System Dynamics . . . . . 2
1.2 Coevolutionary Modeling Approaches for the Anthropocene . . . . . 3
1.3 The copan:GLOBAL model . . . . . 6
1.4 Research Tasks and Overview of the Thesis . . . . . 7

**2 Methodological Preliminaries and Concepts** **9**

2.1 Dynamical Systems . . . . . 9
2.1.1 Definition . . . . . 9
2.1.2 Trajectories and phase portraits . . . . . 11
2.1.3 Notions of stability . . . . . 12
2.1.4 Topological equivalence . . . . . 14
2.1.5 Bifurcations . . . . . 17
2.1.6 Topology of managed dynamical systems with desired states . . . . . 29
2.2 Socio-economic concepts . . . . . 31
2.2.1 The Solow-Swan model of economic growth . . . . . 31
2.2.2 General equilibrium theory . . . . . 34
2.2.3 Demographic models . . . . . 35
2.3 Concepts from Earth sciences . . . . . 38
2.3.1 Global carbon cycle . . . . . 38

**3 Model description** **41**

3.1 Overview of the complete model (c:G) . . . . . 41
3.2 Planet without humans (c:G:LAT, c:G:LA, c:G:LT, c:G:L) . . . . . 44
3.2.1 Functional forms of the dynamics . . . . . 45
3.2.2 Overview of variables and parameters . . . . . 47
3.2.3 Dimension reduction and further simplification . . . . . 47

3.3 Hunter-gatherer and agricultural societies (c:G:LATP, c:G:LAP, c:G:LTP, c:G:LP) . . 50
3.3.1 Functional forms of the dynamics . . . . . 50
3.3.2 Overview of variables and parameters . . . . . 56
3.4 Industrial societies (c:G:LAGTPK, c:G:LAGPK, c:G:LGTPK, c:G:LGPK) . . . . . 57
3.4.1 Functional forms of the dynamics . . . . . 58
3.4.2 Overview of variables and parameters . . . . . 61
3.5 Dimensionless formulation . . . . . 61

**4 Parameter estimation** **65**
4.1 Carbon cycle parameters . . . . . 66
4.2 Demographic parameters . . . . . 69
4.3 Economic parameters . . . . . 73
4.4 Carbon-related planetary boundaries . . . . . 76
4.5 Overview of parameter values and confidences . . . . . 77

**5 Bifurcation analysis** **79**
5.1 Planet without humans . . . . . 80
5.2 Agricultural societies . . . . . 87
5.2.1 With constant population . . . . . 87
5.2.2 With dynamic population . . . . . 92
5.3 Industrial societies . . . . . 106
5.3.1 Equilibria and Stabilities . . . . . 106
5.3.2 Without fossil fuels . . . . . 110
5.3.3 With fossil fuels . . . . . 116

**6 Discussion and Outlook** **121**
6.1 Summary of the main results . . . . . 122
6.2 Carbon cycle dynamics . . . . . 123
6.3 Socio-economic dynamics . . . . . 125
6.3.1 Comparison with real world observations and predictions . . . . . 125
6.3.2 Demographic modeling approaches . . . . . 127
6.3.3 Stabilizing and destabilizing processes and management options . . . . . 128
6.4 Comparison to predator-prey dynamics . . . . . 130
6.5 Further directions . . . . . 130

**7 Conclusion** **133**

**Bibliography** **137**

**Appendix** **151**

**A Supplementary Calculations** **151**
A.1 Dimensionless formulation of c:G:LATP . . . . . 151
A.2 Analytical equilibria of c:G:LAT . . . . . 154
A.3 Linear stability analysis of c:G:LAT and c:G:LP . . . . . 156
A.4 Graphical proof of the number of coexistence equilibria . . . . . 158

**B Supplementary Figures** **161**
B.1 Time series of the economic parameter estimates . . . . . 161
B.2 Bifurcation diagrams of c:G:LAT for varying $a_0$ and $l_0$ . . . . . 164
B.3 Topological classifications for different parameter values . . . . . 165

# CHAPTER 1

## Introduction

The Holocene constitutes the most recent geological epoch within the geologic time scale of Earth's history. The interglacial period whose onset is dated about 11700 years before present, is characterized by remarkably stable climatic and ecological conditions. Amongst other factors these are hypothesized to have facilitated the advent of human settlements and major civilizations in general [28]. Thereby the Holocene period encompasses a series of local and global socio-cultural revolutions from the neolithic revolution through several other agricultural revolutions and the industrial revolution to the proposed *Great Acceleration* [92]. At the same time it witnessed the rise and fall of major regional civilizations [25] while the global human population was more or less steadily increasing [52].

The observation that the accumulated impacts of human activities affected natural processes on a planetary scale led to the proclamation of an entirely new geological epoch, the *Anthropocene*, first by E. J. Stoermer in the early 1980s and later by P. J. Crutzen [23]. While there is an ongoing debate on both *whether* the Anthropocene constitutes indeed a geological epoch [64, 102, 109] and, if this was so, *when* it actually has started [62], the term proved to be expedient for the communication of evidences from environmental and sustainability sciences as it characterizes the fundamentally novel relation between human beings and planet Earth.

As it is an essential goal of Earth science and natural sciences in general to qualitatively and quantitatively understand the processes which constitute planetary dynamics, the Anthropocene poses a huge challenge for the development of suitable models which represent a holistic picture of the Earth system [100, 101]. In particular, a model of the Anthropocene necessitates the inclusion of social processes as well as the accounting for feedbacks between the natural and the human sphere.

## 1.1 Modeling natural Earth System Dynamics

One of the most striking features that reflects the substantial impact of human activities on a planetary scale is constituted by *climate change*. As such it depicts a characteristic of the Anthropocene which has been subject to a large field of research in the past decades. Since it is impossible to carry out experiments with the Earth system as a whole, the findings of climate science necessarily rely on theoretical models and computer simulations of these. There is a great variety of climate models which largely differ in their comprehensiveness, as represented by the number of processes incorporated, and their dimensional complexity given by the spatio-temporal resolution [18, 40].

On the one hand there are *General Circulation models* (GCMs) of the atmosphere and the ocean, which utilize a very detailed representation of physical and chemical processes in the natural Earth system in order to simulate the evolution of the climate of the past or the near future on relatively short timescales [36, 47]. However, these models are criticized for underestimating the role of vegetation dynamics and biogeochemical cycles, while spatial resolution and comprehensiveness might be overestimated [18]. Indeed, the feedbacks which occur when coupling an atmosphere-ocean GCM to a simple carbon cycle model may cause predictions that considerably deviate from those of GCM simulations without such feedbacks [21].

On the other hand there are simple, conceptual climate models which focus on certain components of the Earth system and are typically of low dimension [40, 58]. In contrast to GCMs, simple climate models allow rather long timescales of climate dynamics to be studied [76]. Moreover, there exist very conceptual models of certain components of the Earth system which aim at illustrating qualitative features of its dynamics rather than making quantitative statements [95, 97].

A third category of climate models is depicted by the *Earth system models of intermediate complexity* (EMICs) [18]. These models aim at an increased comprehensiveness compared to GCMs as they also incorporate biological processes and biogeochemical cycles such as the global carbon cycle [16, 32, 77]. Meanwhile they feature a coarser spatial resolution compared to coupled GCMs and allow simulations of climate variability over a wide range of timescales from seasons to multiple millennia [22].

Besides the progress which has been made through the study of climate models, the view on the Earth as a *complex dynamical system* enabled the gaining of new insights [82]. For example the underlying multistability of certain components of the Earth's climate system makes them to *tipping elements*, which might push the state of the whole Earth system into a different regime once a critical threshold ("tipping point") is transgressed [59].

Combining the findings from various fields of climate science there is strong and growing evidence that a large part of the global warming can be attributed directly or indirectly to human activities such as the emission of greenhouse gases and land use change [91, 94]. The observed changes in the natural Earth system impose a bunch of severe threats like droughts, heat waves, floods and rising sea levels to the human habitats in many regions [99]. However, while rising temperatures are generally expected to have negative consequences for both natural and humans systems, the specific local or global impacts are still poorly understood and thus often remain unforeseeable [99].

An own branch of economic models, so-called *Integrated Assessment Models* (IAMs), aims at incorporating the effects of a changing climate into assessments of the future economic evolution [73]. Often these models are designed to study the implications of certain policy instruments rather than to reflect the dynamics of the Earth system as a whole [57].

However, most of the above-mentioned modeling approaches have in common that they focus only on either the natural or the socio-economic component of the Earth system. Most climate models (GCMs, EMICs) include the human impacts only as a static exogenous driver to the dynamics, for example via emission scenarios, rather than describing the socio-economic evolution dynamically. In IAMs in turn, the natural or climate component is often simplified by linearization such that they are only adequate for short-term simulations on the timescale of decades but do not describe the long-term evolution of the Earth system. Moreover, IAMs usually treat the population dynamics as exogenous driver rather than modeling it endogenously and thus lack relevant feedbacks between the natural and the socio-economic subsystems. For these reasons none of the discussed models is able to adequately represent the complex long-term dynamics of the whole Earth system in the Holocene and the Anthropocene [100]. Hence it is desirable to establish a view on the Earth from a systems science perspective which explicitly includes the human sphere, or *anthroposphere*, as a component [86].

## 1.2 Coevolutionary Modeling Approaches for the Anthropocene

One of the first remarkable attempts which accounted for the limitations posed by the natural Earth system for the socio-economic evolution of humanity was undertaken by Meadows et al. in the early 1970s and prominently published in the book *The Limits to Growth* which was initiated by the Club of Rome [67]. The study utilized the *World3* model to project the mid-term evolution of several natural and socio-economic indicators for different scenarios, given by varying assumptions on model parameters. Some of the projections turned out to lack consistency with later observations which motivated follow-up versions of the report [68, 80]. Despite the manifold criticism about the World3 model, it definitely initiated a novel way of thinking about the relation between humans and the planet Earth and can thus be regarded as

the hour of birth of *coevolutionary* modeling.

The concept of coevolution was formally introduced into climate science by H. J. Schellnhuber in the late 1990s [88, 89]. Within this framework the Earth system $\mathcal{E}$ is composed of an ecosphere $\mathcal{N}$ and the human factor $\mathcal{H}$:

$$\mathcal{E} = \{\mathcal{N}, \mathcal{H}\} \qquad \text{where: } \mathcal{H} = \{\mathcal{A}, \mathcal{S}\} \tag{1.1}$$

The ecosphere $\mathcal{N}$ is composed of several sub-spheres like the atmosphere, biosphere, cryosphere and so on. The human factor $\mathcal{H}$ in turn is given by its physical realization, the *anthroposphere* $\mathcal{A}$ and a metaphysical component $\mathcal{S}$, the *Global Subject*, thought of as a collective self-conscious control force. The dynamic evolution of the Earth system can be represented in the coevolution space which is spanned by the ecosphere and the anthroposphere (Figure 1.1). The strong interconnection between these two spheres is reflected by the following abstract temporal evolution equations for the states of the anthroposphere **A** and the ecosphere **N** in which the state of the Global Subject **S** is regarded as a given precondition (or system parameter):

$$\begin{aligned} \dot{\mathbf{N}}(t) &= F_1(\mathbf{N}, \mathbf{A}, t | \mathbf{S}) \\ \dot{\mathbf{A}}(t) &= G_1(\mathbf{N}, \mathbf{A} | \mathbf{S}) \end{aligned} \tag{1.2}$$

Equation (1.2) is a highly comprehensive representation of the Earth system dynamics. Moreover, it is noteworthy that it does not describe a deterministic system, but rather accounts for the *management* or *control* of the dynamics through the human factor.

An important feature of the ecosphere within the coevolution space is displayed by the *ecological niche* which is its subset within which human life (or life in general) on the planet is possible. The limits of the ecological niche are closely related to the more recently suggested *planetary boundaries* [83, 84, 93] by Rockström et al. Within this framework nine crucial interlinked indicators for the integrity of the natural Earth system are identified and threshold values not to be exceeded are set normatively, based on estimated values beyond which the Holocene regime would likely be left. Together these boundaries form the so-called *safe operating space* for humanity although it was recently shown with a dynamical systems approach that reaching a meaningful amount of "safety" probably requires even narrower boundaries due to the internal dynamics of the system [43]. While Rockström et al. focused on the limits of the ecosphere, K. Raworth extended the concept by defining eleven socio-economic boundaries which depict the *social foundation* of the anthroposphere [81]. Combined with the planetary boundaries, which can be viewed as *environmental ceiling*, these are said to form the *safe and just operating pace* for humanity.

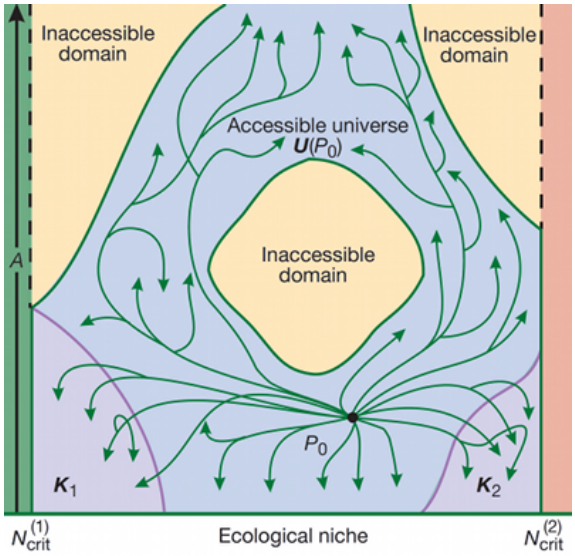


**Figure 1.1:** Schematic of the coevolution space which is spanned by the ecosphere $\mathcal{N}$ and the anthroposphere $\mathcal{A}$. For a given initial point $P_0$ there is a bunch of *pathways* which evolve in the accessible universe. Some regions might be inaccessible and others potentially imply a collapse of the Earth system ($K_{1,2}$). In that case the state of the ecosphere would evolve into undesirable regimes outside the ecological niche. As humanity is able to *control* its actions the system is not deterministic and pathways are allowed to cross each other. Adopted from [88].

Several modeling approaches have been proposed which make first steps towards an understanding of the Earth system in the coevolutionary sense. Brander and Taylor proposed a simple model of coupled population and renewable resource dynamics in order to explain the collapse of the Easter Island civilization [15]. Since then a relatively vast field of *social-ecological* models has emerged which analyze the feedbacks between socio-economic conditions and natural resource systems [42, 54, 55, 90]. However, most of these attempts focus on specific local ecosystems (such as fishery, rangeland or wildlife) rather than on global scale phenomena which are an emergent characteristic of the Anthropocene. The GUMBO model by Boumans et al. in turn aims at a comprehensive representation of the whole Earth system at the price of a large number of variables and parameters which render a qualitative understanding impossible [14]. A more conceptual model which describes the global interaction of humans with the carbon cycle has been investigated by Anderies et al. [2] and allows for a qualitative understanding of the system's *topology*. The framework recently proposed by Heitzig et al. addresses the qualitative classification of a system's state space, especially in the context of planetary boundaries and the safe operating space [43]. Furthermore it suggests a metaphorical framework which is in line with [89] and allows to communicate subtle dynamical properties

of complex systems in an understandable way to laymen.

One potential feedback which is only seldom accounted for in established models are climate impacts on both social and economic entities and processes. Even if there were no efforts to mitigate climate change, the rising temperatures would sooner or later cause damages to physical and human capital what in turn would decelerate the economic evolution and hence decrease the emissions of greenhouse gases [61]. Kellie-Smith and Cox studied a conceptual model which follows this reasoning and find the emergence of oscillations in the coupled climate-economy system [48] even on relatively short timescales of some hundreds of years.

Finally, Motesharrei et al. in their model explicitly investigate the dynamic implications of *inequality* within the society rather than treating all humans in exactly the same way, thereby addressing the "justness" issue of social dynamics [70].

## 1.3 The copan:GLOBAL model

The *copan* project at the Potsdam Institute for Climate Impact Research aims at understanding the mid- and long-term coevolution of the social and natural subsystems of the Earth in the context of the safe and just operating space. The models developed and studied within this scope are mainly of conceptual style and hence allow qualitative insights into complex dynamics rather than quantitative predictions. Thereby they try to fill a gap in the model landscape of the established Earth system models discussed above (Figure 1.2). Wiedermann et al. for instance utilized an agent-based model of social and resource dynamics on a network topology to show that fast imitation rates between agents can induce a phase transition into an unsustainable regime [107].

The model which is studied within this thesis is called *copan:GLOBAL*. It is a conceptual, low-dimensional coevolutionary Earth system model which describes the temporal evolution of globally aggregated or averaged key quantities of the natural and socio-economic subsystems on centennial to millennial timescales. Hence it is capable of reflecting the global natural dynamics of the Holocene as well as characteristics and emergent phenomena of the Anthropocene.

The natural subsystem of the Earth is represented in the model via the global carbon cycle and the global mean surface temperature, reflecting the climate. The socio-economic part on the other hand describes the dynamics of the global human population, the aggregated physical capital and a renewable technology knowledge stock. These quantities influence each other by several processes such as photosynthesis, respiration, economic production, emissions, population growth or climate impacts. From a physical perspective the model constitutes a low-dimensional, *deterministic dynamical system* and can be analyzed using established analytical and numerical techniques from the field of non-linear dynamics.

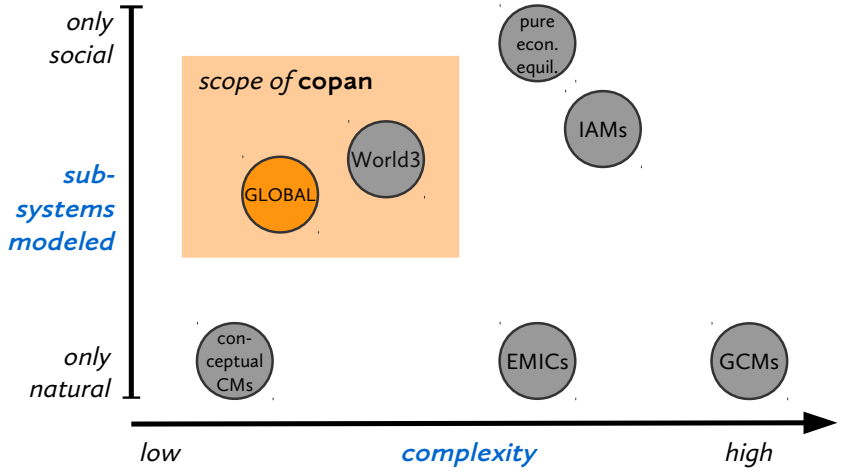


**Figure 1.2:** Landscape of Earth System Models separated according to the modeled subsytems on the vertical axis and the complexity (given by the number of processes and spatio-temporal resolution) on the horizontal axis. Pure climate models (conceptual CMs, EMICs and GCMs) differ considerably with respect to complexity but typically do not account for socio-economic dynamics. Pure economic models also feature different degrees of complexity but treat the natural system exogenously. The relatively complex IAMs strive for an integrated view of natural and social subsystems and typically address quantitative questions relevant for policy-making. The World3 model used by the Club of Rome constitutes a pioneering work for the type of coevolutionary modeling which lies within the scope of the *copan* project. The GLOBAL model studied within this thesis has less variables than World3 which allows for a qualitative analysis from a dynamical systems perspective. Adopted from [106].

## 1.4 Research Tasks and Overview of the Thesis

The state of research on coevolutionary dynamics discussed so far and the scope of the copan project in particular, motivate the following **research tasks** for this thesis:

- Suitable **sub-models** shall be derived from the complete copan:GLOBAL model which correspond to different *stages* of the natural and socio-economic coevolution in the Holocene and the Anthropocene epochs.
- For each identified sub-model the **asymptotic behavior** given by its equilibria and attractors shall be classified. This involves the identification of **dynamic regimes** in the parameter space whose asymptotics feature the same characteristics.
- Moreover, the qualitative influence of the model parameters will be investigated. This involves the analysis of possible **bifurcations** which occur under variation of the free parameters.

- As many **parameters** as possible shall at least roughly be **estimated** from available real-world data in order to curtail the relevant parameter regime and thus identify the most likely qualitative behavior. Meanwhile this will enable the comparison of characteristic quantities of the dynamics with data acquired with differing methodological approaches, thus potentially allowing for a **validation** of the parametrization.

The following chapters are organized as follows. The first section of chapter 2 briefly introduces the concept of a *dynamical system* and gives an overview of *bifurcation theory*, in particular those bifurcations which are of relevance for this thesis are discussed. The part on dynamical systems closes with an introduction into the topology framework by Heitzig et al. [43] as it is applied to the copan:GLOBAL model later on. The following sections introduce concepts from economics (Section 2.2) and Earth science (Section 2.3) which are relevant for the *model design*. The setup of the copan:GLOBAL model is extensively examined in chapter 3. After giving an overview to the complete model which has been developed within the copan project, several submodels are presented which have been defined as a part of the present work. The following two chapters present all relevant findings which have been obtained within the course of this work. Chapter 4 describes the estimation of most of the free model parameters based on real world data and closes with a condensed overview Table in section 4.5. Chapter 5 constitutes the main part of the work as it contains a detailed analysis of the asymptotic dynamics of the studied model versions. This comprises the determination of equilibria, their stabilities, attractors as well as the study of bifurcations which occur when certain parameters are varied. These analytical and numerical calculations are complemented by graphical representations of the phase space of the models and their topology (in the sense of the framework by [43]). Chapter 6 summarizes the main results of this work, discusses these in the context of related research and gives an outlook on further directions of studying and developing the copan:GLOBAL model. Finally, chapter 7 gives a condensed conclusion of the thesis.

# CHAPTER 2

## Methodological Preliminaries and Concepts

This chapter introduces the theoretical background of methods and concepts used for the development and analysis of the model. Section 2.1 reviews the major aspects of dynamical systems theory and gives a brief introduction into the field of bifurcation theory. The following sections are dedicated to the presentation of concepts from economics (2.2) and geoscience (2.3) which are necessary for the model design, presented in the subsequent chapter.

### 2.1 Dynamical Systems

The mathematical concept of an **autonomous deterministic dynamical system** is used to describe deterministic processes from different fields of science [53, Ch. 1.1]. While the processes may originate from physical, chemical and biological as well as economical or social systems, the mathematical description and hence the possible dynamical phenomena are structurally similar.

#### 2.1.1 Definition

All dynamical systems are characterized by the same "ingredients" which make up their formal mathematical definition [53, Ch. 1.1].

Firstly, there is a **state space** $X$ which forms the set of all possible states $x \in X$ that the system can exhibit. Depending on the nature of the system this space can be of very different kind, for example an infinite-dimensional function space or a finite space of discrete states. The systems regarded within this thesis are typically of low finite dimensions $n$ and the state components are given by real numbers, such that $X = \mathbb{R}^n$.

The next ingredient is given by a **time set** $T$ which depicts the set of all possible points in time $t \in T$. One distinguishes between dynamical systems where time is **discrete** and thus $T = \mathbb{Z}$, and those with **continuous** time, where $T = \mathbb{R}$. In this thesis only continuous-time dynamical systems are treated.

Finally a dynamical system needs something which makes it indeed "dynamic". This is achieved by an **evolution law** which prescribes the evolution of the state $x \in X$ of the system with time $t \in T$. In a very general way this can be formulated in terms of a **map**

$$\phi^t : X \to X \, . \tag{2.1}$$

Given an initial state $x_0 \in X$ the state $x_t$ at time $t \in T$ is given by:

$$x_t = \phi^t x_0 \tag{2.2}$$

The **evolution operator** $\phi^t$ needs to fulfill the following properties:

$$\text{(i)} \qquad \phi^0 = \mathrm{id} \tag{2.3}$$

$$\text{(ii)} \qquad \phi^{t+s} x \; = \phi^t(\phi^s x) \tag{2.4}$$

While condition (i) means that the state does not change spontaneously, condition (ii) states that the evolution law does not change with time and thus the system is **autonomous**.

Putting these ingredients together leads to the following general definition [53, Ch. 1.1]:

**Definition 1.** *An **autonomous dynamical system** is a triple $\{X,T,\phi^t\}$, where $T$ is a time set, $X$ is a state space and $\phi^t : X \to X$ is an evolution operator which fulfills conditions (2.3) and (2.4).*

As already mentioned the dynamical systems regarded in this thesis have continuous time ($T = \mathbb{R}$) and a state space of finitely many real variables ($X = \mathbb{R}^n$). For these systems the evolution law is often not given explicitly but rather implicitly via **ordinary differential equations** (ODEs) [53, Ch. 1.4]. Given a state $\mathbf{x} = (x_1,...,x_n)$, its temporal evolution is defined via the velocities

$$\dot{\mathbf{x}} = f(\mathbf{x}) \tag{2.5}$$

where $f : \mathbb{R}^n \to \mathbb{R}^n$ is a smooth function (or vector field). Equation (2.5) represents a set of $n$ autonomous ODEs. The existence and uniqueness of the solution to such an ODE system can be proven. For the definition of a dynamical system the solution curve $\mathbf{x}(t,\mathbf{x}_0)$ (for a given initial state $\mathbf{x}_0$) takes the role of the evolution operator in equation (2.2):

$$\phi^t \mathbf{x}_0 = \mathbf{x}(t,\mathbf{x}_0) \tag{2.6}$$

### 2.1.2 Trajectories and phase portraits

Very basic geometric objects related to a dynamical system are its **trajectories** (or **orbits**) [53, Ch. 1.2].

**Definition 2.** *A **trajectory** starting at $x_0$ is an ordered subset of the state space $X$:*

$$\tau_{x_0} = \{x \in X : x = \phi^t x_0, \text{ for some } t \in T\} \tag{2.7}$$

For a continuous-time dynamical system trajectories correspond to curves in the state space. There are special orbits of which the most simple one is an **equilibrium** (or **fixed point**):

**Definition 3.** *A point $x^* \in X$ is called **equilibrium** if $\phi^t x^* = x^*$ for all $t \in T$.*

Thus, an equilibrium can be seen as a trajectory which exhibits the same state for all times. If the dynamical system is given by an ODE system like (2.5), an equilibrium $\mathbf{x}^*$ fulfills the following condition:

$$f(\mathbf{x}^*) = 0 \tag{2.8}$$

Another class of special trajectories is given by **cycles** which are periodic trajectories:

**Definition 4.** *A **cycle** $\Gamma$ is a non-equilibrium periodic trajectory which satisfies $\phi^{t+T_0} x_0 = \phi^t x_0$ for all $x_0 \in \Gamma$ and $t \in T$ for some $T_0 > 0$. The minimal $T_0$ which fulfills this property is called **period** of the cycle.*

For continuous-time systems cycles correspond to closed curves in the state space. If a cycle $\Gamma$ is **isolated**, meaning that there are no other cycles in a neighborhood of $\Gamma$, it is called a **limit cycle**.

For the qualitative analysis of dynamical systems it is very helpful to have a geometric representation of its dynamics. This is given by the **phase portrait** which is a partitioning of the state space into trajectories. For low-dimensional systems ($n \leq 2$) the phase portrait can actually be drawn, which allows for a graphical analysis of the system. Many important features of the dynamics, like the number and types of **asymptotic** states can be retrieved directly from the phase portrait. In order to obtain a more subtle classification of the phase space objects it is useful to define a notion of **stability** which is done in the following section.

### 2.1.3 Notions of stability

There are different notions of the stability of dynamical systems which have in common that they characterize the behavior of a system after some sort of perturbation. Thus, when a system is called "stable" it needs to be clear which concept of stability is referred to. Furthermore there is some impreciseness about the terminology in the literature [53, 96]. Throughout this thesis the subsequently introduced terminology is used which is mainly in line with [96]. The following definitions are formulated for equilibria of continuous-time, finite-dimensional dynamical systems. However, analogous definitions hold for discrete-time systems and other state spaces.

In the following a continuous-time dynamical system with state space $X = \mathbb{R}^n$ is considered which is defined by the ODE system $\dot{x} = f(x)$, where $x \in \mathbb{R}^n$. The system features an equilibrium state $x^*$.

**Definition 5.** *The equilibrium $x^*$ is said to be **attracting**, if there exists a $\delta > 0$ such that $\lim_{t \to +\infty} x(t) = x^*$ for all $x_0$ with $\|x_0 - x^*\| < \delta$.*

In other words all trajectories which start sufficiently close to $x^*$ will converge eventually to the equilibrium. The subset $B \subseteq X$ which contains all initial conditions which eventually converge to an equilibrium is called its **basin of attraction**.

**Definition 6.** *The equilibrium $x^*$ is called **Lyapunov stable**, if for each $\varepsilon > 0$ there is a $\delta > 0$ such that $\|x(t) - x^*\| < \varepsilon$ for all $t \geq 0$ and all $x_0$ with $\|x_0 - x^*\| < \delta$.*

This means that trajectories which start sufficiently close to $x^*$ will stay in a finite neighborhood around it for all times.

It is worth noting that these notions of stability can hold independently from each other. In many cases, however, they occur simultaneously. An equilibrium which is both attracting and Lyapunov stable is called **asymptotically stable**, or simply **stable**. Whether an equilibrium is (asymptotically) stable can be checked by applying of the following theorem.

**Theorem 1.** *Considering the dynamical system given by $\dot{x} = f(x)$ which has an equilibrium $x^*$, so that $f(x^*) = 0$. Denote by A the Jacobian matrix J of the system, evaluated at $x^*$:*

$$A := J|_{x=x^*} = \left( \left. \frac{\partial f_i(x)}{\partial x_j} \right|_{x=x^*} \right)_{ij} \quad ; \; i,j = 1...n$$

*Then $x^*$ is **stable** if all eigenvalues $\lambda_1,...,\lambda_n$ of A have negative real parts. $x^*$ is **unstable** if at least one eigenvalue $\lambda$ of A has a positive real part.*

This type of analysis is referred to as **linear stability analysis** since the stability is determined from the linearized system. This is legitimate since according to the Hartman-Grobman theorem the phase space of the linearized system around a hyperbolic equilibrium is topologically equivalent to that of the original system [96].[1]

The stability concepts introduced so far can also be transferred to limit cycles. The according definitions and theorems are not shown here but can be found in appropriate textbooks like [53]. The stability analysis of limit cycles is closely related to the stability of fixed point of associated **Poincaré maps** which are discrete-time dynamical systems derived from continuous trajectories. For the following considerations the distinction between stable limit cycles (which are attracting nearby trajectories) and unstable limit cycles (which are repellent) is sufficient.

Finally it remains to be said that there are more, conceptually different notions of stability. While the linear stability analysis focuses on stability against *infinitesimal* perturbations in the state variables and is thus a local measure, the notion of **basin stability** quantifies resistance against *large* perturbations, rendering it a global measure [69]. The basin stability of an equilibrium is given by the volume of its basin of attraction. The response of a system to infinitesimal perturbations in the function $f$ which governs the dynamics is analyzed within the context of **structural stability** analysis [53, Ch. 2.5].

1 The notions of **hyperbolicity** and **topological equivalence** are introduced in section 2.1.4.

### 2.1.4 Topological equivalence

In order to study the qualitative behavior of a dynamical system it is desirable to classify its properties (e.g. number and stabilities of equilibria) and to be able to compare different systems with each other. For this purpose the concept of **topological equivalence** proves to be very useful. It is basically a mathematical formulation of the intuitive requirement that equivalent dynamical systems should have "qualitatively similar" phase portraits [53, Ch. 2.1]. Furthermore the notion of topological equivalence is a precondition for the definition of a **bifurcation** which is explicated in the next section.

**Definition 7.** *A dynamical system* $\{T,\mathbb{R}^n,\phi^t\}$ *is called* ***topologically equivalent*** *to a dynamical system* $\{T,\mathbb{R}^n,\psi^t\}$ *if there is a homeomorphism*[1] $h : \mathbb{R}^n \to \mathbb{R}^n$ *which maps the trajectories of the first onto those of the second system, while the direction of time is preserved.*

An example for two topologically equivalent planar phase portraits is shown in Figure 2.1.

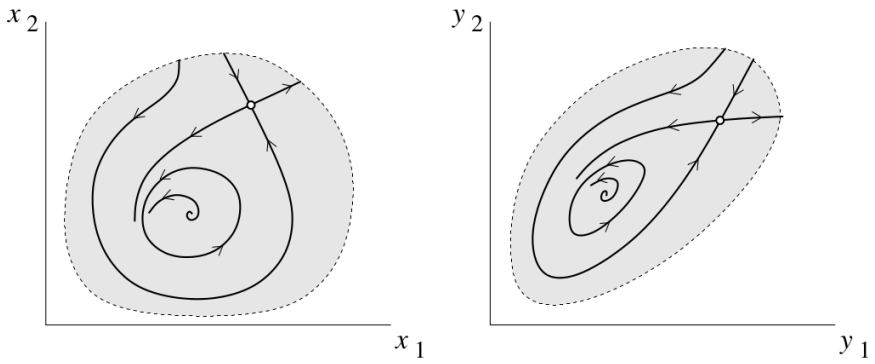


**Figure 2.1:** Phase portraits of two **topologically equivalent** planar dynamical systems. There is a homeomorphism which maps the trajectories of the left onto those of the right system. Taken from [53, Ch. 2.1].

This definition can also be restricted to local neighborhoods $U,V \subset \mathbb{R}^n$ of equilibria $x_0 \in U$ and $y_0 \in V$ of two systems. Applying this concept to the neighborhood of equilibria and limit cycles yields a classification scheme for these special trajectories. While the above definition is also valid for discrete-time systems the following considerations are restricted to systems with continuous time.

1 A homeomorphism is a continuous bijection whose inverse is also continuous.

### Classification of hyperbolic equilibria

As in the previous section a continuous-time dynamical system defined by $\dot{x} = f(x)$, where $x \in \mathbb{R}^n$, is considered. The system has an equilibrium $x^*$ and the Jacobian evaluated at this equilibrium is denoted by $A$. $A$ has $n_+$, $n_-$ and $n_0$ eigenvalues with positive, negative and zero real part, respectively.

**Definition 8.** *The equilibrium $x^*$ is called **hyperbolic** if $n_0 = 0$. A hyperbolic equilibrium is called a **saddle** if $n_+ n_- > 0$.*

This means that a non-hyperbolic equilibrium has at least one eigenvalue exactly on the imaginary axis, which turns out to occur only rarely in systems describing real-world processes with generic parameters. The hyperbolicity condition is typically violated at particular parameter values at which a bifurcation occurs (see Section 2.1.5).

The following theorem allows a topological classification of equilibria:

**Theorem 2.** *The phase portraits near two equilibria $x^*$ and $y^*$ are locally topologically equivalent if and only if they have the same numbers $n_+$ and $n_-$ of eigenvalues with positive and negative real part, respectively.*

A proof of this theorem can be found in appropriate textbooks [53, Ch. 2.2][3, 39].

Applying this theorem to two-dimensional (planar) systems gives a topological classification scheme for its hyperbolic equilibria. The Jacobian evaluated at an equilibrium, $A$, has two eigenvalues $\lambda_1$ and $\lambda_2$. These can be calculated by solving the characteristic equation of the Jacobian:

$$\lambda^2 - \tau\lambda + \Delta = 0 \tag{2.9}$$

where $\tau = \mathrm{tr}(A)$ denotes the trace of the matrix and $\Delta = \det(A)$ its determinant. Hence, for the eigenvalues the following holds:

$$\lambda_{1,2} = \frac{\tau \pm \sqrt{\tau^2 - 4\Delta}}{2} \tag{2.10}$$

Moreover, the following formulas generally hold for the trace and the determinant of $A$:

$$\tau = \lambda_1 + \lambda_2 \tag{2.11}$$

$$\Delta = \lambda_1 \lambda_2 \tag{2.12}$$

If $\Delta < 0$ both eigenvalues are real and have opposite signs ($n_+ = n_- = 1$). According to the above definition such equilibria are called **saddles**.

If $\Delta > 0$ the real parts of the eigenvalues have the same signs. If $\tau > 0$ both eigenvalues have positive real part ($n_+ = 2$, $n_- = 0$) and the equilibrium is unstable. If $\tau < 0$ both have negative real parts and thus the equilibrium is stable. Topologically these are all possible cases. A finer distinction can be achieved by looking at the discriminant term under the square root in equation (2.10). If $\tau^2 - 4\Delta > 0$ the eigenvalues are real, such an equilibrium is called a **node**. If $\tau^2 - 4\Delta < 0$ the eigenvalues are complex conjugates and the corresponding equilibrium is called a **focus** or **spiral**. Topologically, however, nodes and foci of the same stability are equivalent which is explicitly shown in [53, Ch. 2.1]. An overview of this classification scheme is given in Figure 2.2.

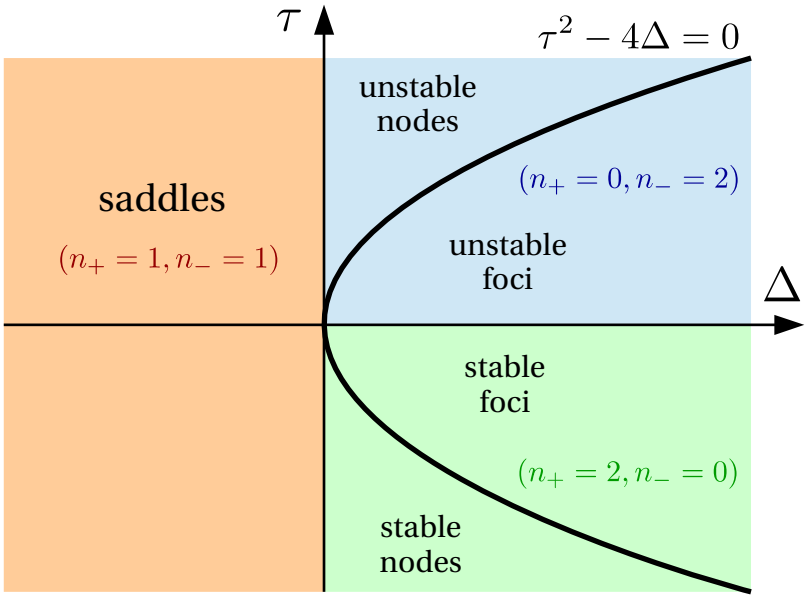


**Figure 2.2:** Topological classification scheme for hyperbolic equilibria in planar system. All saddle points lie in the reddish region with $\Delta < 0$ and are topologically equivalent. All stable equilibria lie in the greenish region with $\Delta > 0$ and $\tau < 0$. The blueish region with $\Delta > 0$ and $\tau > 0$ contains all unstable nodes and foci. The black curve divides the nodes from the foci which are topologically equivalent though, given that they have the same number of eigenvalues $n_+$ and $n_-$ with positive and negative real parts, respectively.

#### Classification of hyperbolic limit cycles

The notion of hyperbolicity can also be applied to limit cycles. A limit cycle is called hyperbolic if the the corresponding fixed point of the Poincaré map derived from the system is hyperbolic [53, Ch. 2.2]. The topological classification of the limit cycle is done according to the eigenvalues of the Jacobian of the Poincaré map, evaluated at its fixed point. These are called called **multipliers of the cycle**.[1] Topologically equivalent limit cycles have the same numbers $n_+$ and $n_-$ of multipliers outside and inside the unit circle, respectively. As the Poincaré map of a cycle of a $n$-dimensional system is of dimension $n-1$, the relation $n_+ + n_- = n-1$ holds. For example, the Poincaré map derived from a two-dimensional system has dimension one. A limit cycle of the two-dimensional system corresponds to a fixed point of the one-dimensional map and has exactly one multiplier $\mu$. Thus, there are just two possible topological classifications of the cycle given by the sign of $\mu$. If $n_+ = 1$ the cycle is unstable, if instead $n_- = 1$ the cycle is stable. For higher dimensional systems ($n \geq 3$) the case $n_+ n_- > 0$ is also possible. Analogous to equilibria, these are called **saddle cycles**.

### 2.1.5 Bifurcations

Having introduced the concept of topological equivalence of dynamical systems enables the introduction of the important notion of **bifurcations** [53, Ch. 2.3, 2.4]. Consider a dynamical system which depends on some $m$-vector of parameters $\alpha$. For the continuous-time case with $X = \mathbb{R}^n$ it can be represented by the following ODE system:

$$\dot{x} = f(x, \alpha) \qquad , x \in \mathbb{R}^n, \alpha \in \mathbb{R}^m \tag{2.13}$$

Generally a change in the parameters $\alpha$ will lead to a change in the vector field $f$ and hence in the phase portrait of the system. The following definition is valid for any time set $T$ and state space $X$:

**Definition 9.** *The occurrence of a topologically non-equivalent phase portrait under variation of parameters is called a* ***bifurcation****.*

The parameter space can be subdivided into maximal connected subsets (**strata**) for which the system has a topologically equivalent phase portrait. The partitioning of the phase space into such regions is called **parametric portrait** or **bifurcation diagram**. The boundaries of these regions in the parameter space are called **bifurcation boundaries** and are typically smooth manifolds of dimension $< m$. This enables the definition of the **codimension** of a bifurcation:

1 The logarithms of the multipliers are called the **Floquet exponents** of the cycle and the real parts of the latter are called **Lyapunov exponents** which quantify the rate of amplification or decay of perturbations.

**Definition 10.** *The difference between the dimension of the parameter space m and the dimension of the bifurcation boundary is called the* ***codimension*** *of the bifurcation.*

For example, if a one-dimensional parameter space $\mathbb{R}$ is divided into two regions by a critical bifurcation value $\alpha_{\text{crit}}$ of dimension zero, the bifurcation is of codimension one. This also means that the codimension sets the minimal number of parameters which need to be varied simultaneously for the bifurcation to occur.

Equivalently, the codimension equals the number of independent *equality conditions* which characterize a bifurcation. These are typically algebraic equations for some quantities derived from the system. Apart from these **bifurcation conditions** there are typically some *inequalities* which need to be fulfilled at a bifurcation point. These are called **non-degeneracy** and **transversality** conditions.[1] A violation of such an inequality can imply a bifurcation of a higher codimension.

Another important distinction is that into **local** and **global** bifurcations [96, Ch. 8.4 ]. A bifurcation is called local when it can be detected by looking at an arbitrarily small neighborhood of an equilibrium. For the observation ob global bifurcations, however, one needs to regard large regions of the phase space.

The mechanisms which lead to some local bifurcation are generally independent of the specific system. They can be studied in simple (polynomial) prototypical systems which feature a certain type of bifurcation. These prototypical systems are called **topological normal forms** for the bifurcation. Systems which feature a bifurcation of the same type are locally topologically equivalent to its normal form.

In the following sections all types of bifurcations of equilibria and cycles which are relevant for this thesis are introduced.

1 In the following examples the non-degeneracy and transversality conditions are only stated explicitly if they are of relevance at a later point.

### Local Bifurcations of Equilibria and Cycles

The most simple local bifurcations of equilibria occur in one-dimensional systems of the form:

$$\dot{x} = f(x,\alpha) \qquad , x \in \mathbb{R}, \alpha \in \mathbb{R} \tag{2.14}$$

Consider at first the following system:

$$\dot{x} = \alpha + x^2 \tag{2.15}$$

which has two equilibria $x^*_{1,2} = \pm\sqrt{-\alpha}$ if $\alpha < 0$, one equilibrium $x^*_0 = 0$ if $\alpha = 0$ and no equilibria for the case $\alpha > 0$. $x^*_1 = +\sqrt{-\alpha}$ is an unstable equilibrium while $x^*_2 = -\sqrt{-\alpha}$ is stable. At $\alpha = 0$ the equilibrium becomes non-hyperbolic as the eigenvalue (the derivative in the 1D case) becomes zero:

$$\lambda = \left.\frac{\partial f}{\partial x}\right|_{x=0} = 0 \tag{2.16}$$

The phase portraits for the cases $\alpha < 0$ , $\alpha = 0$ and $\alpha > 0$ are not topologically equivalent. Thus a bifurcation occurs at the critical value $\alpha_0 = 0$. This bifurcation is called a **fold** or **saddle-node** bifurcation. It is the basic mechanism for equilibria to appear or disappear under variation of a parameter. As there is one equality condition (2.16) which characterizes the bifurcation, it has codimension one. Additionally the non-degeneracy condition

$$\left.\frac{\partial^2 f}{\partial x^2}\right|_{x=0} \neq 0 \tag{2.17}$$

must be fulfilled. Figure 2.3 shows phase portraits and the generic bifurcation diagram of a fold bifurcation.

The next type of bifurcation which is of importance is called **transcritical** bifurcation. It typically occurs in systems which have an equilibrium whose position is independent of the parameter values. If another equilibrium “passes through” the first one when a parameter is varied, the stabilities of the equilibria are “exchanged”. The prototypical example for a transcritical bifurcation reads as follows:

$$\dot{x} = \alpha x - x^2 \tag{2.18}$$

This system has one equilibrium at $x^*_0 = 0$ and one at $x^*_1 = \alpha$. $x^*_0$ is stable for $\alpha < 0$ and unstable for $\alpha > 0$, for $x^*_1$ the situation is reversed. For the case $\alpha = 0$ there is only one equilibrium

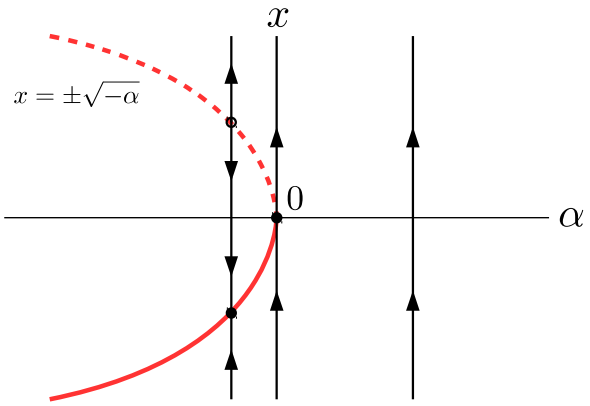


**Figure 2.3:** Generic bifurcation diagram of a **fold bifurcation**. The vertical lines show non-equivalent one-dimensional phase portraits of system (2.15) for different $\alpha$. The red curve corresponds to the positions of the stable (continuous) and unstable (dashed) equilibria.

at $x^* = 0$ which is non-hyperbolic as condition (2.16) holds here as well. Again the phase portraits for $\alpha < 0$ , $\alpha = 0$ and $\alpha > 0$ are topologically non-equivalent and hence a bifurcation occurs (see Figure 2.4). Like the fold bifurcation it is of codimension one.

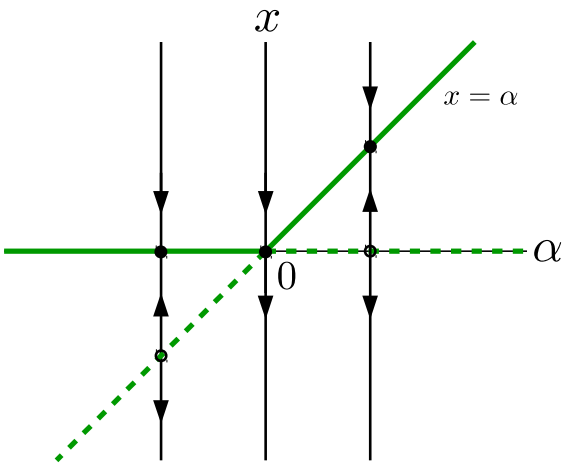


**Figure 2.4:** Generic bifurcation diagram of a **transcritical bifurcation**. The vertical lines show exemplary one-dimensional phase-portraits of system (2.18) for different $\alpha$. The green curves correspond to the positions of stable (continuous) and unstable (dashed) equilibria.

Note that although both saddle-node and transcritical bifurcations are local bifurcations, a saddle-node bifurcation still has “global consequences” since at the critical parameter value,

the limit that a trajectory starting from a far away point converges to makes a discontinuous jump, if that trajectory converged to the eliminated stable equilibrium before the bifurcation. In other words, basins of attraction change locally and smoothly under transcritical bifurcations but globally and non-smoothly under saddle-node bifurcations.

A third type of bifurcation in one-dimensional systems is the **pitchfork** bifurcation for which the normal form is given by $\dot{x} = \alpha x \pm x^3$. It is not explained here as it is not of relevance for this thesis but a discussion can be found in [96, Ch. 3.4].

The next important type of bifurcation occurs in systems which have a minimal dimension of two:

$$\dot{x} = f(x,\alpha) \qquad , x = (x_1,x_2) \in \mathbb{R}^2, \alpha \in \mathbb{R} \tag{2.19}$$

In such systems the hyperbolicity condition ($\mathrm{Re}\lambda \neq 0$ for all eigenvalues) can be violated in two ways. Either one eigenvalue becomes exactly zero when a parameter is varied. This leads to the same bifurcations as discussed above for one-dimensional systems. Another possibility is that two complex conjugate eigenvalues cross the imaginary axis. This leads to the so called **Andronov-Hopf** (AH) bifurcation which is one mechanism for the creation of limit cycles from equilibria.

The following system, given in polar coordinates $(\rho,\phi)$ is a prototypical example in which an Andronov-Hopf bifurcation can be observed:

$$\begin{aligned} \dot{\rho} &= \rho(\alpha - \rho^2) \\ \dot{\phi} &= \omega \end{aligned} \tag{2.20}$$

For $\alpha < 0$ there is one stable equilibrium at $\rho^* = 0$. For $\alpha > 0$ this equilibrium is unstable and there is a stable limit cycle trajectory located at $\rho = \sqrt{\alpha}$. The non-equivalent phase portraits show that a bifurcation occurs at $\alpha_0 = 0$ (see Figure 2.5).

By writing the system in Cartesian coordinates one can show that the eigenvalues of the Jacobian at the equilibrium $\rho^* = 0$ are given by $\lambda_{1,2} = \alpha \pm i\omega$. Thus for $\alpha = 0$ the eigenvalues lie on the imaginary axis as discussed above and the equilibrium becomes non-hyperbolic. The condition

$$\lambda_{1,2} = \pm i\omega \tag{2.21}$$

is the defining condition for all Andronov-Hopf bifurcations. Additionally at an AH bifurcation

point the following non-degeneracy condition must be fulfilled:

$$l_1(\alpha_0) \neq 0 \tag{2.22}$$

where $l_1(\alpha)$ denotes the **first Lyapunov coefficient**, a quantity which is calculated from higher-order derivatives of the vector field (see [53] for a definition).

Depending on whether $l_1$ is negative or positive at the bifurcation point, the limit cycle which appears is either stable or unstable. If $l_1 < 0$ (as in the example above) a stable limit cycle appears, this case is denoted as **super-critical** Andronov-Hopf bifurcation. In the opposite case, $l_1 > 0$, the limit cycle is unstable which is denoted as **sub-critical** Andronov-Hopf bifurcation. If the inequality (2.22) is violated a bifurcation of codimension two occurs which is discussed later in this section.

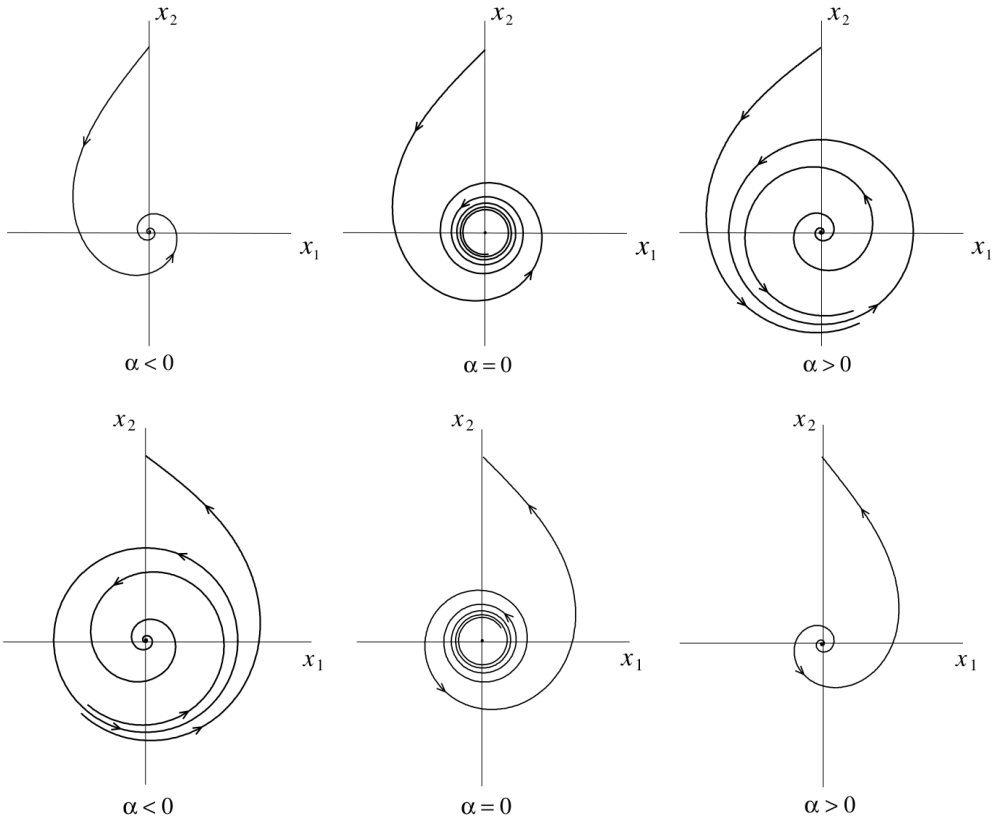


**Figure 2.5:** Phase portrait of generic planar systems which exhibit an **Andronov-Hopf bifurcation** at $\alpha = 0$. Top: Super-critical case given by equations (2.20) in which a stable limit cycle appears for $\alpha > 0$. The first Lyapunov coefficient is negative at the bifurcation point, $l_1 < 0$. Bottom: Sub-critical case given by $\dot{\rho} = \rho(\alpha + \rho^2), \dot{\phi} = \omega$, in which an unstable limit cycle is present for $\alpha < 0$. Here $l_1 > 0$ holds. Taken from [53, Ch. 3.4].

### Global Bifurcations of Cycles

The Andronov-Hopf case discussed above is just one of many mechanisms in which limit cycle trajectories can be created through a bifurcation. There are other bifurcation mechanisms in which limit cycles appear **globally** meaning that the bifurcation cannot be detected locally at an equilibrium [96, Ch. 8.4].

The first case of a global bifurcation is given by the **fold** or **saddle-node bifurcation of cycles**. It can be observed in the following system, given in polar coordinates:

$$\dot{\rho} = \alpha\rho + \rho^3 - \rho^5 \tag{2.23}$$

$$\dot{\phi} = \omega \tag{2.24}$$

It is helpful to look only at the one-dimensional system for $\rho \geq 0$ given by the first equation (see Figure 2.6, top). For $\alpha > 0$ it has two equilibria at $\rho_0^* = 0$ (unstable) and $\rho_1^*(\alpha) > 0$ (stable). The latter one corresponds to a stable limit cycle in the full two-dimensional system. If $\alpha$ is decreased below 0 the unstable equilibrium at $\rho_0^* = 0$ becomes stable and an additional unstable equilibrium occurs at $\rho_2^*(\alpha) < \rho_1^*(\alpha)$. This corresponds to an unstable limit cycle in the full system. Thus a sub-critical Andronov-Hopf bifurcation which was mentioned above occurs at $\alpha_0 = 0$. If $\alpha$ is further decreased the equilibria at $\rho_1^*$ and $\rho_2^*$ approach each other until they coalesce at $\alpha_1 = -1/4$ and disappear for $\alpha < -1/4$. This corresponds to a fold bifurcation in the one-dimensional system. In the two-dimensional system the two limit cycles coalesce and vanish which is denoted as a fold bifurcation of cycles referring to the one-dimensional analog. This bifurcation is global as it is not observable in an arbitrarily small region of the phase space.[1] This bifurcation has codimension one as it is achieved by the variation of one parameter.

1 Some authors like [53] denote this as **local bifurcation of cycles** since the bifurcation corresponds to a local bifurcation in the corresponding Poincaré map.

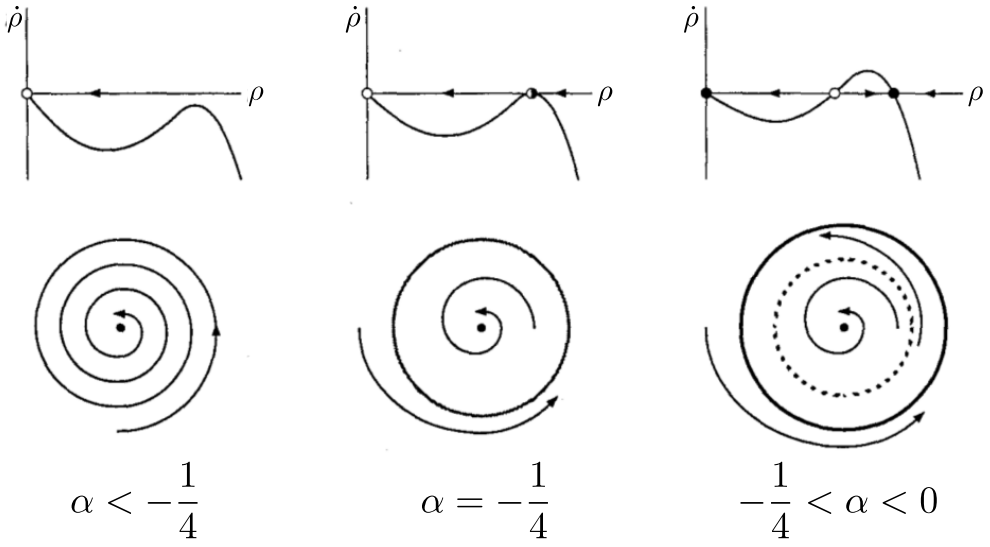


**Figure 2.6:** Mechanism and phase portraits of a **fold bifurcation of cycles**. Top: In the one-dimensional radial system given by equation (2.23) a fold bifurcation occurs at $\alpha = -1/4$. Bottom: The fold bifurcation in the radial system causes a global bifurcation of two limit cycles in the planar system. Modified from [96, Ch. 8.4].

The last codimension one bifurcation to be introduced is the **homoclinic bifurcation** which is another example for a global bifurcation. It requires the definition of a **homoclinic** orbit. Given a continuous-time dynamical system like (2.13) with an evolution operator $\phi^t$ and an equilibrium at $x = x^*$.

**Definition 11.** *An orbit $\Gamma$ starting at some $x \in \mathbb{R}^n$ is called **homoclinic** to the equilibrium $x^*$ if $\phi^t x \to x^*$ for $t \to \pm\infty$.*

A homoclinic orbit can be shown to be structurally unstable, which means that small perturbations in the governing equations will lead to non-equivalent phase portraits and thus to bifurcations of the system. Figuratively spoken a homoclinic bifurcation occurs when a limit cycle touches a saddle point in the phase space and thus becomes a homoclinic orbit at the bifurcation point. If the parameter is changed further the homoclinic orbit vanishes and only the saddle is left (Figure 2.7).

For two-dimensional systems the homoclinic bifurcation is characterized by the **Andronov-Leontovich theorem** [53, Ch. 6.2]. It is not stated completely at this point but just one of its implications. Suppose a saddle point $x^*$ has the two real eigenvalues $\lambda_{1,2}(\alpha)$. One can define the quantity $\sigma(\alpha) = \lambda_1(\alpha) + \lambda_2(\alpha)$ which corresponds to the trace of the Jacobian evaluated at the saddle. If the homoclinic bifurcation occurs at a critical parameter value of $\alpha_0 = 0$, the associated limit cycle is stable if $\sigma(0) < 0$ and unstable if $\sigma(0) > 0$ (Figure 2.7).

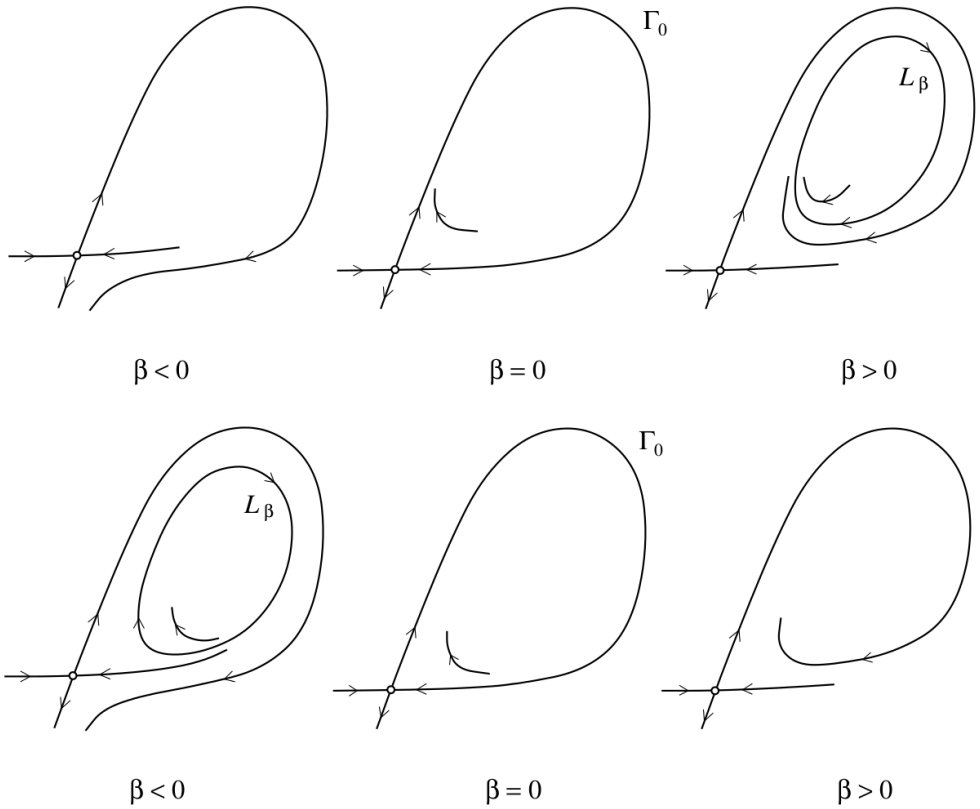


**Figure 2.7:** Phase portraits of a planar system which features a bifurcation of a homoclinic orbit $\Gamma_0$ at a critical parameter $\beta = 0$. For the case $\sigma(0) < 0$ a stable limit cycle appears for $\beta > 0$ (top), for $\sigma(0) > 0$ the situation is reversed and an unstable limit cycle appears (bottom). Taken from [53, Ch. 6.2].

### Two-parameter Bifurcations

The following section is devoted to the introduction of some relevant codimension 2 bifurcations. These can only be observed in systems with a minimum of two free parameters:

$$\dot{x} = f(x,\alpha) \qquad , x \in \mathbb{R}^n,\ \alpha = (\alpha_1,\alpha_2) \in \mathbb{R}^2 \tag{2.25}$$

Suppose the system exhibits a local bifurcation (fold or AH) of some equilibrium $x^*$ at some critical $\alpha = \alpha^* = (\alpha_1^*,\alpha_2^*)$. Generically the equilibrium condition (2.8) together with the respective bifurcation condition, namely the non-hyperbolicity conditions (2.16) or (2.21), implicitly define a one-dimensional **bifurcation curve** in the $(\alpha_1,\alpha_2)$-plane.

If one moves along such a bifurcation curve in the parameter space, additional bifurcation conditions might be fulfilled at some point. If one follows for instance a fold bifurcation curve in a one-dimensional system, the non-degeneracy condition, $\partial_x^2 f(x = x^*, \alpha = \alpha^*) \neq 0$ (Equation (2.17)) might be violated at some particular point. At such a point a so-called **cusp** bifurcation occurs. As this condition involves higher-order derivatives of $f$, it cannot be detected by looking only at the eigenvalues of the Jacobian. The Cusp bifurcation can be observed in systems with $n \geq 1$.

If one follows a fold curve in a two-dimensional system, the second eigenvalue of the non-hyperbolic equilibrium could become zero, $\lambda_2 = 0$. This is referred to as a **Bogdanov-Takens** (BT) or **double zero** bifurcation and is observable in systems with $n \geq 2$. Alternatively one might of course also follow a Andronov-Hopf bifurcation with $\lambda_{1,2} = \pm i\omega$ and would observe a Bogdanov-Takens bifurcation at the point where $\omega = 0$. A generic case of the BT bifurcation is explained in more detail in Figure 2.8.

An Andronov-Hopf bifurcation curve is described by a non-hyperbolic equilibrium with $\lambda_{1,2} = \pm i\omega$ and the non-degeneracy condition $l_1(\alpha^*) \neq 0$, equation (2.22). If one moves along the curve and the latter condition is violated, a **Bautin** or **generalized Hopf** (GH) bifurcation occurs. It corresponds to the change from a sub- to a super-critical Andronov-Hopf bifurcation. Like the cusp bifurcation it cannot be detected by only looking at the eigenvalues of the Jacobian since the computation of $l_1$ involves higher order derivatives of $f$. The GH bifurcation is explained in more detail in Figure 2.9.

In three-dimensional systems one might, by following either a fold or Andronov-Hopf bifurcation curve reach a point at which there is one eigenvalue zero, $\lambda_1 = 0$, and the two others cross the imaginary axis, $\lambda_{2,3} = \pm i\omega$. At such a point a **Gavrilov-Guckenheimer** or **Fold-Hopf** or **zero-pair** bifurcation occurs.

In systems with a minimal dimension of four, one might, by following an Andronov-Hopf bifurcation curve, reach a point at which it touches another Andronov-Hopf curve and thus

simultaneously two pairs of eigenvalues lie on the imaginary axis, $\lambda_{1,2} = \pm i\omega_0$ and $\lambda_{3,4} = \pm i\omega_1$. The corresponding codimension two bifurcation at this point is called **Hopf-Hopf** or **two-pair** bifurcation.

The above-mentioned five different bifurcation types are all possible local codimension-two bifurcations of generic continuous-time dynamical systems. For this thesis only the Bogdanov-Takens (Figure 2.8) and Bautin (Figure 2.9) bifurcations are of relevance.

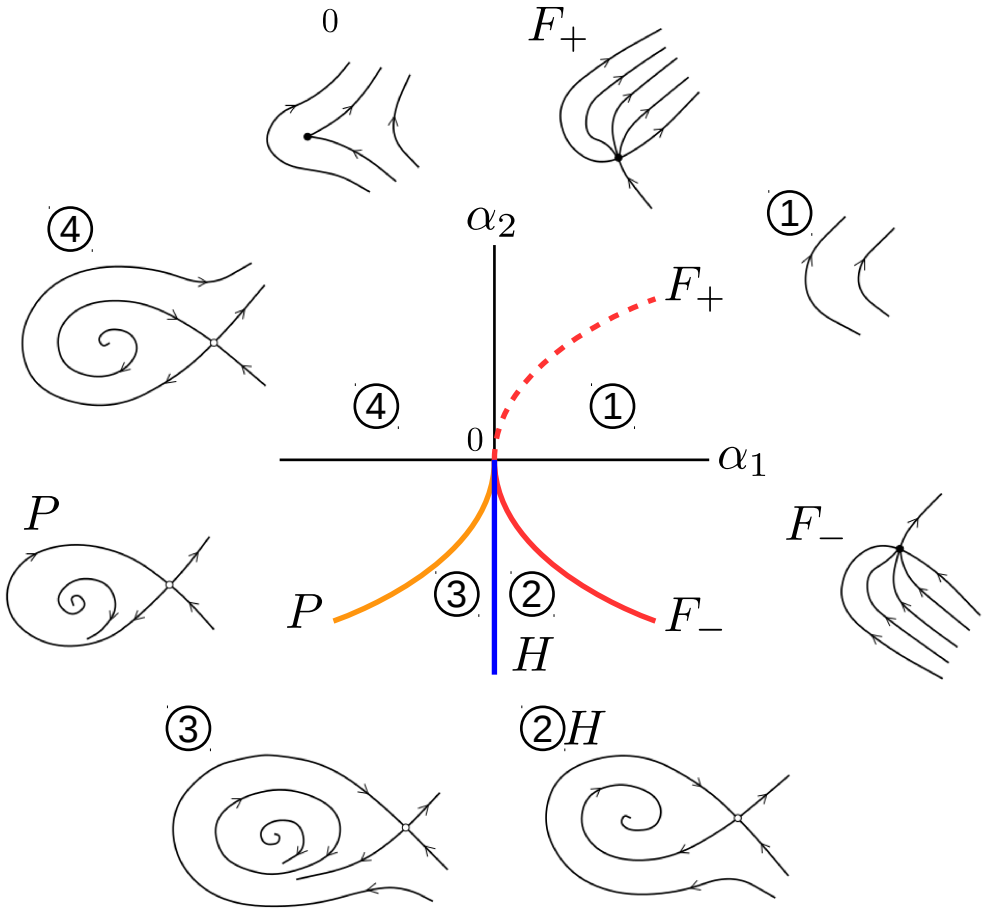


**Figure 2.8:** Bifurcation diagram of a generic **Bogdanov-Takens bifurcation** at the point $(\alpha_1, \alpha_2) = (0,0)$. The bifurcation point lies at the intersection of a fold bifurcation curve ($F_\pm$), an AH curve ($H$) and a homoclinic bifurcation curve ($P$). Crossing $F_-$ from region 1 to region 2 a fold bifurcation of a saddle and a stable node occurs. The stable node becomes unstable in a super-critical AH bifurcation when crossing $H$ from 2 to 3. The stable limit cycle in region 3 becomes homoclinic to the saddle at $P$ and vanishes in region 4. The remaining unstable node coalesces with the saddle in another fold bifurcation when crossing $F_+$. At the bifurcation point (0) the equilibrium is still stable but non-hyperbolic, such that the speed of convergence is slower than exponential. The reversed case in which the limit cycle in region 3 is unstable is also possible. Modified from [53, Ch. 8.4].

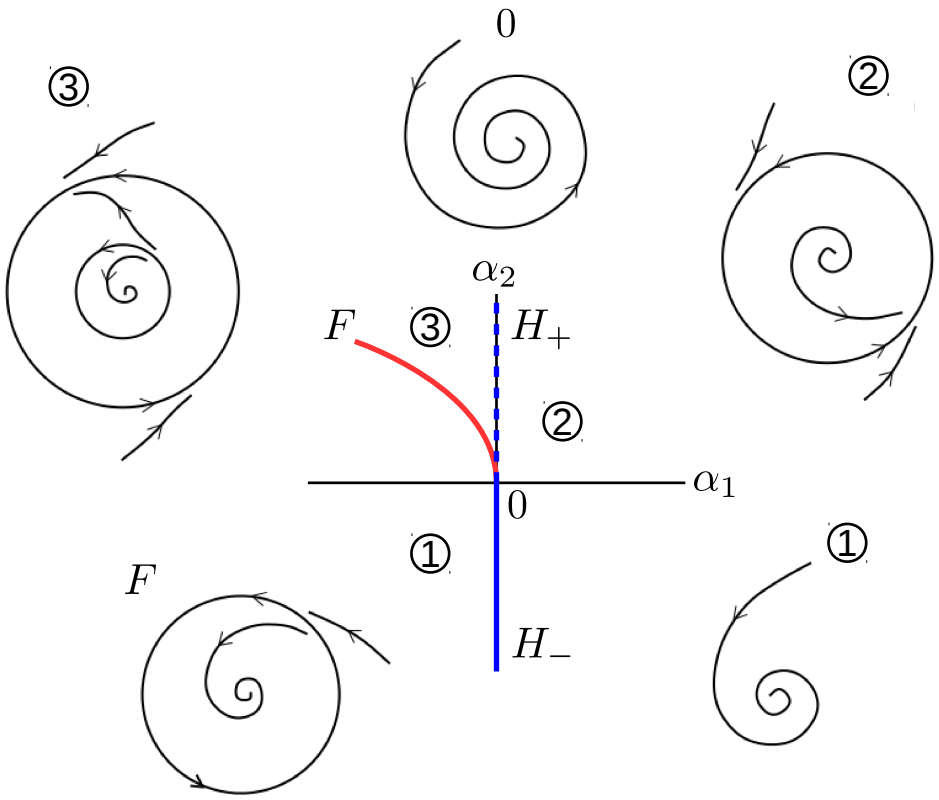


**Figure 2.9:** Bifurcation diagram of a generic **Bautin bifurcation** at the point $(\alpha_1, \alpha_2) = (0,0)$. The bifurcation point lies at the intersection of a super-critical AH curve ($H_-$), a sub-critical AH curve ($H_+$) and a curve of fold bifurcation of cycles ($F$). Region 1 features a stable node which becomes unstable in a super-critical AH bifurcation when crossing $H_-$ to region 2. When crossing $H_+$ from region 2 to 3 the node becomes stable again via a sub-critical AH bifurcation. As the curve $F$ is approached the two limit cycles come closer and ultimately vanish at $F$ in a fold bifurcation of cycles such that only the stable node is left. The reversed situation in which the outer limit cycle is unstable is also possible. Modified from [53, Ch. 8.3].

### 2.1.6 Topology of managed dynamical systems with desired states

In addition to the study of the asymptotic behavior of a dynamical system further topological features of its phase space can be of interest. Its partitioning into different **basins of attraction** reveals important information about the asymptotic behavior. In several applications, however, there might also be normative conditions prescribed which render some states of a dynamical system (un)desirable. Such conditions would give another partitioning of the phase space. The topology might further be influenced if some of the parameters which govern the dynamics are variable, for instance through active control or "management" of the system. Such problems are the subject of the mathematical field of **viability theory** which is closely related to optimal control theory [4–6]. The central goal of a viability problem is to identify the **viability kernel** of an environment within a system's state space, which is given by the subset of initial states which remain within this environment under control. The development of algorithms to compute the viability kernel is subject to recent research [12, 87]

Another comprehensive framework for a topological classification of such dynamical systems has recently been presented in [43]. The work by Heitzig et al. is extending viability theory by singling out one flow of the system as the default one, naturally yielding a partition of the state space called **Topology of Sustainable Management**. It has proven to be particularly useful for applications in Earth system science and can be related to the concepts of planetary boundaries and the safe operating space which have been mentioned in section 1.2.

Within this topology framework a **manageable dynamical system with desirable states** is given by the following ingredients (see [43]):

1. A dynamical system with *state space* $X$ and a *default dynamics* represented by *default trajectories* $\tau_x$ for all $x \in X$.
2. A set of *desirable states* $X^+ \subseteq X$ whose complement $X^- = X - X^-$ forms the *undesired region*.
3. A notion of *management options* represented by a family of *admissible trajectories* $M_x$ for each $x \in X$.

The desirable region is also referred to as the *sunny* part and the undesirable as the *dark* part of the state space.

Given these ingredients one can find a partition of the state space by posing questions like whether one can stay in the sunny region forever with or without management and whether some part is reachable from another. The full possible topological partition of a phase space is shown in Figure 2.10 in the form of a decision tree. The denotations of the different state

space regions are metaphors related to the picture of a boat floating or rowed in some waters. Rigorous mathematical definitions of the regions are given in [43].

An interesting feature of the topological partition is the emergence of several **dilemmas** which the managing agent might face. For example, the so-called "lake dilemma" poses the choice between *uninterrupted* desirability (through active management) and *eventual* safety (without the need for management after a certain time).

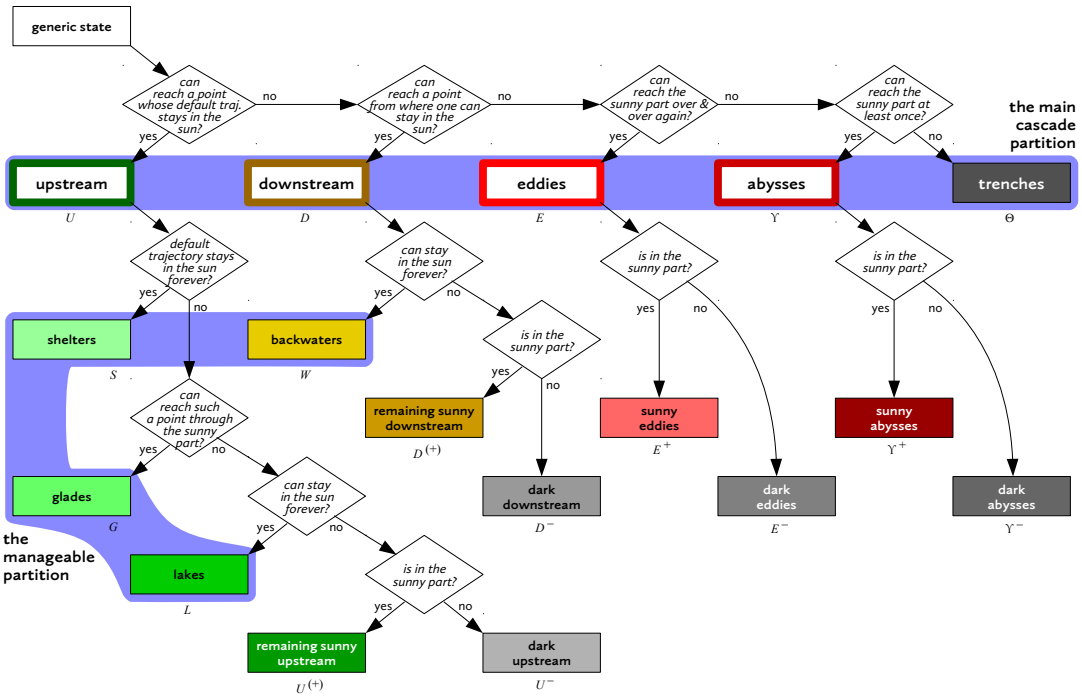


**Figure 2.10:** Decision tree which gives an overview of the topological partition of dynamical systems with desirable states. The so-called **main cascade partition** is divided regarding whether one can ultimately stay in the sunny part forever by default (**upstream** $U$), by management (**downstream** $D$), reach it repeatedly (**eddies** $E$), finitely often (**abyss** $\Upsilon$) or never (**trench** $\Theta$). The **manageable partition** is given by those regions where one can stay in the sunny part forever (with or without managing). Figure taken from [43].

## 2.2 Socio-economic concepts

After having introduced the most important mathematical and physical concepts which are mainly relevant for the model *analysis*, this section is dedicated to the theoretical background of several socio-economic concepts which are relevant for the model *design*. The first section 2.2.1 reviews in a nutshell the most important aspects of neoclassical growth theory in form of the Solow-Swan model. The following section 2.2.2 is dedicated to the microeconomic general equilibrium theory which describes the allocation of production factors between different goods or sectors. In the last section 2.2.3 some concepts concerning population dynamics are introduced.

### 2.2.1 The Solow-Swan model of economic growth

The original *Solow-Swan model* describes economic growth, reflected by the increase in economic output per capita, due to the accumulation of physical capital (such as tools, buildings, infrastructure, etc.). Capital as an economic entity has several properties of which the first is that it is *productive*. This makes it a **factor of production** of an economy [103, Ch. 3]. Furthermore capital is *produced* which makes it different from natural resources or land area which are also factors of production. The property of being *limited in use* distinguishes it from factors like ideas and technological advances. Finally physical capital *depreciates* with usage and time. A growth model which describes the evolution of capital should incorporate these features.

The economic output $Y$ of a whole economy in this type of macroeconomic model is described by a **macroscopic production function** $F$:

$$Y = F(L,K) \tag{2.26}$$

where $L > 0$ and $K > 0$ denote the factors of production labor and capital, respectively.[1] In the Solow-Swan model, the production function $F$ is assumed to fulfill several properties [104]. Firstly, it features **constant returns to scale** which means, mathematically, it is homogeneous of degree one:

$$F(\alpha L, \alpha K) = \alpha F(L,K) \qquad \forall\ \alpha > 0 \tag{2.27}$$

Furthermore $F$ has **positive** but **diminishing marginal returns** which can be expressed via its

1 There are more factors of production than labor and capital such as resources and technology. These are, however, not treated in the classical Solow-Swan model and thus not considered at this point.

derivatives:

$$\frac{\partial F}{\partial X} > 0 \qquad \forall\, X \tag{2.28}$$

$$\frac{\partial^2 F}{\partial X^2} < 0 \qquad \forall\, X \tag{2.29}$$

for $X \in \{L,K\}$. Finally $F$ fulfills the **Inada conditions**:

$$\lim_{X \to 0} \frac{\partial F}{\partial X} = \infty \tag{2.30}$$

$$\lim_{X \to \infty} \frac{\partial F}{\partial X} = 0 \tag{2.31}$$

for $X \in \{L,K\}$.

An often used function which fulfills all of the above conditions is the **Cobb-Douglas** function [103, Ch. 3]:

$$Y = F_{\text{CD}}(L,K) = aL^{1-\kappa}K^{\kappa} \tag{2.32}$$

where $a > 0$ is a constant referred to as **total factor productivity** of the economy. The constant $0 < \kappa < 1$, also called **elasticity**, corresponds to the capital's share of the total income, given that in a perfectly competitive economy the marginal returns $p_K = \frac{\partial F}{\partial K}$ for the factors will be paid (as capital rent to the owners of capital and as wages to workers):

$$\frac{p_K K}{Y} = \frac{\frac{\partial F}{\partial K} K}{Y} = \frac{\kappa a L^{1-\kappa} K^{\kappa-1} K}{a L^{1-\kappa} K^{\kappa}} = \kappa \tag{2.33}$$

So far it was described how capital contributes to the *generation* of the economical production $Y$. To close the loop one needs also to describe how it is produced and how it depreciates. The economy in the Solow-Swan model is a closed system without a government as actor. Thus the economic output is *spent* completely in the forms of **consumption** $C$ and **investments** $I$ (or **savings**):

$$Y = C + I \tag{2.34}$$

While consumption $C$ does not alter the capital stock, investments $I$ do so. Assuming a constant **savings ratio** $0 \leq s \leq 1$ one gets:

$$I = sY \tag{2.35}$$

While investments increase the capital stock $K$, it is also decreased due to depreciation $D$. For simplicity one can assume that this happens at a constant rate $\delta$. Thus the rate of change of $K$ is given as follows:

$$\dot{K} = I - D = sY - \delta K = saL^{1-\kappa}K^{\kappa} - \delta K \tag{2.36}$$

From a mathematical perspective equation (2.36) defines a one-dimensional dynamical system (Figure 2.11). The equilibrium states are obtained by setting $\dot{K} = 0$:

$$K_0^* = 0 \tag{2.37}$$

$$K_1^* = \left(\frac{sa}{\delta}\right)^{\frac{1}{1-\kappa}} L \tag{2.38}$$

$K_0^*$ is always unstable as $\left.\frac{\partial \dot{K}}{\partial K}\right|_{K=0} \propto \left.\frac{\partial Y}{\partial K}\right|_{K=0} = +\infty$. $K_2^*$ is thus necessarily a stable equilibrium which is confirmed by considering the derivative $\left.\frac{\partial \dot{K}}{\partial K}\right|_{K=K_1^*} = \delta(\kappa - 1) < 0$ as $\kappa < 1$ and $\delta > 0$.

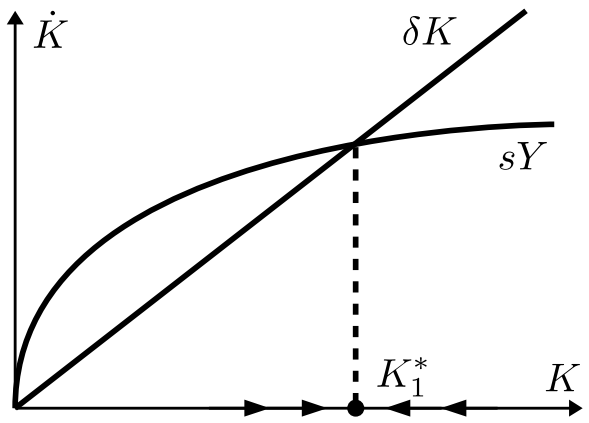


**Figure 2.11:** The Solow-Swan model as one-dimensional dynamical system which describes the evolution of the physical capital stock $K$. Capital increases due to investments $I = sY \propto K^{\kappa}$ and decreases due to depreciation $D = \delta K$. There is a stable equilibrium at $K_1^*$.

Thus the economy will always converge to the equilibrium state $K_1^*$ at which the per-worker income $y^*$ amounts to:

$$y^* = \frac{Y^*}{L} = a^{\frac{\kappa}{1-\kappa}} \left(\frac{s}{\delta}\right)^{\frac{1}{1-\kappa}} \tag{2.39}$$

While savings ratio $s$ and productivity $a$ increase the equilibrium per-worker income, deprecia-

tion $\delta$ decreases it. For consumers more relevant than the average per-worker income $y^*$ is the average per-worker consumption $c^* = (1-s)y^*$. It can be shown that $c^*$ is maximized with respect to the savings ratio by choosing $s = \kappa$. Figuratively spoken this means that the capital's share of income $\kappa$ is invested while the labor's share of income $(1-\kappa)$ is consumed.

So far a constant labor force $L$ was assumed. The number of workers is, however, dependent on the size of the population $P$ which is not constant over time. The classical Solow-Swan model simply assumes exponential population growth. This and other simple models for the dynamics of the population that are more realistic on longer timescales are presented in sections 2.2.3 and 3.3.

Moreover, other factors like the availability and use of resources will in reality affect the output of an economy. A very simple approach to also incorporate resource and land availability into the Solow-Swan model is discussed in [85, Ch. 1]. A more elaborate extension to neoclassical growth theory which accounts for resource and energy use is presented in [8]. These findings have also been incorporated in the model design for this thesis which is discussed in more detail in chapter 3.

### 2.2.2 General equilibrium theory

If an economy is composed of different **sectors of production** the question arises how the available factors of production which are used by all sectors (labor, capital, etc.) are *allocated* amongst them. The sectors might feature different productivities or depend on further factors of production which are not shared with other sectors. Assume for instance the total economic output $Y$ is composed of the outputs of two independent sectors A and B:

$$Y = Y_A + Y_B \tag{2.40}$$

where $Y_A$ and $Y_B$ are given by suitable production functions, for example of Cobb-Douglas form as given by equation (2.32). Any allocation of labor force $L$ and capital $K$ to the sectors A and B needs to fulfill the following constraints:

$$\begin{aligned} L &= L_A + L_B \\ K &= K_A + K_B \end{aligned} \tag{2.41}$$

In *General equilibrium theory* it is assumed that the allocation happens via perfect factor markets which form equilibrium prices for the factors (e.g. wages for labor and rents for capital) [71]. As argued in the previous section, in a perfectly competitive economy these prices equal the marginal returns of the factors of production. These equilibrium conditions can be expressed

as follows:

$$\begin{aligned} \frac{\partial Y_A}{\partial L_A} &= \frac{\partial Y_B}{\partial L_B} \\ \frac{\partial Y_A}{\partial K_A} &= \frac{\partial Y_B}{\partial K_B} \end{aligned} \tag{2.42}$$

Generally, an analytical solution to the equation system (2.42) under the constraints (2.41) might necessitate further assumptions on the elasticities of the factors. Otherwise the solution can be obtained by numerical optimization algorithms. For the model studied in this thesis the sectors refer to different forms of energy which can be used (biomass, fossils, renewables).

### 2.2.3 Demographic models

As already mentioned in section 2.2.1 the evolution of an economy is closely related to the the evolution of the population size. For instance the factor of productivity labor $L$ is mainly determined by the population and in turn the consumption $C$ has to be shared among all people.

A first attempt to account for population dynamics in economic growth models is to extend the Solow-Swan model by an exogenous growth rate $\gamma$ of labor force $L$:

$$\dot{L} = \gamma L \tag{2.43}$$

For the per-worker capital $k = K/L$ this implies the following dynamics:

$$\dot{k} = \frac{\dot{K}L - K\dot{L}}{L^2} = \frac{sY - \delta K}{L} - \frac{\gamma K}{L} = sy - (\delta + \gamma)k \tag{2.44}$$

where equations (2.36) for the capital accumulation and (2.43) for the population dynamics have been used. Equation (2.44) makes clear that the population growth rate $\gamma$ has the same effect for the per-capita quantities $k$ (and thus $y$) as the depreciation rate $\delta$. Thus the dynamics of the per-capita quantities does not change qualitatively compared to the model without population growth, meaning that these will reach constant equilibrium values $k^*$ and $y^*$. The absolute quantities $K$ and $Y$ will, however, grow with the same rate $\gamma$ as the population does.

While a constant exogenous growth rate might be empirically a reasonable assumption for relatively short timescales of several years, it evidently does not hold true for longer timescales of several hundreds of years. Hence it is desirable to determine the reproduction rate of the population endogenously. Indirectly this has been done by the British economist Thomas R. Malthus in the late eighteenth century [65]. He argued that reproduction of humans was mainly limited by the availability of resources (such as land in agricultural societies). If there

is an abundance of resources the population will grow, leading, however, to less available resources (or land) per person. This will in turn prevent further population growth such that ultimately constant levels of population and resources per capita would be reached. Moreover Malthus reasoned that only a deliberate reduction of the offspring would effectuate higher per-capita incomes.

Malthus' argument can be formalized into a mathematical model for the dynamics of the population $P$. Most generally $\dot{P}$ is given as follows:

$$\dot{P} = P(f_{\text{fert}} - f_{\text{mort}}) \tag{2.45}$$

where $f_{\text{fert}}$ and $f_{\text{mort}}$ are functions describing how the fertility and mortality of the people depend on some relevant factors, respectively. Malthus argues that fertility will increase proportional to the available resources (or consumption $C$) per capita. Mortality is simply assumed to have a constant baseline value, thus:

$$\dot{P} = P\left(p\frac{C}{P} - q\right) \tag{2.46}$$

where $p$ and $q$ are parameters. It can easily be seen from equation (2.46) that at equilibrium either the population is zero $P_0^* = 0$ or the per-capita consumption has a constant value of $\left(\frac{C}{P}\right)^* = q/p$. To take up the formulation from above, the consumption can be written as a certain fraction $1-s$ of the total economic output $Y$ [1], which can be described by some production function like 2.32. This leads to the following differential equation for $P$:

$$\dot{P} = P\left(p\frac{(1-s)Y}{P} - q\right) \tag{2.47}$$

$$= p(1-s)Y - qP \tag{2.48}$$

$$= \widetilde{p}P^{1-\kappa}K^{\kappa} - qP \tag{2.49}$$

where $\widetilde{p} = (1-s)ap$ and labor force $L$ is assumed to be proportional to population size $P$. For a constant capital stock $K$ the population dynamics given by equation (2.49) is qualitatively the same as that of the capital dynamics in the Solow model for constant labor force $L$ (Equation (2.36)). As long as there is no accumulation of capital population will remain at a constant equilibrium value.

1 The fraction $1-s$ might be close to one in the agricultural societies described by Malthus, meaning that all produced goods are more or less directly consumed. In other words, the resources in these societies are so scarce that saving is not possible, giving a savings ratio $s \approx 0$.

Even though the Malthus model might be an aid in explaining the long period of constant population levels throughout human history, it definitely broke down with the ascent of the industrial revolution which was accompanied by an acceleration in population growth and simultaneously increasing levels of wellbeing reflected by per-capita incomes [103, Ch. 4]. Moreover, with higher income levels, both fertility and mortality are observed to decrease which is referred to as the **fertility** and **mortality transition**, respectively [103, Ch. 4]. These findings are combined in the empirical **demographic transition** model (Figure 2.12). The explanation of the changes in fertility and mortality are subtle and include many explanatory factors such as nutrition, education (of women) or health care. Therefore low-dimensional models might fail in fully capturing the behavior as predicted by the demographic transition model. In chapter 3.3 an attempt is made to capture the basic effects in a model that uses wellbeing as the sole proxy for for all these explanatory factors in order to keep the system's dimension low.

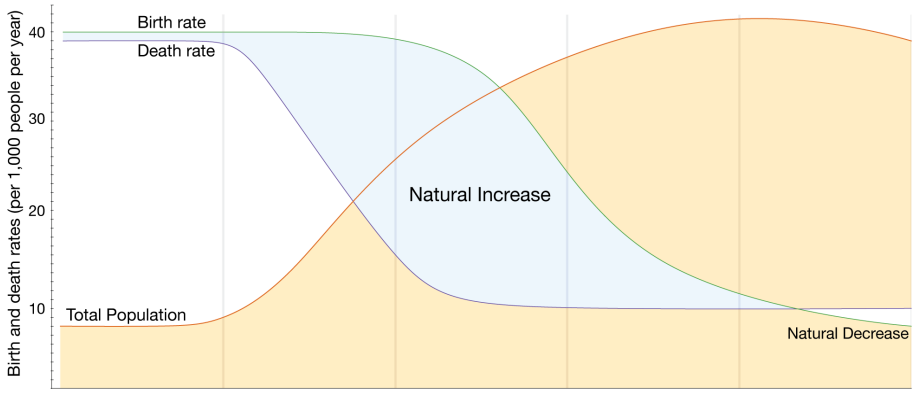


| | Stage 1 | Stage 2 | Stage 3 | Stage 4 | Stage 5 |
|---|---|---|---|---|---|
| Birth rate | *High* | *High* | *Falling* | *Low* | *Very low* |
| Death rate | *High* | *Falls rapidly* | *Falls more slowly* | *Low* | *Low* |
| Natural increase | *Stable or slow increase* | *Very rapid increase* | *Increase slows down* | *Stable or slow increase* | *Stable or slow decrease* |

**Figure 2.12:** Overview of the demographic transition model which describes the evolution of fertility and mortality in dependence of the development level of a country or geographical region. The occurrence and duration of the various stages might differ very much, depending on manifold socio-economic factors. Figure taken from [75].

## 2.3 Concepts from Earth sciences

This section is devoted to the introduction of a concept from Earth science which is relevant for the model *design*, the **global carbon cycle**. It is the main component of the model to reflect the natural dynamics of the Earth system.

### 2.3.1 Global carbon cycle

The global carbon cycle is a biogeochemical cycle which is crucial to the functioning of the Earth system and amongst other factors enables life on the planet. Carbon is present in many different forms and components of the Earth such as the atmosphere, hydrosphere, biosphere or geosphere. Typically the carbon of different spheres is categorized into **stocks** (or **pools**) which contain those carbon amounts which play approximately the same role in the cycle. How fine the distinction of different stocks is, depends on the question posed and timescale of interest. The same is true for the carbon **fluxes** which are the flows of carbon between different stocks. A very common schematic overview of the carbon cycle of the Earth is shown in Figure 2.13.

All carbon in the atmosphere is typically considered as one stock because the mixing between different layers and latitudes happens comparably fast (on the timescale of days). As the Earth is mainly covered with water there is a significant exchange of carbon between the atmosphere and the oceans via the process of diffusion. The oceanic carbon can be subdivided into organic and inorganic carbon of which the latter is the dominant amount. It can further be distinguished between the carbon in the surface layer of the ocean and the carbon in the intermediate and deep sea. There is a significant exchange between the different layers which happens on comparably long timescales. Thus the surface layer carbon stock is the only which interacts with other (non-oceanic) components of the carbon cycle. The next important carbon stock is given by the terrestrial systems which constitute of living vegetation and soils. From both vegetation and soils there is a carbon flux into the atmosphere due to the process of respiration. Photosynthesis of plants in turn constitutes a flow from the atmosphere to the terrestrial systems which is of comparable size under pre-industrial conditions.

There are other carbon stocks like the permafrost soils or fossil fuels which under natural conditions only play a role on very long timescales. Due to the extraction of fossil fuels through humans since the onset of the industrial era, this stock became connected to other parts of the carbon cycle even for short timescales. Since then it has been decreased considerably, thereby exerting a significant perturbation to the natural operating state of the carbon cycle. The extracted carbon from fossil fuels is initially emitted completely into the atmosphere so that the atmospheric carbon content rose considerably over the past centuries and decades. This is the main driver of the anthropogenic greenhouse effect which leads to climate change. However, only the airborne fraction of about 60 % of the emitted carbon stays in the atmosphere while

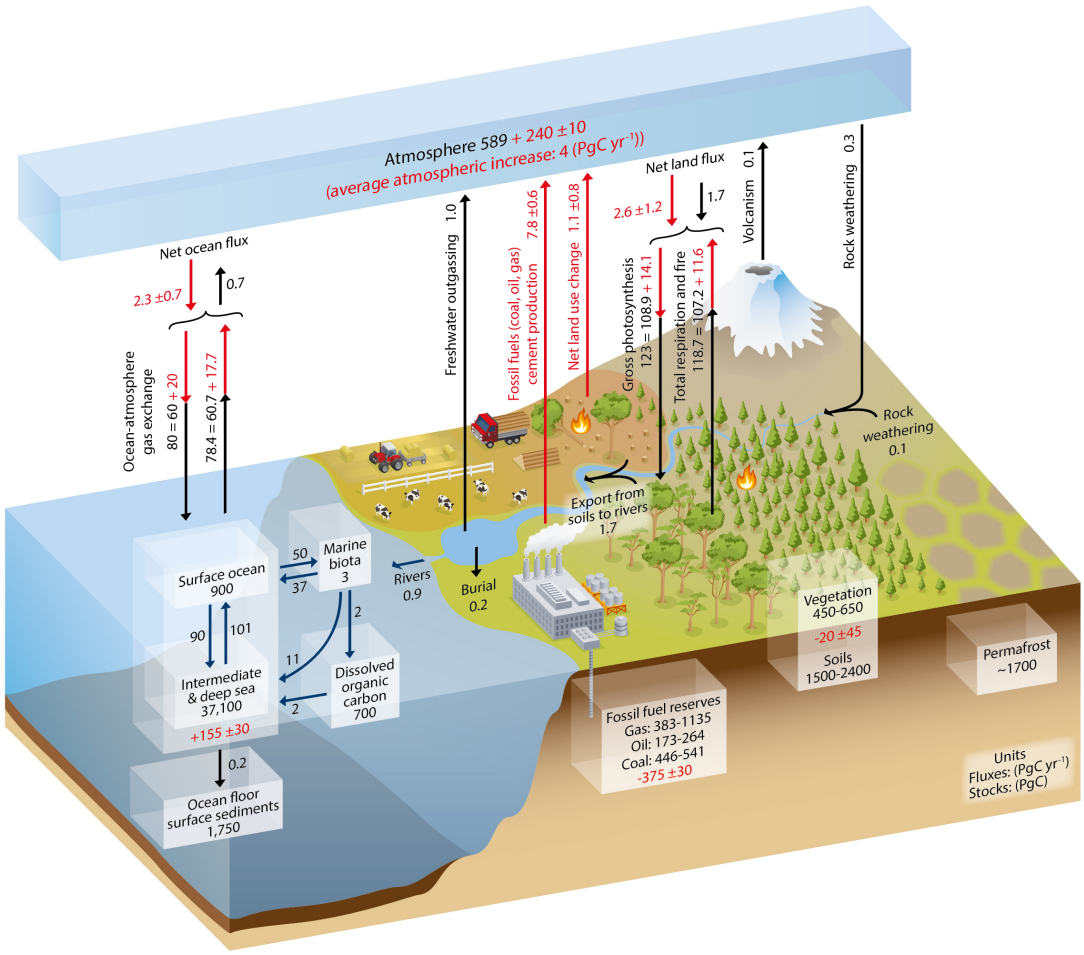


**Figure 2.13:** Schematic overview of the global carbon cycle. Atmosphere, oceans and terrestrial systems together with the processes of photosynthesis, respiration and diffusion are the most important features of the natural (pre-industrial) operating state (black numbers). The combustion of fossil fuels and land use change through humans constitute a significant perturbation to this state, thereby leading to undesirable effects like climate change and ocean acidification (red numbers). 1 PgC = 1 GtC. Figure taken from [17].

the remaining amount is taken up by the maritime and terrestrial systems to a comparable size [30]. Thus due to the diffusion process the oceanic carbon considerably increased due to humans. Also the terrestrial systems serve as a carbon sink as the efficiency of photosynthesis increases with atmospheric carbon content. This effect is referred to as carbon fertilization. It is counteracted by the agricultural activities of humans which are subsumed as net land use change and also constitute a substantial perturbation to the natural operating mode of the carbon cycle.

The situation becomes even more involved if the feedbacks between climate change and the carbon cycle are accounted for. This is due to the facts that the processes of photosynthesis, respiration and diffusion are dependent on the surface temperature [58]. Fully understanding and quantifying these feedback mechanisms is still subject to research in climate science [21, 30, 56].

Finally there are several carbon fluxes which are of negligible size such as freshwater outgasing, rock weathering, rivers or volcanism. Such irregular events as extreme volcano eruptions might, however, be of importance when interested in short timescales.

# CHAPTER 3

## Model description

This chapter introduces all details on the model copan:GLOBAL (c:G) which are relevant for the analyses performed within the scope of this thesis. The first section gives an overview of the **complete seven-dimensional model**. The structure of the model and the general functional forms describing the processes have been developed prior to this thesis within the *copan* project as described in an internal report available from PIK [44].

Part of the present work was to identify and analyze in depth a number of meaningful subsets of the variables and processes which correspond to self-contained submodels representing the dynamics of the Earth system during a real or fictitious period of its history. Thus the following sections are dedicated to the detailed description of **lower-dimensional submodels** of c:G with explicitly stating the governing equations. Additional assumptions on the scenarios described by these lead to a reduction in complexity, dimension and number of parameters of the model.

The final section of this chapter introduces a **dimensionless formulation** of the model equations which will be used for simulations and the presentation of the results.

### 3.1 Overview of the complete model (c:G)

The c:G model aims at describing the dynamics of globally aggregated (extensive) or averaged (intensive) key quantities of the Earth system on centennial to millennial timescales. It tries to incorporate the essential processes which determine the dynamics of the Earth system on a global scale. Several existing models have been used as a basis or source of inspiration for the construction of the complete c:G model. A schematic overview of its structure is given in Figure 3.1.

The left part corresponds to the **natural (or climatic) subsystem** of the Earth which is represented via the main parts of the global carbon cycle introduced in section 2.3.1. The state

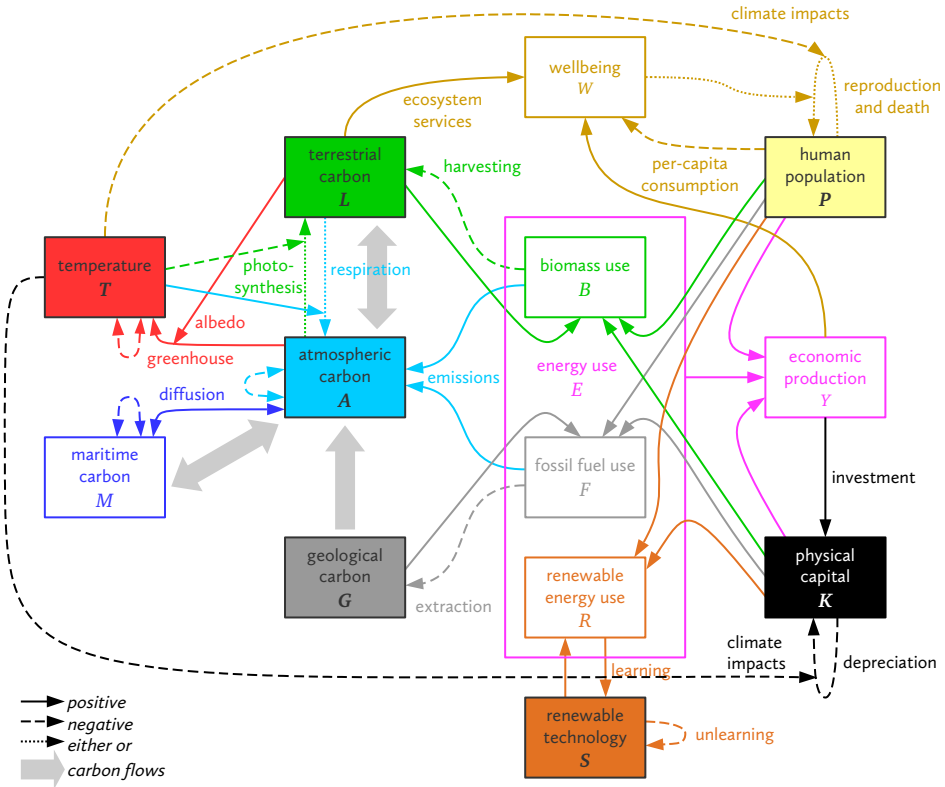


**Figure 3.1:** Overview of the complete copan:GLOBAL model with seven state variables (colored boxes) and several derived variables (white boxes). The arrows represent the coupling processes between the variables. The left part corresponds to the natural subsystem of the Earth (ecosphere) while the right part represents socio-economic entities (anthroposphere). Diagram adapted from [44].

of the natural subsystem is given by the *state variables* terrestrial carbon stock $L$, atmospheric carbon stock $A$, geological carbon stock $G$ (all measured in gigatons carbon, GtC) and global mean surface temperature $T$. The maritime carbon stock $M$ is a *derived variable* since it is assumed that the total available carbon stock $C^*$ is constant over time.

The arrows between the boxes indicate the several *processes* by which the variables interact. Carbon from the atmosphere can be accumulated in the terrestrial stock via photosynthesis of plants whose efficiency is dependent on the temperature. The counter-acting process is the temperature-dependent respiration. Similarly carbon is exchanged between the atmosphere and the oceans via the process of diffusion. There is no direct process between the geological and the other carbon stocks as the generation of fossil fuels from terrestrial carbon happens on

time scales much longer than those of interest. This means that the geological stock cannot increase with time in the model and must thus converge to either zero or a positive value.

The mean surface temperature of the Earth is connected to the atmospheric carbon stock via the greenhouse effect. This in turn is additionally affected by the albedo of the Earth surface which can be calculated from the land carbon stock (forests are darker than desert).

The right part of Figure 3.1 shows the variables and processes of the **socio-economic part** of the Earth system with humans. The economic activity of the humans is basically given by a macroeconomic growth model as described in section 2.2.1. The total economic output $Y$ is derived from the production factors labor (i.e. human population $P$), physical capital $K$ and resources (i.e. total energy use $E$). This total output in turn is partly consumed by the humans and partly reinvested into the physical capital stock. How exactly the production factors are allocated is determined by an underlying general equilibrium model (see section 2.2.2) that is designed in a way that leads to relatively simple functional relationships between the variables.

The use of energy by humans is supposed to be the central coupling mechanism between the natural and the human system. There are three forms of energy flows: the biomass extraction flow $B$ (including agricultural food and biofuel production), the fossil fuel extraction flow $F$ and the renewable energy flow $R$ which are all derived from other variables. Each of these is directly linked to a stock variable which determines the availability of the respective form (land carbon $L$ for biomass, geological carbon $G$ for fossil fuels and renewable technology knowledge stock $S$ for renewables). The energy forms differ qualitatively regarding their influence on other variables. Both biomass and fossil fuel use cause emissions of carbon into the atmosphere while renewable energy does not. Biomass is harvested from the terrestrial carbon stock which can be seen as a renewable resource. The fossil fuels in contrast are extracted from the geological stock which is not renewable on the timescales the model aims to describe. The renewable energy use is fundamentally different from the other in the sense that the related stock variable $S$ increases with its use instead of being decreased like a resource. This “learning-by-doing” mechanism is counter-acted by a natural unlearning rate.

The population dynamics constitute another important element of the model. They are given by a birth rate which has a certain dependence on the wellbeing $W$ of the population and a death rate which is sensitive to wellbeing and competition for space. The wellbeing is composed of per-capita consumption and ecosystem services. The dynamics of the physical capital stock are governed by the processes of investment and depreciation.

Finally the c:G model accounts for climate impacts mediated by rising global mean temperatures. These are assumed to affect the population dynamics (increased death rate) and the physical capital stock (increased depreciation) and thereby introduce another feedback loop between the natural and the socio-economic subsystems.

## 3.2 Planet without humans (c:G:LAT, c:G:LA, c:G:LT, c:G:L)

As a first scenario which can be described by a submodel of c:G we consider a planet without human or negligible human impact. This is supposed to reflect the natural dynamics of the Earth system in Holocene epoch which started some 11700 years ago after the last glacial, however, excluding the "human factor" that became important shortly after that point due to the consequences of the neolithic revolution.

Thus the dynamics is reflected by the global carbon cycle component of the complete model. The dynamic state variables are the terrestrial carbon stock $L$, the atmospheric carbon stock $A$ and the global mean temperature $T$. The maritime carbon stock $M$ is derived from the latter two. The geological carbon stock $G$ is not regarded in this context since there are no humans burning fossil fuels. A schematic overview of this three-dimensional submodel which is abbreviated c:G:LAT is shown in Figure 3.2 (left).

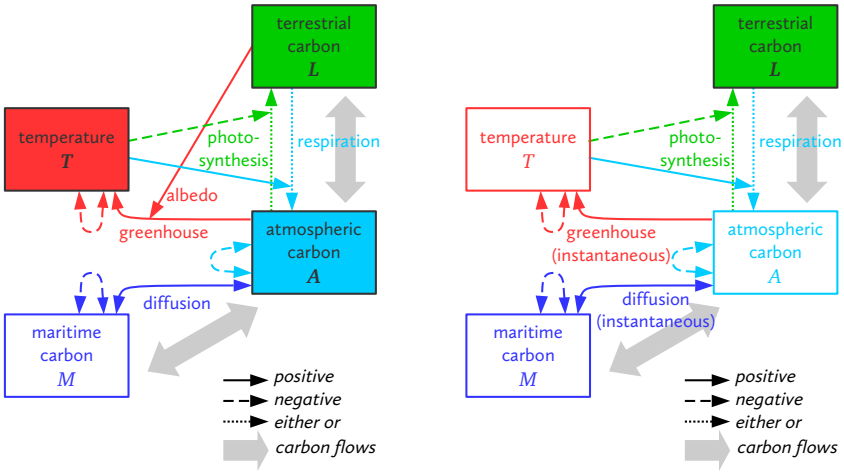


**Figure 3.2:** Left: Schematic overview of the carbon cycle submodel c:G:LAT with the three state variables terrestrial carbon stock $L$, atmospheric carbon stock $A$ and temperature $T$. The maritime carbon stock $M$ follows from a fixed total available carbon stock $C^*_{\mathrm{PI}}$ (without geological carbon stock).
Right: If the greenhouse effect and diffusion are assumed to happen instantaneously, temperature and atmospheric carbon become derived variables. Thus one obtains the one-dimensional submodel c:G:L.

### 3.2.1 Functional forms of the dynamics

Taking into account the processes depicted in the schematic overview the dynamic equations for the carbon stocks $L$ and $A$ may be written in the following general form:

$$\dot{L} = f_{\text{phot}}(L,A,T) - f_{\text{resp}}(L,T) \tag{3.1}$$

$$\dot{A} = -f_{\text{phot}}(L,A,T) + f_{\text{resp}}(L,T) + f_{\text{diff}}(A,M) \tag{3.2}$$

$$\text{where:} \quad M = M(L,A) \tag{3.3}$$

**Photosynthesis** $f_{\text{phot}}$ and **respiration** $f_{\text{resp}}$ are both proportional to the total amount of vegetation, which in turn is assumed to be proportional to $L$. Furthermore the processes are temperature-dependent. Anderies et al. use comparably complicated products of powers and exponential functions to describe this temperature-dependence [2]. However, for the temperature regime of interest one finds that while photosynthesis efficiency is monotonically decreasing with $T$, respiration efficiency monotonically increases with $T$. For simplicity linear dependencies are assumed here.

In addition one needs to account for the effect of **carbon fertilization**. This means an improved photosynthesis efficiency for higher concentrations of atmospheric carbon. The efficiency is concavely increasing with $A$ which is modeled by a square root dependence. Altogether this leads to the following equations:

$$f_{\text{resp}}(L,T) = L(a_0 + a_T T) \tag{3.4}$$

$$f_{\text{phot}}(L,T,A) = L(l_0 - l_T T)\sqrt{A/\Sigma} \tag{3.5}$$

where $a_0$, $a_T$, $l_0$ and $l_T$ are non-negative parameters. $\Sigma$ denotes the available Earth surface area and is introduced to guarantee the correct scaling behavior of the dynamical system, so that if the planet was doubled, also the photosynthesis flow would be doubled. Mathematically spoken the functions are homogeneous of degree one.

The **diffusion** between the atmosphere and the ocean is described equivalently to the Anderies model via a simple linear relationship.

$$f_{\text{diff}}(A,M(L,A)) = \delta\,(M - mA) \tag{3.6}$$

where $\delta$ sets the diffusion rate and $m$ is the dimensionless solubility coefficient which reflects the equilibrium ratio of carbon concentrations between atmosphere and oceans. The maritime carbon stock $M$ is a derived variable given the constant total pre-industrial available carbon

stock $C^*_{\mathrm{PI}}$:

$$M = C^*_{\mathrm{PI}} - L - A \tag{3.7}$$

The dynamic equation for the global mean temperature $T$ can be written in the following general form:

$$\dot{T} = f_{\mathrm{greenh}}(A, T, \Omega(L)) \tag{3.8}$$

where $\Omega$ denotes the albedo of the planet. It is an intensive quantity which is assumed to decrease linearly with the vegetation cover:

$$\Omega(L) = \Omega_0 - \frac{\omega_L}{\Sigma} L \tag{3.9}$$

The greenhouse effect is assumed to be linearly increasing with the excess of atmospheric carbon concentration and decreasing with albedo due to reflection. This can be expressed in the following explicit equation:

$$\begin{aligned} f_{\mathrm{greenh}}(A, T, \Omega(L)) &= g\left(\frac{1}{\Sigma} A - T - \Omega\right) \\ &= g\left(\frac{1}{\Sigma} A - T + \frac{\omega_L}{\Sigma} L - \Omega_0\right) \end{aligned} \tag{3.10}$$

where $g$ denotes a rate which sets the timescale of the process. For convenience $T$ is measured on a non-linear scale in units of $\mathrm{GtC\,km^{-2}}$.[1]

1 The unit can be interpreted as "carbon per area equivalent degrees". I. e. $T = x\,\mathrm{GtC\,km^{-2}}$ is the thermodynamic equilibrium temperature of an atmosphere with a carbon concentration of $x\,\mathrm{GtC\,km^{-2}}$ at zero albedo.

Putting the functional forms for the several processes into the dynamic equations for the state variables leads to the following system of differential equations:

**c:G:LAT**

$$\dot{L} = L\left((l_0 - l_T T)\sqrt{A/\Sigma} - (a_0 + a_T T)\right) \tag{3.11}$$

$$\dot{A} = -\dot{L} + \delta\,(M - mA) \tag{3.12}$$

$$\dot{T} = g\left(\frac{1}{\Sigma}A - T + \frac{\omega_L}{\Sigma}L - \Omega_0\right) \tag{3.13}$$

where: $$M = C^*_{\mathrm{PI}} - L - A \tag{3.14}$$

### 3.2.2 Overview of variables and parameters

The model has several free parameters which need to be set for quantitative calculations and simulations. These are shown together with all state and derived variables in Table 3.1.

**Table 3.1:** Overview of the variables and free parameters of the c:G:LAT model which describes the essential dynamics of the natural subsystem of the Earth via the global carbon cycle.

| variable | unit | range | description |
|---|---|---|---|
| $L$ | GtC | $0 \le L \le C^*$ | terrestrial carbon stock |
| $A$ | GtC | $0 \le A \le C^*$ | atmospheric carbon stock |
| $T$ | $\mathrm{GtC\,km^{-2}}$ | $0 \le T \le C^*/\Sigma$ | global mean surface temperature |
| $M$ | GtC | $0 \le M \le C^*$ | maritime carbon stock |
| parameter | unit | range | description |
| $\Sigma$ | $\mathrm{km^2}$ | $> 0$ | available Earth surface area |
| $C^*_{\mathrm{PI}}$ | GtC | $> 0$ | total pre-industrial carbon stock |
| $a_0$ | $\mathrm{a^{-1}}$ | $\ge 0$ | respiration baseline coefficient |
| $a_T$ | $\mathrm{km^2\,a^{-1}\,GtC^{-1}}$ | $\ge 0$ | respiration sensitivity to temperature |
| $l_0$ | $\mathrm{km\,a^{-1}\,GtC^{-1/2}}$ | $\ge 0$ | photosynthesis baseline coefficient |
| $l_T$ | $\mathrm{km^3\,a^{-1}\,GtC^{-3/2}}$ | $\ge 0$ | photosynthesis sensitivity to temperature |
| $\delta$ | $\mathrm{a^{-1}}$ | $> 0$ | diffusion rate |
| $m$ | 1 | $> 0$ | solubility coefficient |
| $g$ | $\mathrm{a^{-1}}$ | $> 0$ | speed of greenhouse effect |
| $\Omega_0$ | $\mathrm{GtC\,km^{-2}}$ | $\ge 0$ | albedo at zero vegetation |
| $\omega_L$ | 1 | $\ge 0$ | albedo sensitivity to terrestrial carbon |

### 3.2.3 Dimension reduction and further simplification

Equations (3.11), (3.12) and (3.13) define the three-dimensional submodel of the natural subsystem of the Earth. The dimension of this model can be reduced if one assumes the process

of diffusion or the greenhouse effect to occur instantaneously.

An **instantaneous diffusion** corresponds to the limit $\delta \to +\infty$ in which equation (3.6) can be rewritten as the algebraic identitiy:

$$M = mA \tag{3.15}$$

Plugging this into the mass conservation law $L + A + M = C^*_{\mathrm{PI}}$ gives a fixed relation between the terrestrial and the atmospheric carbon stocks:

$$L = C^*_{\mathrm{PI}} - (1+m)A \qquad \Leftrightarrow \qquad A = \frac{C^*_{\mathrm{PI}} - L}{1+m} \tag{3.16}$$

These relations can be used to either eliminate $L$ or $A$ in the dynamic equations of the model, leading to a two-dimensional model. For example, if one eliminates $A$ in equation (3.11) one gets the two-dimensional system which is abbreviated c:G:LT:

**c:G:LT**

$$\dot{L} = L\left((l_0 - l_T T)\sqrt{\frac{C^*_{\mathrm{PI}} - L}{\Sigma(1+m)}} - (a_0 + a_T T)\right) \tag{3.17}$$

$$\dot{T} = g\left(\frac{C^*_{\mathrm{PI}} - L}{\Sigma(1+m)} - T + \frac{\omega_L}{\Sigma}L - \Omega_0\right) \tag{3.18}$$

Similarly one may assume the **greenhouse effect** to happen **instantaneously** which corresponds to letting $g \to +\infty$. In this case equation (3.10) becomes an algebraic identity:

$$T = \frac{1}{\Sigma}A + \frac{\omega_L}{\Sigma}L - \Omega_0 \tag{3.19}$$

Using this expression for $T$ in equations (3.11) and (3.12) leads to the following two-dimensional system which is abbreviated c:G:LA:

**c:G:LA**

$$\dot{L} = L\left[\left(l_0 - l_T\left(\frac{1}{\Sigma}A + \frac{\omega_L}{\Sigma}L - \Omega_0\right)\right)\sqrt{\frac{1}{\Sigma}A} - \left(a_0 + a_T\left(\frac{1}{\Sigma}A + \frac{\omega_L}{\Sigma}L - \Omega_0\right)\right)\right] \tag{3.20}$$

$$\dot{A} = -\dot{L} + \delta\,(M - mA) \tag{3.21}$$

Another assumption which does not lead to a reduction of the dimension but to a reasonable simplification of the equations is to **neglect the albedo effect** on the greenhouse process by simply setting $\Omega = 0$ in (3.10). In that case the dynamic equation for the temperature becomes:

$$\dot{T} = g\left(\frac{1}{\Sigma}A - T\right) \tag{3.22}$$

For the case of instantaneous greenhouse effect the algebraic identity (3.19) reads as follows:

$$T = \frac{1}{\Sigma}A \tag{3.23}$$

If not stated otherwise, for the rest of this thesis the albedo effect is neglected and thus $\Omega_0$ and $\omega_L$ are set to zero. The legitimation for this approximation is discussed in section 6.2.

The assumptions and simplifications presented above can be combined at will. For example, if all of them hold, the model reduces to the one-dimensional c:G:L model whose structure is shown in Figure 3.2 (right):

**c:G:L**

$$\dot{L} = L\left[\left(l_0 - \frac{l_T(C^*_{\mathrm{PI}} - L)}{\Sigma(1+m)}\right)\sqrt{\frac{C^*_{\mathrm{PI}} - L}{\Sigma(1+m)}} - \left(a_0 + \frac{a_T(C^*_{\mathrm{PI}} - L)}{\Sigma(1+m)}\right)\right] \tag{3.24}$$

It should be emphasized at this point already that depending on the assumptions the asymptotic behavior of the system might change. The positions of the equilibria (if such exist) are, however, not influenced by making a process instantaneous, only their stabilities might be.

Moreover the same simplifications can be made for any of the following more complex submodels, meaning that the dimension of the model can be reduced independently from the socio-economic system.

## 3.3 Hunter-gatherer and agricultural societies (c:G:LATP, c:G:LAP, c:G:LTP, c:G:LP)

The next scenario also accounts for humans interacting with the natural Earth system and thus depicts a **minimal coevolutionary submodel** of the ecosphere and the anthroposhere. For this the c:G:LAT model described in the previous section is extended by a state variable for the human population ($P$) and is thus abbreviated c:G:LATP (see Figure 3.3).

The population $P$ interacts with the natural system by harvesting biomass from the terrestrial carbon stock $L$ which is consumed and ultimately emitted as carbon into the atmosphere $A$. The availability of biomass determines the wellbeing $W$ of mankind which in turn governs the reproductivity of the human species. Accumulation of physical capital besides a fixed capital per person is not regarded in this scenario.

With respect to the Earth history this submodel might correspond to a hunter-gatherer or agricultural society as the energy demand is solely satisfied by biomass and there is no accumulation of physical capital. Thus it might be valid for period before the onset of substantial capital accumulation due to the agricultural revolution after roughly 1500 AD. Additionally the results gathered from this submodel could be interpreted as representing alternative histories in which capital accumulation and fossil fuels have never been introduced into the economic system.

### 3.3.1 Functional forms of the dynamics

In order to obtain the governing equations of c:G:LATP the schematic from Figure 3.3 can be translated into the following **general form**:

$$\dot{L} = f_{\text{phot}}(L,T,A) - f_{\text{resp}}(L,T) - f_{\text{harv}}(B) \tag{3.25}$$

$$\dot{A} = -f_{\text{phot}}(L,T,A) + f_{\text{resp}}(L,T) + f_{\text{diff}}(A,M) + f_{\text{emis}}(B) \tag{3.26}$$

$$\dot{T} = f_{\text{greenh}}(A,T,\Omega(L)) \tag{3.27}$$

$$\dot{P} = P(f_{\text{fert}}(W) - f_{\text{mort}}(T,P,W)) \tag{3.28}$$

where:

$$M = M(L,A) \tag{3.29}$$

$$B = B(L,P,K) \tag{3.30}$$

$$W = W(L,P,Y) \tag{3.31}$$

$$Y = Y(P,K,B) \tag{3.32}$$

$$K = K(P) \tag{3.33}$$

The temperature evolution $\dot{T}$ and the processes of photosynthesis $f_{\text{phot}}$ and respiration $f_{\text{resp}}$ are identically modeled as described in section 3.2.

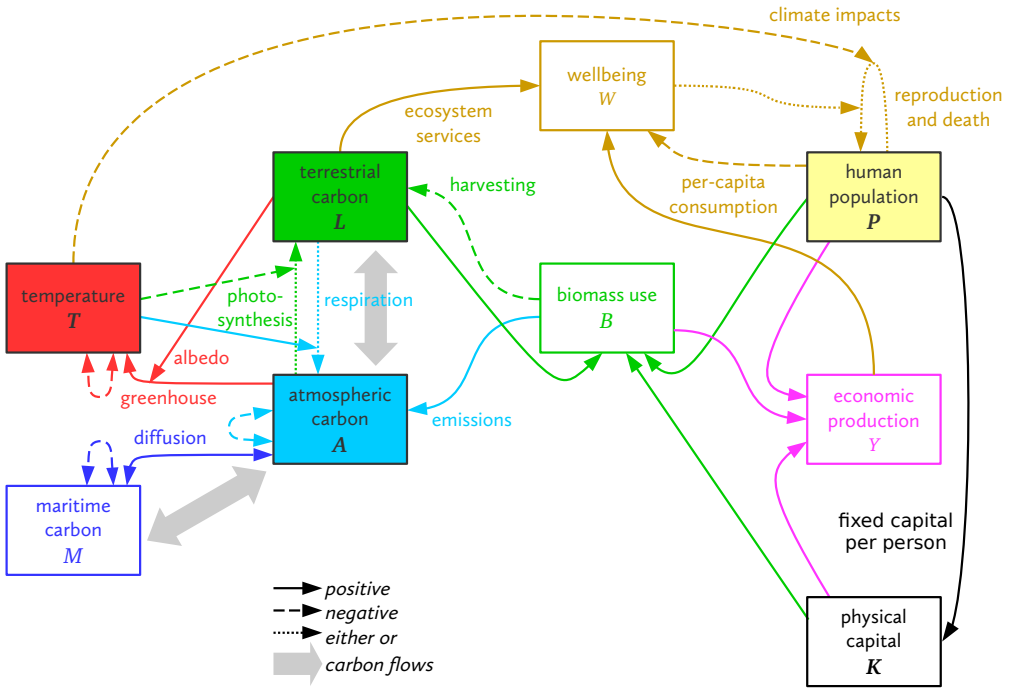


**Figure 3.3:** Overview of the minimal co-evolutionary submodel c:G:LATP which models a global hunter-gatherer or agricultural society without capital accumulation. The carbon cycle model is extended by a human population stock $P$ which affects the natural subsystem by harvesting biomass $B$ and emitting carbon into the atmosphere. The wellbeing $W$ determines the reproduction dynamics of the humans. The physical capital stock $K$ is derived from a fixed capital amount per person.

As already mentioned the carbon content of the harvested biomass is assumed to be completely emitted into the atmosphere on rather short timescales.[1] Hence the terms for harvesting and emissions are identical and equal to the biomass use $B$.

$$f_{\text{harv}}(B) = f_{\text{emis}}(B) = B(L,P,K) \tag{3.34}$$

The biomass use $B$ is ultimately determined by the **general equilibrium model** which is part of the complete c:G model and has been introduced in section 2.2.2. In this case the biomass sector

1 The forms of biomass use are mainly nutrition, building materials and firewood. Through the processes of respiration, rotting and combustion almost the complete carbon from the biomass is released to the atmosphere on rather short time scales. The carbon amount which goes into soils remains in the terrestrial stock (consisting of both vegetation and soils) and is thus not included in the harvesting term $B$.

is the only economic sector. The output function $B$ has a Cobb-Douglas form with constant returns to scale:

$$B = \frac{1}{e_B} X_B^{\frac{1}{5}} P^{\frac{2}{5}} K^{\frac{2}{5}} N^{-\frac{1}{5}} \tag{3.35}$$

where $e_B$ is the energy density of biomass (measured in GJ/GtC), $X_B$ is the "energy availability" of biomass and $N \geq 1$ reflects the degree of fragmentation of the global economic system.[1] The auxiliary quantity $X_B$ is calculated from the terrestrial carbon stock:

$$X_B = a_B L^2 \tag{3.36}$$

The physical capital stock $K$ in this scenario is assumed to be directly proportional to the population. Each person has (on average) a fixed capital amount $k_P$, thus:

$$K = k_P P \tag{3.37}$$

Finally the degree of fragmentation $N$ is assumed to be proportional to the total population $P$. This is motivated by the idea that the hunter-gatherer or agricultural communities described by this scenario have (on average) the same size $n_P^{-1}$:

$$N = n_P P \tag{3.38}$$

Plugging equations (3.36), (3.37) and (3.38) into the general form (3.35) one obtains:

$$B = \frac{a_B^{\frac{1}{5}} k_P^{\frac{2}{5}}}{e_B n_P^{\frac{1}{5}}} L^{\frac{2}{5}} P^{\frac{3}{5}} \tag{3.39}$$

$$= b L^{\frac{2}{5}} P^{\frac{3}{5}} \tag{3.40}$$

where in the second step the auxiliary parameter $b = a_B^{\frac{1}{5}} k_P^{\frac{2}{5}} e_B^{-1} n_P^{-\frac{1}{5}}$ is introduced. The right hand side of equation (3.40) is very similar to a comparable term in the renewable resource use model of Brander and Taylor [15] where the resource use is given as:

$$B_{\mathrm{BT}} = bLP \tag{3.41}$$

1 $N = 1$ means one global perfectly interconnected economic system while $N = 100$ would mean a fragmentation into 100 independent sub-economies.

However, in the c:G model $B(L,P,K,N)$ is a homogeneous function of degree one, meaning that if all extensive input quantities ($L$, $P$, $K$, $N$) are multiplied by some factor $\alpha$, also the output $B$ is multiplied by $\alpha$ as it is an extensive quantity. Equation (3.41) in contrast implies that a doubling of $L$ and $P$ would result in a fourfold renewable use $B_{\mathrm{BT}}$ which is not realistic.

The next extension compared to the c:G:LAT model is the additional equation (3.28) which governs the **dynamics of the population** $P$ (measured in the unit "humans" H). It consists of the processes of reproduction and death which are both proportional to the total population.

Like in ecological models for population growth of non-human species, fertility $f_{\mathrm{fert}}$ is assumed to increase linearly with wellbeing for very low values of $W$ accounting for the basic nutritional needs for reproduction. After the birth rate reaches a maximum value $p$ at a wellbeing of $W_p$ it is assumed to decrease inversely proportional to $W$ due to wealth and education effects. This dependence can be expressed as follows:

$$f_{\mathrm{fert}} = \frac{2pWW_p}{W^2 + W_p^2} \tag{3.42}$$

Mortality $f_{\mathrm{mort}}$ is composed of a natural death rate which is assumed to decrease inversely proportional to $W$ but increases linearly with $T$ due to potential climate impacts. In addition to this there is a term which accounts for competition for space, somewhat similar to a logistic growth model, which constitutes a natural limit against overpopulation of the planet.

$$f_{\mathrm{mort}} = \frac{(q_0 + q_T T)}{W} + \frac{q_P P}{\Sigma} \tag{3.43}$$

The shapes of both fertility and mortality functions are shown in Figure 3.4.

The upper limit on population posed by the competition term, $P^+$ can be calculated analytically. For this one needs maximize the difference between fertility and mortality without the competition term with respect to $W$, setting it equal to the competition term and solve for $P$. The wellbeing $W^+$ at which the difference between natural fertility and mortality (without competition term) are maximal is given as follows:

$$W^+ = W_p \sqrt{\frac{pW_p + q_0}{2pW_p - q_0} + \sqrt{\left(\frac{pW_p + q_0}{2pW_p - q_0}\right)^2 + \frac{q_0}{2pW_p - q_0}}} \tag{3.44}$$

Setting equal (3.42) and (3.43) at $W^+$ and solving for $P$ gives the **upper limit to population**:

$$P^+ = \frac{\Sigma}{q_P}\left(\frac{2pW_pW^+}{W^{+2}+W_p^2} - \frac{q_0}{W^+}\right) \tag{3.45}$$

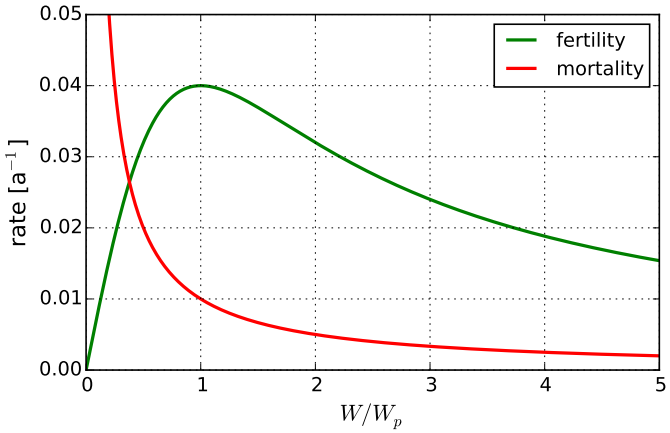


**Figure 3.4:** Qualitative dependence of fertility and mortality (without the competition term) on wellbeing $W$. Parameters: $p = 0.04$, $q_0 = 0.01$, $W_p = 1$, $q_T = 0$, $q_P = 0$.

It remains to choose a functional form for the wellbeing $W = W(L,P,Y)$. It is assumed to be composed of per capita consumption $Y/P$ and ecosystem services (such as biodiversity and recreational and aesthetic aspects) which are modeled proportional to the spatial density of available terrestrial carbon $L/\Sigma$. [1]

$$W = \frac{Y}{P} + \frac{w_L}{\Sigma}L \tag{3.46}$$

where $w_L$ is a parameter which appraises the relative weighting of ecosystem services compared to consumption.

The general equilibrium model makes the assumption that the total energy use $E$ sets an upper limit on the total economic output $Y$ (measured in \$/a). Therefore $Y$ is directly proportional to $E$. As in this scenario biomass is the only form of energy used, $E = e_B B$ holds, which gives,

1 The wellbeing contributions derived from consumption and ecosystem services are here assumed to be perfect substitutes which is probably not true but sufficient for investigating the qualitative effects.

using equation (3.40):

$$Y = y_E E \tag{3.47}$$
$$= y_E e_B B \tag{3.48}$$
$$= y_B b L^{\frac{2}{5}} P^{\frac{3}{5}} \tag{3.49}$$

where $y_E$ and $y_B = y_E e_B$ are parameters linking energy and biomass use to economic output in monetary units.

Putting together all functional forms and considerations made above, the c:G:LATP model is described by the following system of differential equations:

**c:G:LATP**

$$\dot{L} = L\left((l_0 - l_T T)\sqrt{A/\Sigma} - (a_0 + a_T T)\right) - B \tag{3.50}$$
$$\dot{A} = -\dot{L} + \delta\,(M - mA) \tag{3.51}$$
$$\dot{T} = g\left(\frac{1}{\Sigma}A - T + \frac{\omega_L}{\Sigma}L - \Omega_0\right) \tag{3.52}$$
$$\dot{P} = P\left(\frac{2pWW_p}{W^2 + W_p^2} - \frac{q_0 + q_T T}{W} - \frac{q_P P}{\Sigma}\right) \tag{3.53}$$

where:
$$M = C^*_{\mathrm{PI}} - L - A \tag{3.54}$$
$$B = bL^{\frac{2}{5}} P^{\frac{3}{5}} \tag{3.55}$$
$$W = y_B \frac{B}{P} + \frac{w_L}{\Sigma} L \tag{3.56}$$

### 3.3.2 Overview of variables and parameters

The additional variables and parameters of the c:G:LATP model compared to c:G:LAT (Table 3.1) are shown in Table 3.2.

**Table 3.2:** Overview of the additional variables and free parameters of the coevolutionary c:G:LATP model which describes hunter-gatherer and agricultural societies.

| variable | unit | range | description |
|---|---|---|---|
| $P$ | H | $0 \leq P$ | human population stock |
| $K$ | \$ | $0 \leq K$ | physical capital stock |
| $B$ | $\mathrm{GtC\,a^{-1}}$ | $0 \leq B$ | biomass harvesting flow |
| $W$ | $\mathrm{\$\ H^{-1}a^{-1}}$ | $0 \leq W$ | wellbeing flow |
| $Y$ | $\mathrm{\$\,a^{-1}}$ | $0 \leq Y$ | total economic output flow |
| parameter | unit | range | description |
| $p$ | $\mathrm{a^{-1}}$ | $> 0$ | fertility rate maximum |
| $W_p$ | $\mathrm{\$a^{-1}\,H^{-1}}$ | $> 0$ | fertility saturation wellbeing |
| $q_0$ | $\mathrm{\$a^{-2}\,H^{-1}}$ | $\geq 0$ | mortality baseline coefficient |
| $q_T$ | $\mathrm{km^2\,\$a^{-2}\,H^{-1}GtC^{-1}}$ | $\geq 0$ | mortality sensitivity to temperature |
| $q_P$ | $\mathrm{km^2a^{-1}H^{-1}}$ | $\geq 0$ | mortality sensitivity to population density |
| $b$ | $\mathrm{GtC^{3/5}\,a^{-1}\,H^{-3/5}}$ | $\geq 0$ | biomass harvesting rate |
| $y_B$ | $\mathrm{\$\,GtC^{-1}}$ | $\geq 0$ | economic output per biomass input |
| $w_L$ | $\mathrm{\$\,km^2\,GtC^{-1}\,a^{-1}\,H^{-1}}$ | $\geq 0$ | wellbeing sensitivity to land carbon |

## 3.4 Industrial societies (c:G:LAGTPK, c:G:LAGPK, c:G:LGTPK, c:G:LGPK)

Historically the non-capitalistic agricultural societies of the middle age were followed by technical revolutions which made physical capital a replacement for labor force in the economic production and later on the industrial revolution starting roughly around 1750 which was accompanied by the advent of fossil fuels. The submodel which aims at describing this period of the human history therefore includes a physical capital stock $K$ as state variable and allows the use of fossil fuels $F$ which are extracted from a geological carbon stock $G$ (see Figure 3.5). This "industrialization scenario" is abbreviated c:G:LAGTPK and is a six-dimensional submodel of c:G.

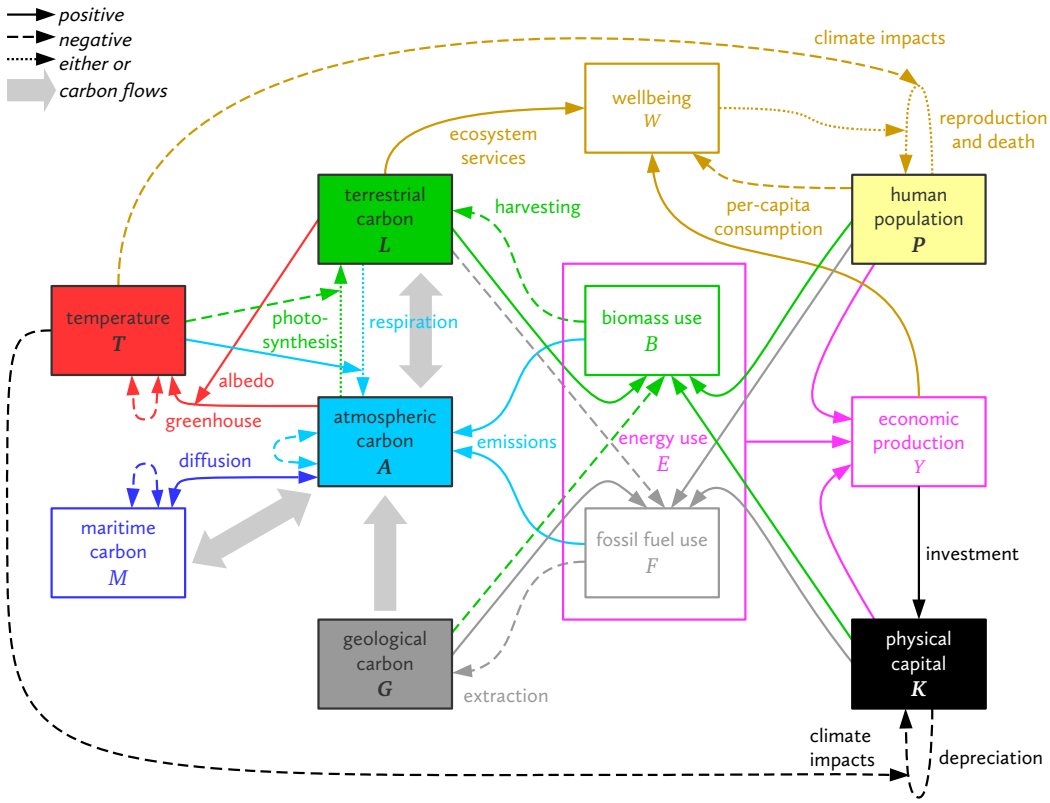


**Figure 3.5:** Overview of c:G:LAGTPK submodel which corresponds to industrial societies. The pre-industrial model versions are extended by a geological carbon stock $G$. From this fossil fuels $F$ can be extracted which lead to additional emissions of carbon into the atmosphere. Moreover a physical capital stock $K$ as independent production factor is added which grows due to investments.

### 3.4.1 Functional forms of the dynamics

Again the general form of the model equations can be extracted from the diagram in Figure 3.5.

$$\dot{L} = f_{\text{phot}}(L,T,A) - f_{\text{resp}}(L,T) - f_{\text{harv}}(B) \tag{3.57}$$

$$\dot{A} = -f_{\text{phot}}(L,T,A) + f_{\text{resp}}(L,T) + f_{\text{diff}}(A,M) + f_{\text{emis}}(B,F) \tag{3.58}$$

$$\dot{G} = -f_{\text{extr}}(F) \tag{3.59}$$

$$\dot{T} = f_{\text{greenh}}(A,T,\Omega(L)) \tag{3.60}$$

$$\dot{P} = P(f_{\text{fert}}(W) - f_{\text{mort}}(T,P,W)) \tag{3.61}$$

$$\dot{K} = f_{\text{inv}}(Y) - f_{\text{depr}}(K,T) \tag{3.62}$$

where:

$$M = M(L,A,G) \tag{3.63}$$

$$B = B(L,G,P,K) \tag{3.64}$$

$$F = F(L,G,P,K) \tag{3.65}$$

$$W = W(L,P,Y) \tag{3.66}$$

$$Y = Y(P,K,B,F) \tag{3.67}$$

The first extension to the c:G:LATP submodel is the **additional geological carbon pool** $G$ which can only be decreased by the use of fossil fuels. The extraction function is given by:

$$f_{\text{extr}}(F) = F(L,G,P,K) \tag{3.68}$$

The carbon contained in fossil fuels is emitted almost immediately into the atmosphere through the process of combustion. Thus the emission process is given by:

$$f_{\text{emis}}(B,F) = f_{\text{harv}}(B) + f_{\text{extr}}(F) = B + F \tag{3.69}$$

It is important to note that the total available carbon stock $C^* > C^*_{\text{PI}}$ is enlarged by the initial size of the carbon pool $G(t = 0)$. The maritime carbon $M$ is derived from the three other carbon pools:

$$M = C^* - L - A - G \tag{3.70}$$

Biomass use $B$ and fossil fuel use $F$ are determined by the general equilibrium model. The economy in this case consists of two competing sectors, the biomass and the fossil sector. Thus the availability of biomass has a negative effect on fossil use and vice versa.

Similar to equation (3.35) the total energy use $E$ is of Cobb-Douglas form:

$$E = X^{\frac{1}{5}} P^{\frac{2}{5}} K^{\frac{2}{5}} N^{-\frac{1}{5}} \tag{3.71}$$

where $X = X_B + X_F$ is the total "energy availability" given by the sum of biomass and fossil availabilities. While the biomass availability is given by equation (3.36), $X_F$ is determined by the geological carbon stock:

$$X_F = a_F G^2 \tag{3.72}$$

As the total energy use is the sum of biomass energy and fossil energy use $E$ must fulfill:

$$E = e_B B + e_F F \tag{3.73}$$

where $e_B$ and $e_F$ are the energy densities of biomass and fossil fuels, respectively. Together with equation (3.71) one can conclude for the individual carbon use flows:

$$B = \frac{1}{e_B} \frac{X_B}{X^{\frac{4}{5}}} P^{\frac{2}{5}} K^{\frac{2}{5}} N^{-\frac{1}{5}} = \frac{a_B}{e_B} \frac{L^2 P^{\frac{2}{5}} K^{\frac{2}{5}} N^{-\frac{1}{5}}}{(a_B L^2 + a_F G^2)^{\frac{4}{5}}} \tag{3.74}$$

$$F = \frac{1}{e_F} \frac{X_F}{X^{\frac{4}{5}}} P^{\frac{2}{5}} K^{\frac{2}{5}} N^{-\frac{1}{5}} = \frac{a_F}{e_F} \frac{G^2 K^{\frac{2}{5}} P^{\frac{2}{5}} N^{-\frac{1}{5}}}{(a_B L^2 + a_F G^2)^{\frac{4}{5}}} \tag{3.75}$$

In contrast to the pre-industrial societies described by the previous submodels the economic system in the industrialized scenario is assumed to be not fragmented at all, so that subsequently $N = 1$ is assumed.

The **physical capital** stock $K$ in this scenario is a state variable which is increased by the process of investment and decreased through depreciation. Assuming that a fixed share $i$ of the total economic output $Y$ is invested gives:

$$f_{\text{inv}}(Y) = iY \tag{3.76}$$

The depreciation rate is assumed to be composed of a natural baseline coefficient $k_0$ and a part which increases linearly with temperature $T$ due to climate impacts:

$$f_{\text{depr}} = (k_0 + k_T T)K \tag{3.77}$$

As now a certain share $i$ of $Y$ is invested, only the remainder of $(1 - i)Y$ is available for consumption and thus the first term of the wellbeing function (3.46) is slightly changed.

Altogether the considerations above lead to the following system of differential equations for the c:G:LAGTPK submodel:

**c:G:LAGTPK**

$$\dot{L} = L\left((l_0 - l_T T)\sqrt{A/\Sigma} - (a_0 + a_T T)\right) - B \tag{3.78}$$

$$\dot{A} = -\dot{L} + \delta\,(M - mA) \tag{3.79}$$

$$\dot{G} = -F \tag{3.80}$$

$$\dot{T} = g\left(\frac{1}{\Sigma}A - T + \frac{\omega_L}{\Sigma}L - \Omega_0\right) \tag{3.81}$$

$$\dot{P} = P\left(\frac{2pWW_p}{W^2 + W_p^2} - \frac{q_0 + q_T T}{W} - \frac{q_P P}{\Sigma}\right) \tag{3.82}$$

$$\dot{K} = iY - (k_0 + k_T T)K \tag{3.83}$$

where:

$$M = C^* - L - A - G \tag{3.84}$$

$$B = \frac{a_B}{e_B}\frac{L^2 P^{\frac{2}{5}} K^{\frac{2}{5}}}{(a_B L^2 + a_F G^2)^{\frac{4}{5}}} \tag{3.85}$$

$$F = \frac{a_F}{e_F}\frac{G^2 P^{\frac{2}{5}} K^{\frac{2}{5}}}{(a_B L^2 + a_F G^2)^{\frac{4}{5}}} \tag{3.86}$$

$$W = \frac{(1-i)Y}{P} + \frac{w_L}{\Sigma}L \tag{3.87}$$

$$Y = y_E E = y_E(e_B B + e_F F) \tag{3.88}$$

#### Further submodels

Even if instantaneous greenhouse effect and diffusion are assumed (see section 3.2.3) the submodel for the industrialization scenario (c:G:LGPK) is four-dimensional and hence hard to analyze by graphical means like portraits of the phase space. Thus it is instructive to reduce the dimension further in order to obtain three-dimensional submodels.

A scenario in which only capital accumulation is considered but biomass is still the only form of energy used might correspond to **capitalistic agricultural societies**. Technically this is achieved by ignoring the geological carbon stock $G$ in equations (3.78) to (3.88) or, equivalently, setting $a_F = 0$. This model version is denoted by c:G:LPK.

Alternatively one might think of fictitious societies which makes use of fossil fuels (such as lignite) but do not accumulate physical capital to do so. The governing equations can be derived from those of the industrial scenario by assuming a constant per-capita capital as in

(3.37). This model version is denoted by c:G:LGP but is not analyzed within the context of this thesis.

### 3.4.2 Overview of variables and parameters

The additional variables and parameters of the c:G:LAGTPK model compared to c:G:LAT and c:G:LATP (Tables 3.1 and 3.2) are shown in Table 3.3.

**Table 3.3:** Overview of the additional variables and free parameters of the c:G:LAGTPK model which describes a scenario of industrialized societies.

| variable | unit | range | description |
|---|---|---|---|
| $G$ | GtC | $0 \leq G \leq C^*$ | geological carbon stock |
| $K$ | \$ | $0 \leq K$ | physical capital stock |
| $F$ | $\mathrm{GtC\,a^{-1}}$ | $0 \leq F$ | fossil fuel extraction flow |
| parameter | unit | range | description |
| $C^*$ | GtC | $> 0$ | total available carbon stock |
| $y_E$ | $\mathrm{\$\,GJ^{-1}}$ | $> 0$ | economic output per energy input |
| $a_B$ | $\mathrm{GJ^5 a^{-5} GtC^{-2} \$^{-2} H^{-2}}$ | $> 0$ | biomass sector productivity |
| $a_F$ | $\mathrm{GJ^5 a^{-5} GtC^{-2} \$^{-2} H^{-2}}$ | $> 0$ | fossil fuel sector productivity |
| $e_B$ | $\mathrm{GJ\,GtC^{-1}}$ | $> 0$ | biomass energy density |
| $e_F$ | $\mathrm{GJ\,GtC^{-1}}$ | $> 0$ | fossil fuel energy density |
| $i$ | 1 | $0 < i < 1$ | investment ratio |
| $k_0$ | $\mathrm{a^{-1}}$ | $> 0$ | capital depreciation rate |
| $k_T$ | $\mathrm{km^2\,a^{-1} GtC^{-1}}$ | $\geq 0$ | capital depreciation sensitivity to temperature |

## 3.5 Dimensionless formulation

As the variables and parameters are of diverse physical dimensions and expected be of unlike orders of magnitude it is instructive to introduce a dimensionless version of the governing equations. This will be used during simulations to preclude numerical issues as well as to present the results. For each variable and parameter a non-dimensional version is introduced which will be decorated with a hat ($\hat{x}$) to be distinguishable from the dimensional value.

The theoretical foundation for the "non-dimensionalization" of the equations is given by the **Buckingham Π-Theorem** [9]. It states that a physical system described by $N$ physcial quantities which feature $D$ independent physical dimensions can be described by $P = N - D$ dimensionless physical quantities.

Practically one can choose $D$ parameters whose dimensions include all of the independent dimensions present in the system and set them to 1. The other parameters' and variables' dimensions can then be expressed in terms of those "reference parameters".

The dimensionless formulation of the model equation is subsequently done for the c:G:LAGTPK

model but meanwhile the same definitions hold for all other submodels. As an exception a slightly different dimensionless formulation is introduced for the c:G:LATP model as it involves the auxiliary parameter $b$ (see appendix A.1).

The physical quantities of the model variables involve six independent physical dimensions (GtC, km, a, H, \$, GJ). Therefore the number of free parameters can be reduced by six according to the Buckingham Π-Theorem. The parameters $C^*$, $\Sigma$, $\delta$, $W_p$, $y_E$ and $e_B$ are chosen as reference parameters which are set to 1.[1] Using these the following non-dimensional variables are defined:

$$\hat{t} = \delta t \tag{3.89}$$

$$\hat{L} = \frac{L}{C^*} \tag{3.90}$$

$$\hat{A} = \frac{A}{C^*} \tag{3.91}$$

$$\hat{G} = \frac{G}{C^*} \tag{3.92}$$

$$\hat{T} = \frac{T\Sigma}{C^*} \tag{3.93}$$

$$\hat{P} = \frac{PW_p}{C^*\delta y e_B} \tag{3.94}$$

$$\hat{K} = \frac{K}{C^* y e_B} \tag{3.95}$$

$$\hat{M} = \frac{M}{C^*} \tag{3.96}$$

$$\hat{B} = \frac{B}{C^*\delta} \tag{3.97}$$

$$\hat{F} = \frac{F}{C^*\delta} \tag{3.98}$$

$$\hat{W} = \frac{W}{W_p} \tag{3.99}$$

$$\hat{Y} = \frac{Y}{C^*\delta y e_B} \tag{3.100}$$

1 Those model versions with instantaneous diffusion effectively assume $\delta = +\infty$. Their dimensionless quantities are, however, scaled with respect to the estimated value of $\delta$ given in Table 4.3. Therefore in this case the number of model parameters is not reduced by the scaling of the time.

Plugging these into the dimensional equations (3.78) to (3.88) leads to the following **non-dimensional equations**:

**c:G:LAGTPK dimensionless**

$$\dot{\hat{L}} = \hat{L}\left((\hat{l_0} - \hat{l_T}\hat{T})\sqrt{\hat{A}} - (\hat{a_0} + \hat{a_T}\hat{T})\right) - \hat{B} \tag{3.101}$$

$$\dot{\hat{A}} = -\dot{\hat{L}} + \left(\hat{M} - m\hat{A}\right) \tag{3.102}$$

$$\dot{\hat{G}} = -\hat{F} \tag{3.103}$$

$$\dot{\hat{T}} = \hat{g}\left(\hat{A} - \hat{T}\right) \tag{3.104}$$

$$\dot{\hat{P}} = \hat{P}\left(\frac{2\hat{p}\hat{W}}{1+\hat{W}^2} - \frac{\hat{q_0} + \hat{q_T}\hat{T}}{\hat{W}} - \hat{q_P}\hat{P}\right) \tag{3.105}$$

$$\dot{\hat{K}} = i\hat{Y} - (\hat{k_0} + \hat{k_T}\hat{T})\hat{K} \tag{3.106}$$

where:

$$\hat{M} = 1 - \hat{L} - \hat{A} - \hat{G} \tag{3.107}$$

$$\hat{B} = \frac{\hat{a_B}^{\frac{1}{5}}\hat{L}^2\hat{P}^{\frac{2}{5}}\hat{K}^{\frac{2}{5}}}{(\hat{L}^2 + \hat{a_F}\hat{G}^2)^{\frac{4}{5}}} \tag{3.108}$$

$$\hat{F} = \frac{\hat{a_B}^{\frac{1}{5}}\hat{a_F}\hat{G}^2\hat{P}^{\frac{2}{5}}\hat{K}^{\frac{2}{5}}}{\hat{e_F}(\hat{L}^2 + \hat{a_F}\hat{G}^2)^{\frac{4}{5}}} \tag{3.109}$$

$$\hat{W} = \frac{(1-i)\hat{Y}}{\hat{P}} + \hat{w_L}\hat{L} \tag{3.110}$$

$$\hat{Y} = \hat{E} = \hat{B} + \hat{F} \tag{3.111}$$

These have now 15 non-dimensional instead of 21 dimensional (except for $m$ and $i$) free parameters. These are defined as follows:

$$\hat{a_0} = a_0 \frac{1}{\delta} \tag{3.112}$$

$$\hat{a_T} = a_T \frac{C^*}{\delta \Sigma} \tag{3.113}$$

$$\hat{l_0} = l_0 \frac{C^{*\frac{1}{2}}}{\delta \Sigma^{\frac{1}{2}}} \tag{3.114}$$

$$\hat{l_T} = l_T \frac{C^{*\frac{3}{2}}}{\delta \Sigma^{\frac{3}{2}}} \tag{3.115}$$

$$\hat{g} = g \frac{1}{\delta} \tag{3.116}$$

$$\hat{p} = p \frac{1}{\delta} \tag{3.117}$$

$$\hat{q_0} = q_0 \frac{1}{\delta W_p} \tag{3.118}$$

$$\hat{q_T} = q_T \frac{C^*}{\delta \Sigma W_p} \tag{3.119}$$

$$\hat{q_P} = q_P \frac{C^* y e_B}{\Sigma W_p} \tag{3.120}$$

$$\hat{k_0} = k_0 \frac{1}{\delta} \tag{3.121}$$

$$\hat{k_T} = k_T \frac{C^*}{\delta \Sigma} \tag{3.122}$$

$$\hat{a_B} = a_B \frac{C^* y^4}{\delta^3 W_p^2 e_B} \tag{3.123}$$

$$\hat{a_F} = \frac{a_F}{a_B} \tag{3.124}$$

$$\hat{e_F} = \frac{e_F}{e_B} \tag{3.125}$$

$$\hat{w_L} = w_L \frac{C^*}{\Sigma W_p} \tag{3.126}$$

# CHAPTER 4

## Parameter estimation

The model as described in chapter 3 possesses various free parameters which are shown in Tables 3.1, 3.2 and 3.3. In order to be able to compute trajectories of the variables these need to be set to reasonable values. As the model is conceptual by nature it is mostly sufficient to make rough estimates. “Reasonable” thus means that the parameter values are at least in the right order of magnitude.

For some parameters it turns out to be practically impossible to obtain even rough estimates as they do not correspond to established quantities for which there are data available. These will be the primary candidates for variation in bifurcation analyses.

It is worth noting that in order to investigate the qualitative behavior of the system the absolute values of the scaling parameters introduced in section 3.5 ($C^*$, $\Sigma$, $\delta$, $W_p$, $y_E$, $e_B$) are not necessary as they just set the scale of the physical dimensions involved. However, to be able to compare the results with real world data, also these values should be reasonably estimated.

In analogy to the distinction of the submodels the parameters can be divided into several categories: those related to the global carbon cycle, those governing the demography of the society and those related to the economic model components. This chapter is subdivided according to this classification of the parameters. It closes with an overview Table of all estimated parameter values in section 4.5.

## 4.1 Carbon cycle parameters

The parameters of the global carbon cycle model c:G:LAT are listed in Table 3.1.

The available earth surface area $\Sigma$ can be estimated by the land surface of the earth:

$$\Sigma \approx 150 \cdot 10^6 \,\mathrm{km}^2 \tag{4.1}$$

The parameters $C^*$, $a_0$, $a_T$, $l_0$, $l_T$, $m$ and $\delta$ are calibrated using actually estimated carbon pools and flows as reported in the latest assessment report of the Working Group I of the IPCC [17] (see Figure 2.13) in section 2.3.1.[1] Table 4.1) shows the values for the relevant stocks and flows extracted from Figure 2.13. Vegetation and soils are regarded as one terrestrial pool $L$. Also the different forms of fossil fuels (gas, oil, coal) are regarded as one geological stock $G$. Even though there are relatively high ranges given for $L_{\mathrm{PI}}$ and $G_{\mathrm{PI}}$ the average values are taken and assumed to be without uncertainty. The uncertainties given for the changes to the present values are used to estimate also uncertainties of the parameter values.

**Table 4.1:** Pre-industrial carbon stocks and flows and changes to present with uncertainties which are relevant to the c:G model. Numbers are extracted from Figure 2.13 and partly rounded.

| parameter | pre-industrial | change to present |
|---|---|---|
| $L$ [GtC] | 2500 | $-20 \pm 45$ |
| $A$ [GtC] | 600 | $+240 \pm 10$ |
| $M$ [GtC] | 900 | $+155 \pm 30$ |
| $G$ [GtC] | 1500 | $-375 \pm 30$ |
| $f_{\mathrm{resp}}$ [GtC a$^{-1}$] | 107.2 | $+11.6 \pm 1.2$[2] |
| $f_{\mathrm{phot}}$ [GtC a$^{-1}$] | 108.9 | $+14.1 \pm 1.2$ |
| $f_{\mathrm{diff}}$ [GtC a$^{-1}$] | 0.7 | $-3.0 \pm 0.7$ |

The total available carbon $C^*$ on the timescales of interest ($10^2$ to $10^3$ years) constitutes of the terrestrial stock $L$, the atmospheric stock $A$, the maritime stock $M$ and the geological stock $G$. It can be calculated from the preindustrial values for each stock:

$$C^* = L_{\mathrm{PI}} + A_{\mathrm{PI}} + M_{\mathrm{PI}} + G_{\mathrm{PI}} = 5500\,\mathrm{GtC} \tag{4.2}$$

1 Since the c:G:LAT model is very similar to the conceptual carbon cycle model presented in [2] another strategy would be to adjust the parameters such that the resulting dynamics is comparable to that presented there. This has been done with the result that it is possible to find parameter values which generate a phase space that is topologically equivalent to that of the Anderies model. These results however are not shown here because the Anderies paper is not transparent about the estimation of the parameter values used. The following analysis thus relies on the direct parameter estimates from the IPCC data.

2 As there are no uncertainties given for the individual flows, the uncertainty estimate of the net flow is assigned to both the respiration and photosynthesis flow.

For the preindustrial value $C^*_{\mathrm{PI}}$ the geological stock is not regarded:

$$C^*_{\mathrm{PI}} = L_{\mathrm{PI}} + A_{\mathrm{PI}} + M_{\mathrm{PI}} = 4000\,\mathrm{GtC} \tag{4.3}$$

The carbon exchange between land and atmosphere is given by the flows of **respiration** $f_{\mathrm{resp}}$ and **photosynthesis** $f_{\mathrm{phot}}$. They are given in the model by equations (3.4) and (3.5). For simplicity the temperature is estimated via equation (3.23), assuming an instantaneous greenhouse effect and no albedo, thus:

$$f_{\mathrm{resp}} = L\left(a_0 + \frac{a_T}{\Sigma}A\right) \tag{4.4}$$

$$f_{\mathrm{phot}} = L\left(l_0 + \frac{l_T}{\Sigma}A\right)\sqrt{\frac{A}{\Sigma}} \tag{4.5}$$

Using the values from Table 4.1 for $f_{\mathrm{resp}}$, $f_{\mathrm{phot}}$, $L$ and $A$ these equations can be written for both the preindustrial and the present state. By solving these equations the unknown parameters $a_0$, $a_T$, $l_0$ and $l_T$ can be determined. The uncertainties of the parameter values can be estimated using Gaussian error propagation:

$$a_0 = (0.0298 \pm 0.0026)\,\mathrm{a}^{-1} \tag{4.6}$$

$$a_T = (3.2 \pm 0.6) \cdot 10^3\,\mathrm{km}^2\,\mathrm{a}^{-1}\,\mathrm{GtC}^{-1} \tag{4.7}$$

$$l_0 = (26.4 \pm 2.4)\,\mathrm{km}\,\mathrm{a}^{-1}\,\mathrm{GtC}^{-1/2} \tag{4.8}$$

$$l_T = (1.1 \pm 0.6) \cdot 10^6\,\mathrm{km}^3\,\mathrm{a}^{-1}\,\mathrm{GtC}^{-3/2} \tag{4.9}$$

As one can see the relative uncertainties of parameters that determine the temperature sensitivity, $a_T$ and $l_T$ is considerably larger than that of the baseline coefficients $a_0$ and $l_0$ which have a relative uncertainty of roughly 10 %.

The net **diffusive flux** $f_{\mathrm{diff}}$ from the ocean to the atmosphere is described in the model by equation (3.6):

$$f_{\mathrm{diff}} = \delta(M - mA)$$

Again from the preindustrial and present values this equation can be solved for the unknown parameters inclusive of uncertainties. The estimated values are rounded in order to obtain

nicer values for the scaling parameter $\delta$ and the solubility coefficient $m$.

$$\delta = (0.016 \pm 0.005)\,\mathrm{a}^{-1} \approx 0.01\,\mathrm{a}^{-1} \tag{4.10}$$

$$m = 1.43 \pm 0.02 \approx 1.5 \tag{4.11}$$

The remaining parameters of the c:G:LAT submodel are related to the greenhouse effect ($g$, $\Omega_0$ and $\omega_L$). As the assumption of a negligible albedo effect is made throughout this thesis, $\Omega_0$ and $\omega_L$ are effectively set to zero.

A straight forward estimation of $g$ from climate data or other climate models is not possible as the greenhouse effect is typically described in a more complex manner or on shorter timescales (see for instance [58]). A similar functional form to describe the dynamics of the global mean temperature is used in [48] where the characteristic time of the greenhouse effect is estimated as $\tau_T = 50\,\mathrm{a}$. This corresponds to a value for $g$ of

$$g = 0.02\,\mathrm{a}^{-1} \tag{4.12}$$

which is used as best estimate in the following. However, it is often argued that for long term simulations over centuries and millennia it is sufficient to use the steady state value of $T$ which can directly be derived from other variables [2, 58]. Therefore for most of the results presented in chapter 5 the assumption of an instantaneous greenhouse effect is made such that equation (3.23) holds.

An overview of all estimated parameters and their non-dimensional default values is given in Section 4.5.

## 4.2 Demographic parameters

The dynamics of the human population is governed by equations (3.42) and (3.43) which model the fertility and mortality of the population in dependence of other model variables. These equations introduce the parameters $p$, $W_P$, $q_0$, $q_T$ and $q_P$ (listed in Table 3.2) which need to be estimated in order to compute trajectories of the model.

The effect of climate impacts on mortality is not regarded in the context of this thesis so that $q_T = 0$ holds in the following.

Furthermore the mortality sensitivity to population density is set to zero: $q_P = 0$. This is motivated by the assumption that the population densities of the scenarios regarded (agricultural, industrial) are fairly below critical values. The limited availability of resources (biomass and fossil fuels) guarantees that there is still an upper limit to the population size.

The parameters $p$, $W_p$ and $q_0$ are estimated by means of a **(weighted) least square regression**, in which the model functions (3.42) and (3.43) are fitted to available data. The dependent variables of the regression are the fertility $f_{\text{fert}}$ and mortality $f_{\text{mort}}$ respectively, for which data on crude birth and death rates are used. These are available country-wise and yearly for a period from 1960 until 2013 from the World Bank [11, 24]. The predictor variable in this case is given by the wellbeing $W$, for which data on the gross domestic product (GDP) per capita are used. The World Bank offers country-wise, yearly data on the GDP per capita based on purchasing power parities[1] (PPP) and measured in 2011 international \$ [2] for the period from 1990 until 2014 [33].

The data are shown in Figure 4.1 on linear an logarithmic scales. Each data point corresponds to an available birth or death rate value for a single year and country in dependence of its GDP per capita. The data feature quite large variances in both directions. The birth rate is generally quite high ( $0.04\ \mathrm{a^{-1}\,H^{-1}}$) for low GDP per capita ($< 5000\,\$\,\mathrm{a^{-1}H^{-1}}$). This regime is followed by a regime with decreasing birth rates down to around $0.01\ \mathrm{a^{-1}\,H^{-1}}$ for the high-income countries. The death rates decline fast for low incomes from roughly $0.02\ \mathrm{a^{-1}\,H^{-1}}$ to around $0.01\ \mathrm{a^{-1}\,H^{-1}}$ at $10000\,\$\,\mathrm{a^{-1}H^{-1}}$. Beyond this point the death rates stay more or less on a constant level or decrease only slowly.

For the least squares regression the data points are weighted according to the population size of the particular country, for which the values are also retrieved from the World Bank [79]. The resulting estimates for the parameters are given in Table 4.2 as “original model”.

1 The concept of purchasing power parities ensures that the GDP data are comparable between different countries and currencies. [98]

2 The GDP values are inflation-adjusted to the reference year 2011 which makes the data comparable between different points in time.

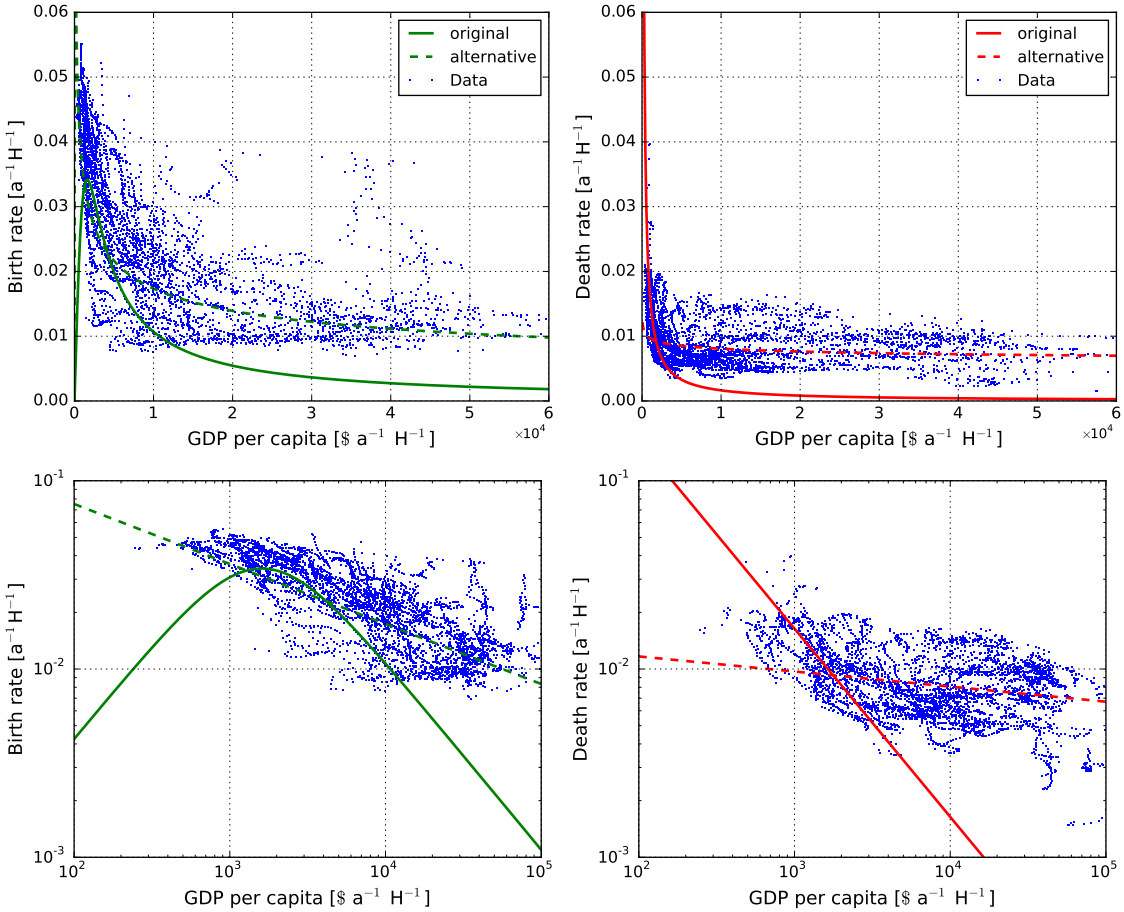


**Figure 4.1:** Country-wise yearly data on curde birth (left) and death rates (right). The continuous curves result from a least squares regression of the model equations (3.42) and (3.43), respectively. While they reflect basic characteristics of the data, the decrease towards large incomes is too fast. The fitted curves of the alternative model equations (4.13) and (3.43) (shown as dashed lines) do better capture the data but introduce additional parameters. For the mortality curves $q_P = q_T = 0$ is assumed. The lower panel shows the data and curves on double-logarithmic scales for which the differing speeds of decrease between the model versions are visible. The modeled increase of fertility for very low incomes is not reflected by the data but rather motivated from theoretical evidences.

The fertility and mortality curves for the fitted parameter values are also shown in Figure 4.1) as “original” model. The fertility curve captures the plateau with high birth rates for low incomes; the decrease for larger incomes appears to be too fast. For very low incomes the model assumption of a linear increase of fertility with wellbeing is not backed up by the available data. For this regime the model equation draws its legitimation from ecological theory as discussed in section 6.3.2. The estimated curve for the mortality dependence also appears to decrease

too fast for higher income levels.

**Table 4.2:** Overview of the regressed parameter values of the different demographic models. For the "original model" $\omega_p = \omega_q = 1$ holds.

| parameter | estimated value |
|---|---|
| original model | |
| $p\ [\mathrm{a}^{-1}]$ | $0.0342 \pm 0.0004$ |
| $W_p\ [\$\,\mathrm{H}^{-1}\mathrm{a}^{-1}]$ | $1600 \pm 30$ |
| $q_0\ [\$\,\mathrm{H}^{-1}\mathrm{a}^{-2}]$ | $16.39 \pm 0.24$ |
| alternative model | |
| $p\ [\mathrm{a}^{-1}]$ | $0.4 \pm 523$ |
| $W_p\ [\$\mathrm{H}^{-1}\mathrm{a}^{-1}]$ | $0.1 \pm 231$ |
| $\omega_p$ | $0.322 \pm 0.008$ |
| $q_0\ [\$^{\omega_q}\mathrm{H}^{-\omega_q}\mathrm{a}^{-(1+\omega_q)}]$ | $0.0169 \pm 0.0008$ |
| $\omega_q$ | $0.080 \pm 0.005$ |

For this reason an **alternative model** is proposed in order to better capture the decreasing behavior at higher incomes. In the original model equation (3.53) the decrease of both birth and death rates for high wellbeing is assumed to be inversely proportional to $W$. A different exponent $W^\omega$ could lead to a slower decrease for large $W$. The following alternative functional forms for $f_{\mathrm{fert}}$ and $f_{\mathrm{mort}}$ introduce such exponents as additional parameters:

$$f_{\mathrm{fert}}^{\mathrm{alt}} = \frac{2pWW_p^{\omega_p}}{W^{1+\omega_p} + W_p^{1+\omega_p}} \tag{4.13}$$

$$f_{\mathrm{mort}}^{\mathrm{alt}} = \frac{q_0}{W^{\omega_q}} \tag{4.14}$$

Here $\omega_p$ and $\omega_q$ denote the exponents which set the speed of decrease of birth and death rates with wellbeing. The original model can be retrieved from these equations by setting $\omega_p = \omega_q = 1$.

The parameters of these alternative model equations are also estimated via a least squares regression. The resulting values are given in Table 4.2 while the corresponding curves are shown in Figure 4.1 as "alternative" model.

The fertility fit of the alternative model does not converge to reasonable parameter values for $p$ and $W_p$, which is indicated by the large uncertainty ranges. The estimated value for the exponent is $\omega_p \approx 0.32$ which means considerably slower decreasing compared to the original model. Also the mortality curve matches the data better as the speed of the decrease is slower. The estimated exponent of $\omega_q \approx 0.08$ would mean a by far slower decreasing compared to the original model.

Since the original model is able to capture the dependencies in the data at least qualitatively and the overall model complexity is tried to be kept as low as possible, in the following analysis the alternative model will not be considered. In more quantitatively oriented studies the alternative model is worth being considered. A general discussion of an accurate model for the population dynamics is elaborated in section 6.3.

The values for $p$, $W_p$ and $q_0$ from the regression analysis give an orientation for the order of magnitude and the proportions of the model parameters. The following rounded values will be used subsequently as best estimates for the demographic parameters:

$$p \approx 0.04\,\mathrm{H}^{-1}\mathrm{a}^{-1} \tag{4.15}$$

$$W_p \approx 2000\,\$\mathrm{H}^{-1}\mathrm{a}^{-1} \tag{4.16}$$

$$q_0 \approx 20\,\$\mathrm{H}^{-1}\mathrm{a}^{-2} \tag{4.17}$$

## 4.3 Economic parameters

It remains to find estimates for the parameters related to the economic part of the model. For the agricultural submodel c:G:LATP these are $b$, $y_B$ and $w_L$ (see Table 3.2).

The parameter $b$ is introduced in equation (3.40) and quantifies the biomass harvesting sensitivity to the terrestrial carbon stock $L$ and the human population $P$. There are barely any data available which quantify the amount of harvested biomass for the period in time before 1900. This is particularly unfavorable since the c:G:LATP submodel aims at describing preindustrial times. Thus one has to be satisfied with restricting the estimation of $b$ to data past 1900.

The amount of harvested biomass through humans is assessed within the concept of the **Human Appropriation of Net Primary Production** (HANPP) [35, 38, 49, 50]. HANPP is a measure for to which extent the biomass production of the natural ecosystem is altered due to human activities. HANPP is composed of a part due to land use change ($\mathrm{HANPP_{luc}}$) and a part due to harvesting ($\mathrm{HANPP_{harv}}$). The latter corresponds approximately to the notion of biomass use $B$ in the c:G model.

Assessments of the global $\mathrm{HANPP_{harv}}$ for the years 1910-2005 can be found in [50] and the corresponding online resource [51]. The datasets also include estimates of the global population $P$ for those points in time. For the terrestrial carbon stock a constant value of $L_{\mathrm{pres}} = 2480\,\mathrm{GtC}$, corresponding to the present estimate from the IPCC (see Table 4.1) is assumed for all years. Rephrasing equation (3.40) and using these data $b$ can be estimated as follows:

$$b = \frac{B}{L^{\frac{2}{5}} P^{\frac{3}{5}}} = \frac{\mathrm{HANPP_{harv}}}{L_{\mathrm{pres}}^{\frac{2}{5}} P^{\frac{3}{5}}} \tag{4.18}$$

The estimates for different years are shown in Figure B.1 in appendix B.1. The arithmetic mean and the standard deviation of the estimated values are:

$$b \approx (5.4 \pm 0.5) \cdot 10^{-7}\,\mathrm{GtC^{3/5}\,a^{-1}\,H^{-3/5}} \tag{4.19}$$

The available data on $\mathrm{HANPP_{harv}}$ can also be used to validate the model equation for the biomass harvesting (3.40). The model states that $B \propto P^{\pi}$ with $\pi_{\mathrm{model}} = 0.6$. The exponent $\pi$ can also be estimated from the data by a least squares regression analysis. This gives a value of $\pi_{\mathrm{data}} = 0.77 \pm 0.04$. Even though the model value lies outside the confidence interval, the exponents are of comparable size. If one would assume a global economy ($N = 1$) rather than a fragmented ($N \propto P$) the model term for the biomass use would state $B \propto P^{\frac{4}{5}}$. For this case the exponent of $\pi_{\mathrm{model}} = 0.8$ lies within the confidence interval of $\pi_{\mathrm{data}}$. As the data come

from a period (past 1900) in which the economy is rather global than fragmented this can be seen as a validation for the model equations.

The parameter $y_B$ (measured in $\$\,\mathrm{GtC}^{-1}$) quantifies the global economic output $Y$ per biomass input $B$. However, it is introduced for the scenario of hunter-gatherer or agricultural societies. Thus, when recent data are used for the estimation, the total economic output $Y$ should be restricted to that of the agricultural sector. The global economic output is identified with the gross world product (GWP) for which there are data available from the World Bank for the years 1990-2014 [34].[1] It also offers data for the global agricultural sector's share of the GWP ($s_{\mathrm{agri}}$) for the years 1995-2013 [1]. The global biomass use is again estimated using the $\mathrm{HANPP}_{\mathrm{harv}}$ data from [50] which are available from 1990-2005 in ten-year-periods. From equation (3.48) follows:

$$y_B = \frac{Y}{B} \approx \frac{s_{\mathrm{agri}} \cdot \mathrm{GWP}}{\mathrm{HANPP}_{\mathrm{harv}}} \tag{4.20}$$

For the years 1990, 2000 and 2005 there are data on GWP, $s_{\mathrm{agri}}$ and HANPP available so that $y_B$ can be calculated (see Figure B.2 in appendix B.1).[2] The arithmetic mean and the standard deviation of the estimated values are:

$$y_B \approx (2.47 \pm 0.07) \cdot 10^{11}\,\$\,\mathrm{GtC}^{-1} = (247 \pm 7)\,\$\,\mathrm{tC}^{-1} \tag{4.21}$$

As the unit of $y_B$ indicates, it is basically an average price for biomass. Hence it is instructive to compare it to actual market prices for biomass. If one takes for example the maize price from the 2014 Global Food Price Monitor of the FAO [29] of about 200 $ per ton and assumes that the mass share of carbon in maize is about 50 %, one gets a price of 400 $ per ton carbon which compares very nicely to the estimate of $y_B$. This can be seen as an independent confirmation of the estimate being of a reasonable order of magnitude.

Instead of $y_B$ the model for industrial societies c:G:LAGTPK has the parameter $y_E$ which relates global economic output $Y$ to energy input $E$. [3] Energy here means primary energy since

1 It is important to note that the economic data which are used for parameter estimations need to be given in the same monetary units. As the demographic parameters were estimated using GDP data in 2011 international $, the same reference year is used for the GWP data used here.

2 The agricultural share of the GWP for the year 1990 is estimated to be 5 %, extrapolating the trend from recent years back into the past.

3 As this scenario is comparable to the present global situation in which the global share of non-biomass renewables on primary energy use is very low, the economic output $Y$ here does not need to be restricted to the agricultural sector.

$E$, according to equation (3.73), amounts to the total energy content of extracted biomass $B$ and fossil fuels $F$. The World Bank offers data on the "primary energy intensity" of the global economy which is basically the reciprocal value of $y_E$ [26]. Averaging the available data from the years 1990-2012 leads to the following estimate (see Figure B.3 in appendix B.1):

$$y_E \approx (147 \pm 15)\,\$\,\mathrm{GJ}^{-1} \tag{4.22}$$

Similarly to the estimate of $y_B$, this estimate of $y_E$ can be independently checked using current energy prices or costs. For example, the "levelized cost of electricity" for a conventional coal power plant amounts to about $100\,\$\,\mathrm{MWh}^{-1} \approx 28\,\$\,\mathrm{GJ}^{-1}$ [60]. The production costs for crude oil lie in a range of about 100 \$ per barrel which is equivalent to approximately $16\,\$\,\mathrm{GJ}^{-1}$ [74]. Even though these values lie rather below the previous estimate of $y_E$, their order of magnitude is comparable and thus the estimate is reasonable.

The parameters $e_B$ and $e_F$ indicate the energy density of biomass and fossil fuels, respectively. According to the definition of the "ton oil equivalent" (toe) one crude oil has an energy density of about 42 GJ/t. Similar values hold for natural gas ($\approx 50$ GJ/t) and coal ($\approx 30$ GJ/t). Recognizing the typical mass share of carbon of fossil fuels is about 90%, this gives an energy density with respect to carbon of:

$$e_F \approx 47\,\mathrm{GJ\,tC}^{-1} \tag{4.23}$$

Typical energy densities of biomass (wood, miscanthus, ...) amount to about $GJ\mathrm{kg}$ [66]. The mass share of carbon is typically about 50%, resulting in a value for $e_B$ of:

$$e_B \approx 40\,\mathrm{GJ\,tC}^{-1} \tag{4.24}$$

Due to the very similar values, $e_B = e_F = 40$ GJ/tC is assumed subsequently.

The capital dynamics introduced with the c:G:LAGTPK submodel (Equation (3.83)) are parametrized via $i$, $k_0$ and $k_T$. Climate impacts on physical capital will not be regarded in the context of this thesis, thus $k_T = 0$ holds.

The World Bank offers a global time series of "gross capital formation" in % of the GWP from 1970-2013 [37] (see Figure B.4 in appendix B.1). This can be identified with the parameter $i$ in the model. The arithmetic mean and standard deviation from the time series are:

$$i \approx (0.244 \pm 0.014) \approx 0.25 \tag{4.25}$$

Various estimates of the physical capital depreciation rate $k_0$ can be found in [72, Table II] and indicate the following value to be reasonable:

$$k_0 \approx 0.1\,\mathrm{a}^{-1} \tag{4.26}$$

With the exception of $w_L$, $a_B$ and $a_F$ all parameters of the submodels have, at least roughly, been estimated. Due to a lack of suitable data for estimation these remaining parameters will not be estimated but varied during bifurcation analyses in the further studies.

## 4.4 Carbon-related planetary boundaries

As the topology framework presented in section 2.1.6 is applied to the c:G model it is necessary to define a *desirable region* of the state space. For the natural sub-system the concept of *planetary boundaries* can be deployed as this notion is comparable to that of the desirable region in the topology framework [43, 83, 93]. The carbon-related boundaries have been used in combination with the carbon cycle model by Anderies et al. [2] in a recent study by Heck et al. which conceptually assessed effects of climate engineering on the carbon cycle [41]. For the topological analyses in this thesis comparable estimates of the desirable region are used.

The *climate change* boundary is given in terms of atmospheric $CO_2$ concentration and is estimated to be in the range of $350 - 450\,\mathrm{ppm}$ $CO_2$. The mean value of 400 ppm can be translated into an absolute atmospheric carbon content of some 840 GtC [41]. In terms of the ratio of the total available pre-industrial carbon this gives the following estimate of the atmospheric carbon boundary $\beta_A$:

$$\beta_A \approx 0.2\,C^*_{\mathrm{PI}} \tag{4.27}$$

The boundary to *ocean acidification* is defined via the surface ocean saturation state of aragonite. This measure is related to the carbon content in the surface oceans but cannot be directly transferred to the model as it lacks necessary chemical processes. Heck et al. estimate the ocean acidification boundary in terms of absolute maritime carbon content, $\beta_M$ as:

$$\beta_M \approx 0.3\,C^*_{\mathrm{PI}} \tag{4.28}$$

Since the topological framework is only applied to model versions which assume instantaneous diffusion and thus $M = mA$ holds according to equation (3.15), the climate change boundary and the ocean acidification boundary are (coincidentally) transgressed simultaneously because $\beta_M = m\beta_A$ for the default solubility coefficient $m = 1.5$.

The *land-system change* boundary can be related to the amount of carbon in the terrestrial

systems as it is defined via the area of forested land relative to the original (pre-human) forest cover. For simplicity forest cover is assumed to be proportional to the carbon stored in vegetation. Using the values by Ciais et al. given in Figure 2.13 the boundary of 75 % can be translated to the a terrestrial carbon boundary of $\beta_L \approx 0.6\, C^*_{\mathrm{PI}}$. In the topological analyses presented in chapter 5 a slightly smaller boundary value is assumed:

$$\beta_L \approx 0.5\, C^*_{\mathrm{PI}} \tag{4.29}$$

This choice is motivated by the practical reason that for these estimates of the boundaries $\beta_L + \beta_A + \beta_M = C^*_{PI}$ holds, and hence for the case of instantaneous diffusion all boundaries are transgressed simultaneously.

One could also try to define socio-economic boundaries, for example on the basis of the concept of the “safe and just operating space” [81]. These could for instance represent a minimum amount of calories per capita and day or a maximal tolerable death rate.

## 4.5 Overview of parameter values and confidences

The following table 4.3 gives an overview of all parameters introduced so far and their best estimates from available data. Furthermore the estimations are classified according to the confidence associated with them. The classification is based in part on the relative uncertainty of the estimates but also more generally on the suitability of the available data used for the estimation.

Parameters associated with a high confidence will mostly be kept constant during the further analyses. Those which could not be estimated from data or which feature a high uncertainty are the primary candidates for variation during bifurcation analyses.

**Table 4.3:** Overview of all estimated parameter values. Dimensional parameters can be converted to corresponding dimensionless values using the formulas given in section 3.5. These values serve as default if not stated otherwise. The background color classifies the estimates with respect to the following categories: high confidence ( green ), low confidence ( yellow ), no estimate ( red ) and neglected ( gray ).

| parameter | unit | best estimate (dimensional) | default value (dimensionless) |
|---|---|---|---|
| $\Sigma$ | $\mathrm{km}^2$ | $1.5 \cdot 10^8$ | 1 |
| $C^*_{\mathrm{PI}}$ | GtC | 4000 | 1 |
| $C^*$ | GtC | 5500 | 1 |
| $a_0$ | $\mathrm{a}^{-1}$ | $0.0298 \pm 0.0026$ | 3.0 |
| $a_T$ | $\mathrm{km}^2\,\mathrm{a}^{-1}\,\mathrm{GtC}^{-1}$ | $(3.2 \pm 0.6) \cdot 10^3$ | 11.9 |
| $l_0$ | $\mathrm{km}\,\mathrm{a}^{-1}\,\mathrm{GtC}^{-1/2}$ | $26.4 \pm 2.4$ | 16.0 |
| $l_T$ | $\mathrm{km}^3\,\mathrm{a}^{-1}\,\mathrm{GtC}^{-3/2}$ | $(1.1 \pm 0.6) \cdot 10^6$ | 25.0 |
| $\delta$ | $\mathrm{a}^{-1}$ | $0.016 \pm 0.005$ | 1 |
| $m$ | 1 | $1.43 \pm 0.02$ | 1.5 |
| $g$ | $\mathrm{a}^{-1}$ | 0.02 | 2 |
| $\Omega_0$ | $\mathrm{GtC}\,\mathrm{km}^{-2}$ | 0 | 0 |
| $\omega_L$ | 1 | 0 | 0 |
| $p$ | $\mathrm{a}^{-1}$ | 0.04 | 4 |
| $W_p$ | $\$\mathrm{a}^{-1}\,\mathrm{H}^{-1}$ | 2000 | 1 |
| $q_0$ | $\$\mathrm{a}^{-2}\,\mathrm{H}^{-1}$ | 20 | 1 |
| $q_T$ | $\mathrm{km}^2\,\$\mathrm{a}^{-2}\,\mathrm{H}^{-1}\mathrm{GtC}^{-1}$ | 0 | 0 |
| $q_P$ | $\mathrm{km}^2\mathrm{a}^{-1}\mathrm{H}^{-1}$ | 0 | 0 |
| $b$ | $\mathrm{GtC}^{3/5}\,\mathrm{a}^{-1}\,\mathrm{H}^{-3/5}$ | $(5.4 \pm 0.5) \cdot 10^{-7}$ | 1 |
| $y_B$ | $\$\,\mathrm{GtC}^{-1}$ | $(2.47 \pm 0.07) \cdot 10^{11}$ | 0.1 |
| $w_L$ | $\$\,\mathrm{km}^2\,\mathrm{GtC}^{-1}\,\mathrm{a}^{-1}\,\mathrm{H}^{-1}$ | — | varied |
| $y_E$ | $\$\ \mathrm{GJ}^{-1}$ | $147 \pm 15$ | 1 |
| $a_B$ | $\mathrm{GJ}^5\mathrm{a}^{-5}\mathrm{GtC}^{-2}\$^{-2}\mathrm{H}^{-2}$ | — | varied |
| $a_F$ | $\mathrm{GJ}^5\mathrm{a}^{-5}\mathrm{GtC}^{-2}\$^{-2}\mathrm{H}^{-2}$ | — | varied |
| $e_B$ | $\mathrm{GJ}\,\mathrm{GtC}^{-1}$ | $40 \cdot 10^9$ | 1 |
| $e_F$ | $\mathrm{GJ}\,\mathrm{GtC}^{-1}$ | $40 \cdot 10^9$ | 1 |
| $i$ | 1 | $0.244 \pm 0.014$ | 0.25 |
| $k_0$ | $\mathrm{a}^{-1}$ | 0.1 | 10 |
| $k_T$ | $\mathrm{km}^2\,\mathrm{a}^{-1}\mathrm{GtC}^{-1}$ | 0 | 0 |
| $\beta_L$ | GtC | 2000 | 0.5 |
| $\beta_A$ | GtC | 800 | 0.2 |
| $\beta_M$ | GtC | 1200 | 0.3 |

# CHAPTER 5

## Bifurcation analysis

In this chapter the qualitative *asymptotic* behavior of the model is investigated. That is, the equilibria, their stabilities and possible other attractors of the dynamical system are determined. As far as possible this is done analytically in a most general way for arbitrary parameter values. If this is not possible, numerical techniques are applied to complement the analytical findings. The number and types of equilibria and attractors depend on the parameter values. Due to the relatively large number of free parameters (see Table 4.3) it is not feasible to investigate the complete parameter space. Instead those parameters for which there is a high confidence in the estimate are fixed to their best estimates, while those which could only very roughly or not be estimated are varied during numerical bifurcation analyses.

These investigations are done separately for the different model scenarios presented in chapter 3, starting from the most simple and ending with the most complex version. All in all the findings presented in this chapter will lead to a comprehensive picture of the asymptotic dynamics of the model.

## 5.1 Planet without humans

### Equilibria

The first scenario to be considered is the planet without humans, introduced in section 3.2. If the albedo effect is neglected, the system is governed by equations (3.11), (3.12) and (3.22). The equilibrium states are calculated by setting $\dot{L} = \dot{A} = \dot{T} = 0$. For the temperature this gives the same condition as for the instantaneous greenhouse effect (see equation (3.23)):

$$T^* = \frac{1}{\Sigma} A^* \tag{5.1}$$

From the equation for the atmospheric carbon the following equilibrium can be calculated:

$$A^* = \frac{C^*_{\mathrm{PI}} - L^*}{1+m} \tag{5.2}$$

which corresponds to the condition that the diffusion is in equilibrium (see equation 3.16). Thus the equilibrium values for the terrestrial carbon $L$ are the same as those of the one-dimensional c:G:L system, given by equation (3.24).

There is no general analytic solution to this equation, however, it can be shown from the properties of the photosynthesis and respiration functions, that there is a **maximum of three equilibria** for which $\dot{L} = 0$ holds. Independent of the parameter values, one equilibrium is always located at

$$L^*_0 = 0 \tag{5.3}$$

$$A^*_0 = \frac{C^*_{\mathrm{PI}}}{1+m} \tag{5.4}$$

$$T^*_0 = \frac{C^*_{\mathrm{PI}}}{\Sigma(1+m)} \,. \tag{5.5}$$

As this corresponds to a planet without vegetation and a high temperature, it is refereed to as **desert state** of the planet. If there exist one or more equilibria with $L^* > 0$ that with the highest terrestrial carbon will be referred to as **forest state** of the planet.

If and how many additional equilibria exist depends on the specific parameter values. The analytical solutions for certain special cases are shown in Appendix A.2. For the general case where all parameters are non-zero, the solutions can be found numerically.

### Stabilities

In addition to the number and position of the equilibria, their *stability* is of interest for a qualitative analysis. For the application of linear stability analysis one need to determine the Jacobian $\mathbf{J}_{LAT}$ of the three-dimensional c:G:LAT system, evaluate it at the positions of the equilibria and compute its eigenvalues. The general Jacobian matrix is shown in appendix A.3.

However, there is a simpler way of argumentation to determine the stability. For this the system is written in the following form:

$$\dot{L} = f(L,A,T) \tag{5.6}$$

$$\dot{A} = -f(L,A,T) + \delta(C_{\mathrm{PI}}^{*} - L - (1+m)A) \tag{5.7}$$

$$\dot{T} = g\left(\frac{1}{\Sigma}A - T\right) \tag{5.8}$$

where $f(L,A,T) = f_{\mathrm{phot}}(L,A,T) - f_{\mathrm{resp}}(L,T)$ according to equation (3.1). If the system is in an equilibrium $(L^{*},A^{*},T^{*})$, then $f(L^{*},A^{*},T^{*}) = 0$ holds. Now the dynamics in the $A$-$T$-plane at fixed $L = L^{*}$ in a small neighborhood around the equilibrium is considered, which is given by the following system:

$$\dot{A} = \delta(C_{\mathrm{PI}}^{*} - L^{*} - (1+m)A) \tag{5.9}$$

$$\dot{T} = g\left(\frac{1}{\Sigma}A - T\right) \tag{5.10}$$

This is a two-dimensional linear system whose Jacobian $\mathbf{J}_{AT}$ can easily be computed:

$$\mathbf{J}_{AT} = \begin{pmatrix} -\delta(1+m) & 0 \\ g/\Sigma & -g \end{pmatrix} \tag{5.11}$$

As $\delta$, $m$ and $g$ are always positive, the determinant $\Delta_{AT} = \delta(1+m)g$ is strictly positive and the trace $\tau_{AT} = -\delta(1+m) - g$ is strictly negative. According to the classification shown in Figure 2.2 the equilibrium is asymptotically stable in the $A$-$T$-plane projection. For the determination of the stabilities of the equilibria it is hence sufficient to limit the analysis to the one-dimensional c:G:L system, given by equation (3.24). If $\left.\frac{\partial \dot{L}}{\partial L}\right|_{L=L^{*}} > 0$ the equilibrium is unstable, while it is stable for the opposite case $\left.\frac{\partial \dot{L}}{\partial L}\right|_{L=L^{*}} < 0$.

### Bifurcations via $a_T$ and $l_T$

As already mentioned the number, positions and types of equilibria are dependent on the specific parameter values. Thus an interesting question is how the properties of the equilibria are affected by variations in different parameters. As a starting point for this *bifurcation analysis* serve the default parameters which have been estimated in the previous chapter 4. As indicated in Table 4.3 the uncertainty on the parameters $a_T$ and $l_T$ is comparably higher than that on $a_0$ and $l_0$. Therefore $a_T$ and $l_T$ are chosen to be varied separately in a bifurcation analysis while all other parameters are set to their default values. The analysis has been performed numerically using the `Python` package `PyCont` which is part of `PyDSTool` [19, 20]. The resulting bifurcation diagrams are shown in Figure 5.1.

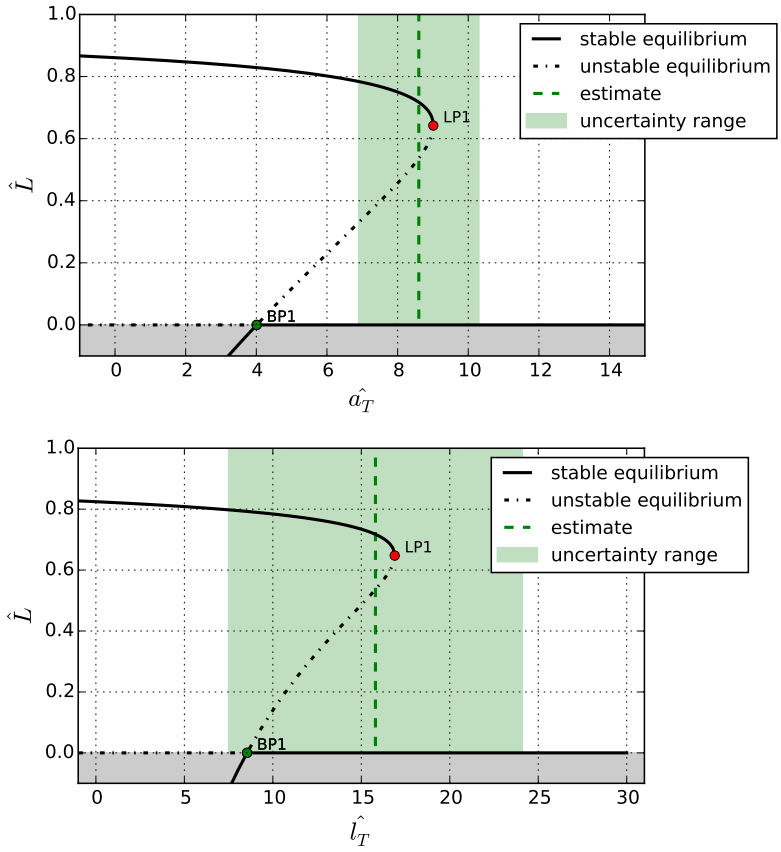


**Figure 5.1:** Bifurcation diagrams of the c:G:LAT system for a variation in $a_T$ (top) and $l_T$ (bottom), respectively. There are three regimes of which each features a different number of equilibria. At the boundaries of the regimes transcritical (BP1) and fold (LP1) bifurcations occur. For the best estimates (see Table 4.3) the system is bistable but the uncertainty ranges cover all regimes. Moreover the system exhibits a hysteresis effect if the parameters are increased above the fold bifurcation point. All parameters but the bifurcation parameter are set to default values from Table 4.3. Gray shaded regions are unphysical as $0 \leq \hat{L} \leq 1$.

The parameter space can be subdivided into three qualitatively different regimes. For low values of either $a_T$ or $l_T$ there are two equilibria, namely an unstable desert state and a stable forest state.[1] If $a_T$ (or $l_T$) are further increased a **transcritical bifurcation** occurs in which the desert state becomes stable and an additional unstable equilibrium "moves" into the region with $L > 0$. Thus there is a bistable regime in which both desert and forest state are stable. When $a_T$ (or $l_T$) are further increased the unstable saddle coalesces with the stable forest equilibrium in a **fold bifurcation**, leaving the desert state as only (stable) equilibrium.

Figure 5.1 also shows the estimates of $a_T$ and $l_T$ from section 4.1 together with their uncertainty ranges. According to the values of these best estimates the carbon cycle is characterized by a **bistable topology**. There is, however, a large uncertainty associated with the parameters such that for $l_T$ all three regimes and for $a_T$ two regimes lie within the $1\sigma$-uncertainty range. Hence from the parameter estimates a definitive classification of the topology is not possible. As the bistable scenario gained from the best estimates is also interesting from a dynamical systems' perspective this will serve as the default case throughout the rest of this thesis.

Another interesting feature of the bifurcation diagrams in Figure 5.1 is a **hysteresis effect**. Suppose the planet is in the forest state in the bistable regime. If now for instance due to some large environmental changes in the terrestrial ecosystems the parameter $a_T$ (or $l_T$) would be effectively increased, the system might change into the regime where the desert state is the only attractor. Thus the system would move towards the desert state. If now the environmental conditions would again be altered such that $a_T$ (or $l_T$) is effectively decreased to its previous value, the system would still remain in the desert state's basin of attraction. Thus for the same environmental conditions the forest state cannot be achieved anymore. Only a further decrease in $a_T$ (or $l_T$) beyond the transcritical bifurcation point would destabilize the desert state and enable a return to the forest state.

The bifurcation analysis presented above has also been conducted for the parameters $a_0$ and $l_0$ for which there is a higher confidence in the estimates. The corresponding bifurcation diagrams are shown in appendix B.2 and are qualitatively the same as those presented for $a_T$ and $l_T$.

It would also be possible to study the bifurcations which occur when two parameters are varied simultaneously. This has been done with the result that no codimension-two bifurcations occur. This is the expected outcome since the asymptotic dynamics is determined by the one-dimensional c:G:L equation (3.24) and most codimension-two bifurcations require a minimal dimension of two. Thus only the codimension-one bifurcation diagrams are shown.

1 In this parameter regime the phase portrait is topologically equivalent to that of the carbon cycle model by Anderies et al. [2].

### Phase portrait

In order to get a better impression of the dynamics of the system it is instructive to have a look at the phase portrait. As this is problematic for three-dimensional systems the phase plane is shown in Figure 5.2 for the c:G:LA system which assumes an instantaneous greenhouse effect. There are three equilibria which are located at the intersections of the nullclines (the subsets of the state space for which one derivative vanishes). Of these equilibria the desert state at $L = 0$ and the forest state at $L \approx 0.72\, C^*_{\mathrm{PI}}$ are asymptotically stable, while there is a saddle point in between, located at $L \approx 0.54\, C^*_{\mathrm{PI}}$. The stable manifold of the saddle (the trajectories with approach the saddle for $t \to \infty$) divides the phase plane into the basins of attraction of desert and forest state.

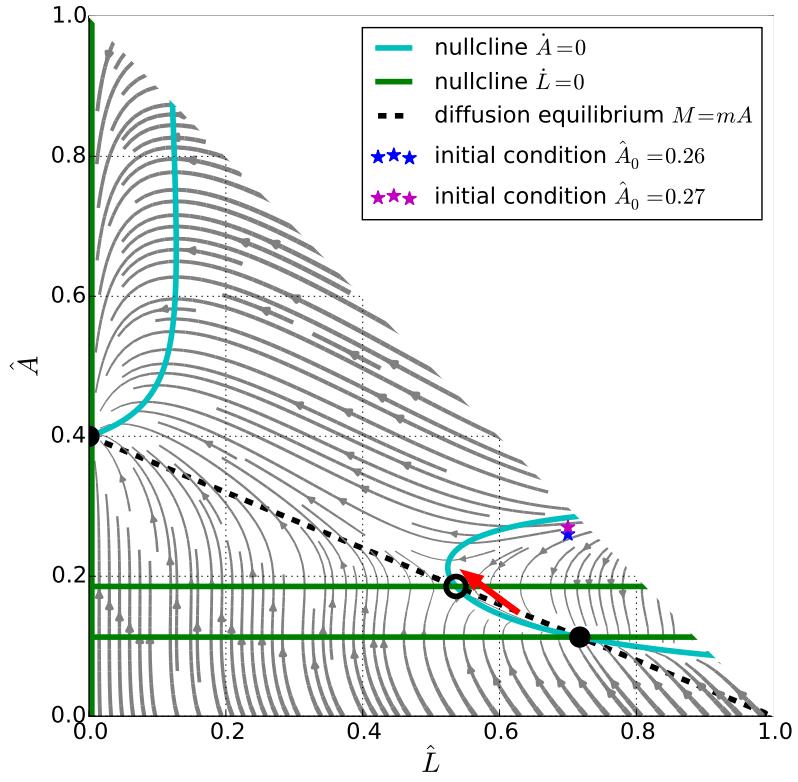


**Figure 5.2:** Phase portrait of the c:G:LA system. Gray arrows show the direction of the flow, thicker lines correspond to faster flow. There are three equilibria located at the intersections of the nullclines which are indicated by the colored lines. On the black dashed line diffusion is in equilibrium. The upper right corner is not part of the phase space due to the mass constraint $L + A \leq C^*_{\mathrm{PI}}$. The star markers correspond to the initial conditions of the trajectories shown in Figure 5.3. The red arrow reflects the actual evolution of the carbon pools from the pre-industrial state until today. Parameters are set to the default values from Table 4.3.

### Exemplary trajectories and recent evolution

Depending on the initial conditions the state of the system will either converge to the desert state or to the forest state. Figure 5.3 shows two exemplary trajectories for nearby initial conditions which are marked in Figure 5.2. In both initial states most of the carbon is stored in the terrestrial systems ($L_0 = 0.7\,C^*_{\mathrm{PI}}$) while most of the remaining carbon is airborne ($A_0 = 0.26\,C^*_{\mathrm{PI}}$ and $A_0 = 0.27\,C^*_{\mathrm{PI}}$, respectively) and only a small fraction remains in the maritime stock. Thus the initial behavior is dominated by the diffusion from the atmosphere to the oceans. Simultaneously the terrestrial carbon stock shrinks as the temperatures (derived from $A$) are relatively high. However, after a time of $t \approx 100\,\mathrm{a}$ the trajectories diverge from each other. While for the initial state with $A_0 = 0.26\,C^*_{\mathrm{PI}}$ the terrestrial systems are able to accumulate net carbon ($\dot{L} > 0$) and converge to the forest state, the trajectory starting at $A_0 = 0.27\,C^*_{\mathrm{PI}}$ ultimately ends in the desert state.

The initial conditions chosen for the exemplary trajectories are somewhat arbitrary and rather far away from the state of the carbon cycle which has been or is observed. The red arrow in Figure 5.2 schematically indicates the actual evolution of the carbon pools from the pre-industrial era until today based on the values given in Table 4.1.[1]

Two features about the evolution of the recent past are remarkable. Firstly, the actual evolution of the state of the carbon cycle (red arrow in Figure 5.2) *diametrically opposes* the "natural" direction of the flow in the model (gray arrows in 5.2), which one would expect solely from the unaffected carbon cycle dynamics. This fact can only be explained due to the considerable interference of humans with the earth system on global scales (as indicated by the numbers in Figure 2.13). In particular, the emissions of fossil carbon and land use change push the carbon cycle away from the naturally stable forest state equilibrium. The second remarkable fact is that, if the human interference is continued in the same way (corresponding to an extrapolation of the red arrow in Figure 5.2), the carbon cycle might be pushed into another basin of attraction, possibly leading to an unavoidable collapse of the terrestrial systems, even if all human activity would be stopped at that point. It should be pointed out, however, that these statements are just of a qualitative nature and that there is a high uncertainty about the parameters which generate the topology shown in Figure 5.2.

The findings presented above highlight the human impact on the earth system and hence emphasize the necessity to include the "human factor" into the model which is the topic of the next section.

1 The indicated evolution in the c:G:LA phase space should only be regarded as schematic since through the considerable emissions of fossil carbon the two-dimensional picture of the c:G:LA model is not thoroughly valid anymore.

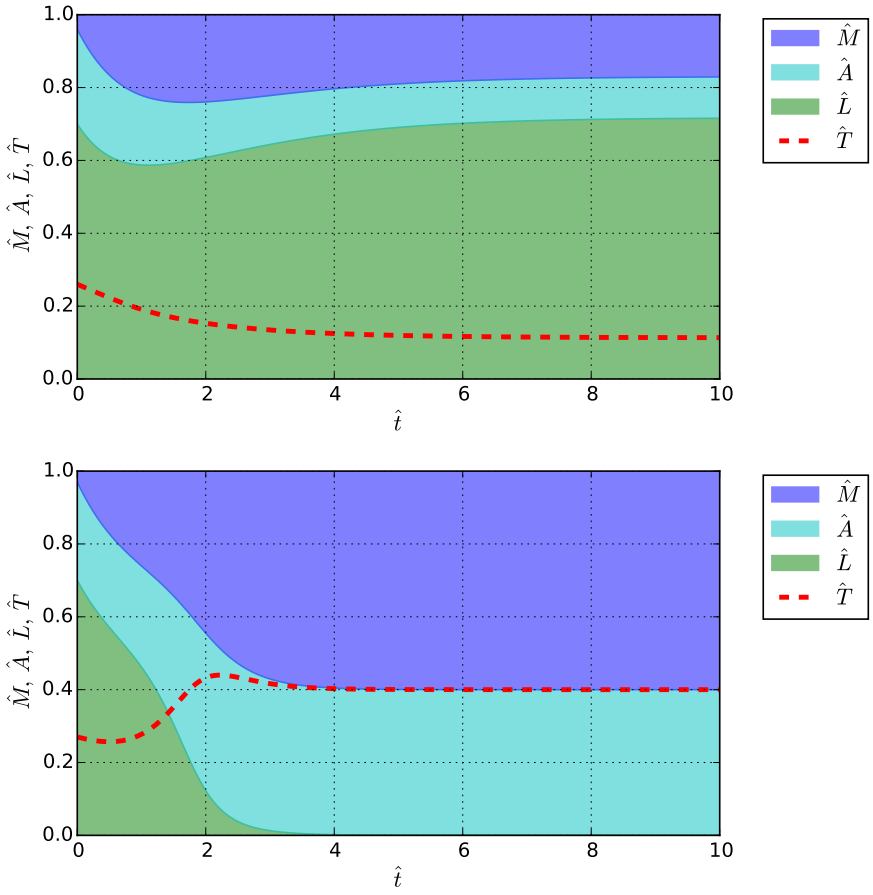


**Figure 5.3:** Exemplary trajectories of the c:G:LA system for nearby initial conditions (marked in Figure 5.2). After a similar initial behavior which is dominated by the diffusion from the atmosphere to the oceans, the trajectories diverge from each other an run into the forest and desert state, respectively. Parameters are set to the default values from Table 4.3. Initial conditions: $L_0 = 0.7\, C^*_{\mathrm{PI}}$; top: $A_0 = 0.26\, C^*_{\mathrm{PI}}$; bottom: $A_0 = 0.27\, C^*_{\mathrm{PI}}$.

## 5.2 Agricultural societies

This section focuses on the analysis of the c:G:LATP model which has been introduced in section 3.3 and includes the global human population $P$ as an additional variable. The scenario which is described by the model is comparable to hunter-gatherer or agricultural societies. In the first subsection 5.2.1 the human population $P$ is assumed to be constant over time and hence modeled as exogenous parameter. In the second part 5.2.2 an endogenously determined, dynamic population is considered which is more realistic when resources become scarce.

Throughout this section the albedo effect will be neglected and the greenhouse effect is assumed to be instantaneous since it has been shown that this does not affect the asymptotic behavior of the system.

### 5.2.1 With constant population

If the population is assumed to be constant $P$ can be treated as a parameter and the dynamics is governed by equations (3.50), (3.51) and the algebraic condition (3.23). Thus, the harvesting of biomass $B$ according to equation (3.40) is the only extension compared to the c:G:LA model.

#### Bifurcations via $P$ and $b$

As $B \propto L^{\frac{2}{5}}$ the position of the equilibrium at $L_0^* = 0$ is unaffected by the additional harvesting term. However, its stability properties might change. Whether there are more equilibria is now also dependent on the additional parameters $b$ and $P$. As under the equilibrium conditions $\dot{L} = \dot{A} = 0$ the diffusion is in equilibrium (see equation (3.51)) the positions of the equilibria can still be derived from the roots of the one-dimensional equation (3.24) under consideration of the harvesting term $B$:

$$\dot{L} = L\left[\left(l_0 - \frac{l_T(C_{\mathrm{PI}}^* - L)}{\Sigma(1+m)}\right)\sqrt{\frac{C_{\mathrm{PI}}^* - L}{\Sigma(1+m)}} - \left(a_0 + \frac{a_T(C_{\mathrm{PI}}^* - L)}{\Sigma(1+m)}\right)\right] - bP^{\frac{3}{5}}L^{\frac{2}{5}} \tag{5.12}$$

The shape of this curve is shown in Figure 5.4 for the default parameter values from Table 4.3 and different population levels $P$. For $P = 0$ the natural dynamics of the carbon cycle is reflected. For increasing $P$ the saddle equilibrium and the forest state equilibrium come closer and coalesce. Above a certain population level the desert state is left as only equilibrium.

The behavior described above corresponds to a **fold bifurcation** which occurs as $P$ is varied. The corresponding bifurcation diagram has been calculated numerically and is shown in Figure 5.5 (top).

The critical level $P_{\mathrm{cc}}$ at which the bifurcation occurs can be interpreted as a potential planetary **carrying capacity** for a fictitious agricultural society that manages its population so that is does not grow. Above this population level the planet is not able to sustain a state with an

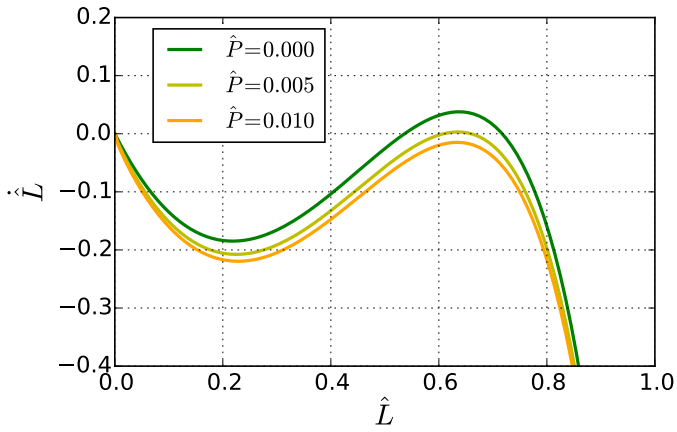


**Figure 5.4:** One-dimensional dynamics of the terrestrial carbon stock $L$ as given by equation (5.12) for different population levels. While the stable desert state equilibrium at $L = 0$ is unaffected by $P$ the stable forest state vanishes for large values of $P$. The corresponding bifurcation diagram is shown in Figure 5.5.

intact natural system. For the default parameter estimates the value of $P_{cc}$ amounts to

$$P_{cc} \approx 300 \cdot 10^6 \,\mathrm{H} \tag{5.13}$$

Interestingly, this value lies in the order of magnitude of the actual global population in medieval which will be discussed in section 6.3.

Note, that at $P_{cc}$ the equilibrium terrestrial carbon $L$ is still above the planetary boundary estimated in section 4.4.

Since the parameter $b$ which reflects the harvesting rate of biomass, has qualitatively the same effect on the dynamics as the population $P$, a variation of $b$ will also affect the value of the carrying capacity. Therefore a two-dimensional bifurcation analysis in the $b$-$P$-space has been performed in order to visualize the dependence of the carrying capacity on the harvesting rate (Figure 5.5 bottom). The boundary of the fold bifurcation divides the parameter space into two dynamically different regimes. For both low $P$ and $b$ there is a stable equilibrium with intact natural systems. For large $P$ or $b$ the carrying capacity is exceeded and the state of the system is attracted by the desert equilibrium with extinguished vegetation. Of course in that regime the assumption of a constant $P$ becomes absurd which necessitates an endogenous dynamical modeling of $P$ (see section 5.2.2).

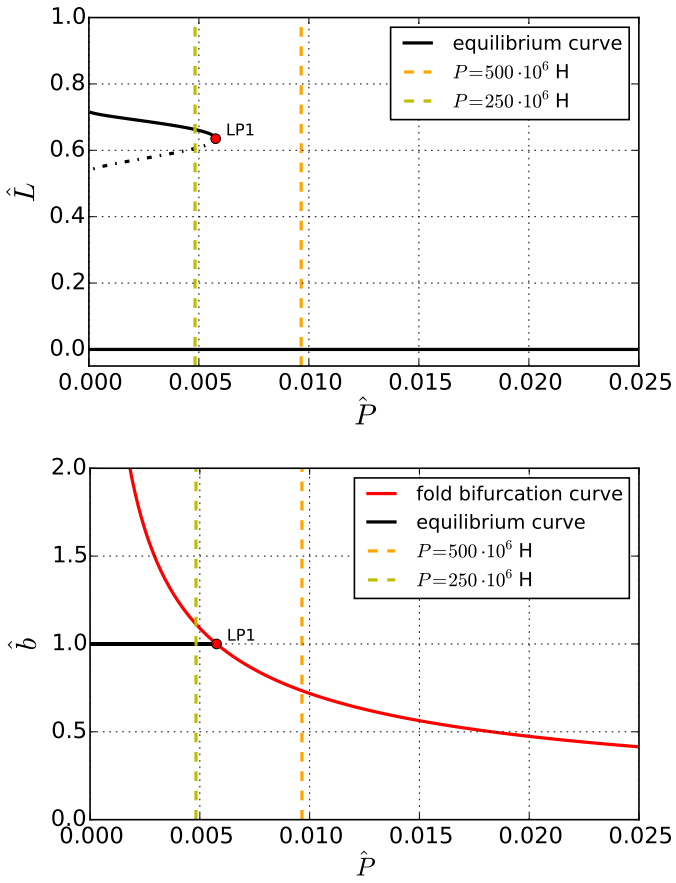


**Figure 5.5:** Bifurcation diagrams of the c:G:LAP system with static population. Top: Variation of $P$ which leads to a fold bifurcation at a critical value of $P_{cc}$ (LP1). $\hat{b} = 1$. Bottom: Two-dimensional bifurcation diagram in the $b$-$P$-space which is divided into two dynamical regimes by the fold bifurcation curve. The dashed lines serve as orientation and correspond to the population levels chosen for the topology analysis in Figures 5.6 and B.7. Parameters are set to the default values from Table 4.3.

### Topology of the managed system

The harvesting rate $b$ is modeled as a constant parameter. However, humans might be able to adjust their harvesting efforts, for instance in response to the scarcity of resources. If locally several humans will change their behavior this will effectively alter the value of the globally averaged harvesting rate. Thus one can argue that humans are to some extent able to *manage* the dynamics of the system. If additionally a *desirable region* of the phase space is defined, the topological concept presented in section 2.1.6 can be applied.

The *default dynamics* is assumed to be given by equations (3.50) and (3.51) and the default parameters from Table 4.3. The *management option* is assumed to lie in the possibility to reduce

the harvesting effort from the default value $b^+$ to a minimal value of $b^- = 0.5b^+$. Thus $b$ can be "chosen" from the interval $b \in [b^-; b^+]$. Finally, for the *desirable region* the planetary boundaries on $L$ and $A$, $\beta_L$ and $\beta_A$, which have been estimated in section 4.4 are used. The population has been set to a value of $P = 500 \cdot 10^6$ H (see also the marking in Figure 5.5) which lies within the range of estimates for the global population around the year 1500 [52] but above $P_{cc}$ such that the default dynamics with $b = b^+$ will lead to extinction of nature and management is necessary for humans to survive. The topology analysis in the sense of [43] leads to a partition of the phase space as shown in Figure 5.6.

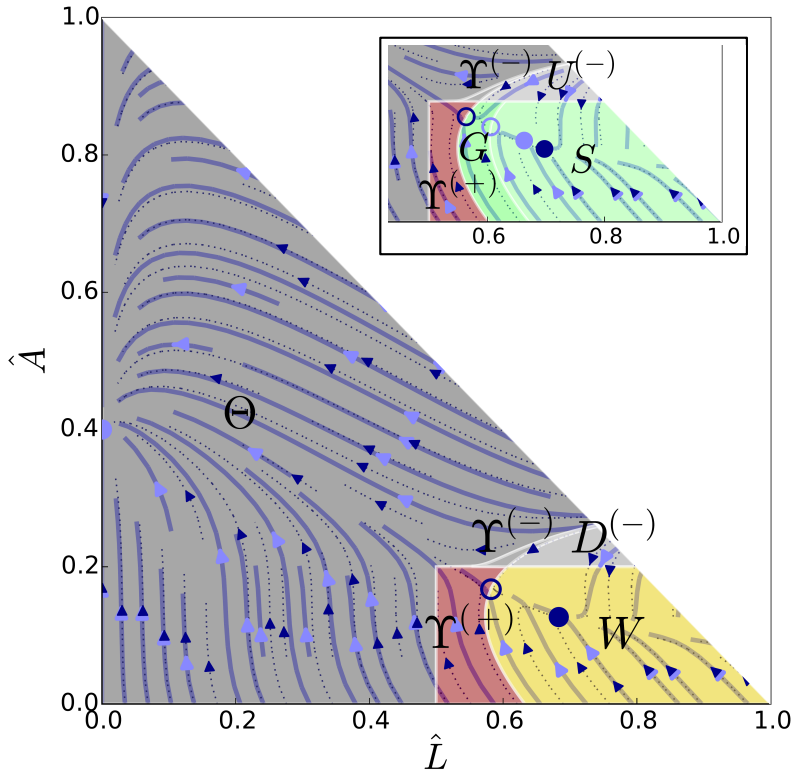


**Figure 5.6:** Partitioning of the phase space of the c:G:LAP model with constant population, according to the topology classification introduced in section 2.1.6. While the default dynamics (pale blue arrows) with $\hat{b} = 1$ has only one equilibrium at $L = 0$ the managed flow (dotted dark blue arrows) with $\hat{b} = 0.5$ has an additional attractor within the desired region. Via managing the system can thus stably stay in the sunny part forever (backwaters $W$). The other regions are explained in the text. Parameters are set to the default values from Table 4.3. $P = 500 \cdot 10^6$ H.
The inlet in the upper right corner shows a detail of the phase space partition for a constant population of $P = 250 \cdot 10^6$ H which is shown completely and discussed in Figure B.7 in appendix B.3.

As it is clear from Figure 5.5 the default flow (with $\hat{b} = 1$) for the given population of $P = 500 \cdot 10^6$ H has no equilibrium within the desired region. Therefore there is **no shelter**

and thus **no upstream region** in the phase space (recall Figure 2.10 for definitions of the topological regions). The managed flow (with $\hat{b} = 0.5$) in turn has a stable equilibrium and a saddle which lie within the sunny part of the phase space. The basin of attraction of the stable equilibrium of the managed system corresponds to the **downstream region**. The sunny part of the downstream is called **backwaters** $W$ reflecting that one can stay within the desired region forever but only with appropriate managing. From the **dark downstream** $D^{(-)}$ one can reach the backwaters. All trajectories — if managed or not — starting outside the downstream ultimately converge to the stable desert state equilibrium. The set of initial conditions which lies in the sunny part but inside the basin of attraction of the desert state form the **sunny abyss** $\Upsilon(+)$. Those who start in the dark but cross the sunny region form the **dark abyss** $\Upsilon^{(-)}$. Finally that part of the phase space from which the sunny part cannot be reached is called the **trench** $\Theta$.

A possible interpretation of these findings is, that agricultural societies of a certain size which lies above the carrying capacity and does not change over long periods are ultimately damned to overuse the natural systems unless they decrease their harvesting efforts appropriately. This could for instance be done by improving agricultural techniques which lead to higher yields. Similar developments have been observed in the human history in the form of several agricultural revolutions.

If the human population level lies below the carrying capacity also the default flow features a stable equilibrium within the desired region. In this case the topological partitioning of the phase space will look different. An example for a population of $P = 250 \cdot 10^6$ H is shown in appendix B.3.

The population level has been found to be of major importance for the qualitative dynamics of the system. So far it was prescribed as a constant parameter. This assumption, however, becomes obviously unrealistic if the resources which nourish the people get scarce. In that case one would expect the population to shrink, possibly taking pressure from the natural systems and enabling them to recover. This feedback is accounted for in the following section.

### 5.2.2 With dynamic population

The dynamics of the population $P$ is governed by equation (3.53), whereby $q_P = 0$ is assumed subsequently as the expected population densities $P/\Sigma$ in the agricultural scenario are far below critical values.

#### Equilibria

At $P = 0$ also $\dot{P} = 0$ holds so that the system is equivalent to the c:G:LAT system. Thus it has equilibria at the same positions (see sections 5.1 and A.2). However, the asymptotic stability of these is affected by the additional dimension. In particular all equilibria with $L > 0$ become unstable while only the desert state at $L = 0$ remains stable.

More interesting are those equilibria with $P > 0$ and $L > 0$ which will be called **coexistence equilibria** as they correspond to situations in which the natural and the human sphere coexist in a steady state. These equilibria also require the steady state conditions of diffusion ($M = mA$) and greenhouse effect ($T = A/\Sigma$). Hence the c:G:LATP model features the same equilibria as c:G:LP. These equilibria lie at the intersections of the nullclines where $\dot{L} = 0$ and $\dot{P} = 0$, respectively.

Setting $\dot{L} = 0$ in equation (5.12) for $L > 0$, solving for $P$ gives:

$$P(L|\dot{L} = 0) = b^{-\frac{5}{3}} L \left(f_{\text{phot}}(L) - f_{\text{resp}}(L)\right)^{\frac{5}{3}} \tag{5.14}$$

For $P > 0$ equation (3.53) has a root which is obtained at the specific wellbeing level $W^*$ at which birth and death rates are identical:

$$W^* = W_p \sqrt{\frac{q_0}{2pW_p - q_0}} \qquad \text{for: } 2pW_p > q_0 \tag{5.15}$$

Thus the equilibrium wellbeing level is solely determined by the demographic parameters $p$, $q_0$ and $W_p$. If the inequality condition $2pW_p > q_0$ is violated, death rates are higher than birth rates for all $W$ and hence no coexistence equilibrium possible. For the default parameter values estimated in section 4.2 the inequality condition holds.

It is worth noting that the equilibrium wellbeing $W^*$ (given in units of \$ per capita and year) can be easily translated into a primary energy supply per capita and year using the parameters $y_B$ and $e_B$. For the estimated parameter values from Table 4.3 this yields:

$$\frac{W^* e_B}{y_B} \approx 122\,\text{GJ}\,\text{H}^{-1}\,\text{a}^{-1} \tag{5.16}$$

which is equivalent to a daily energy supply of about 80000 kcal per person. This number is

discussed in section 6.3.

The nullclines $P(L|\dot{P}=0)$ can be calculated by setting $W^*$ to the general wellbeing function given by equation (3.56). At this point it is useful to make a distinction of cases:

**Case 1: $y_B = 0$ , wellbeing solely given by ecosystem services**
In this case the nullcline fulfills $W^* = w_L L/\Sigma$; solving for $L$ gives:

$$L(\dot{L}=0) = \frac{W^*\Sigma}{w_L} =: L^*_{\text{coex}} \tag{5.17}$$

Plugging this into (5.14) gives the coexistence equilibrium population level:

$$P^*_{\text{coex}} = \frac{W^*\Sigma}{b^{\frac{5}{3}} w_L}\left(f_{\text{phot}}(L^*_{\text{coex}}) - f_{\text{resp}}(L^*_{\text{coex}})\right) \qquad \text{for: } f_{\text{phot}}(L^*_{\text{coex}}) > f_{\text{resp}}(L^*_{\text{coex}}) \tag{5.18}$$

If the inequality condition is violated there exists no coexistence equilibrium.

**Case 2: $y_B > 0$ , per-capita consumption contributes to wellbeing**
In this case $W^* = y_B b L^{\frac{2}{5}}/P^{\frac{2}{5}} + w_L L/\Sigma$ holds for the nullcline; solving for $P$ gives:

$$P(L|\dot{P}=0) = \left(\frac{y_B b}{W^* - w_L L/\Sigma}\right)^{\frac{5}{2}} L \tag{5.19}$$

Setting equations (5.14) and (5.19) equal and raising the expression to the power of $\frac{1}{5}$ gives a conditional equation for potential coexistence equilibria $L^*_{\text{coex}}$:

$$\left[\left(l_0 - l_T\frac{C^*-L}{\Sigma(1+m)}\right)\sqrt{\frac{C^*-L}{\Sigma(1+m)}} - \left(a_0 + a_T\frac{C^*-L}{\Sigma(1+m)}\right)\right]^{\frac{1}{3}}\left(W^* - \frac{w_L}{\Sigma}L\right)^{\frac{1}{2}} = \phi_{\text{agri}} \tag{5.20}$$

$$\text{where:} \qquad \phi_{\text{agri}} = b^{\frac{5}{6}} y_B^{\frac{1}{2}} \tag{5.21}$$

For the general case it is not possible to give analytical expressions for the solutions. From the functional forms it can, however, be argued that there is a **maximum of two coexistence equilibria** (see Appendix A.4 for a graphical proof). Thus, together with the maximal number of three equilibria of c:G:LAT there is a **maximum of five equilibria** in the c:G:LATP system.

If the scalar $\phi_{\text{agri}}$ on the right-hand side of equation (5.20) is larger than the maximum of the left hand side, no coexistence equilibria exist. This means that large values of either of the

economic parameters $b$ or $y_B$ can preclude a coexistence. If $w_L = 0$ holds, $W^*$ can be included in the scalar on the right-hand side, which then, using (5.15) reads as:

$$\widetilde{\phi}_{\text{agri}} = \frac{b^{\frac{5}{6}} y_B^{\frac{1}{2}} (2pW_p - q_0)^{\frac{1}{4}}}{q_0^{\frac{1}{4}}} \tag{5.22}$$

This shows that large values of the demographic parameters $p$ and $W_p$ also might preclude coexistence equilibria while large values of $q_0$ renders them possible.

#### Stabilities

The stabilities and types of the equilibria depend on the actual parameter values. As for the c:G:LAT model it can be argued that the $T$ and $A$ dimensions do not affect the asymptotic stabilities of the equilibria and it thus is sufficient to restrict the stability analysis to the c:G:LP system.

To assess the stability of an equilibrium the eigenvalues of the Jacobian $\mathbf{J}_{LP}$, evaluated at the equilibrium position, have to be determined. As the system is two-dimensional the stability can directly be determined from the trace $\tau_{LP}$ and determinant $\Delta_{LP}$ of $\mathbf{J}_{LP}$. An analytical expression for $\mathbf{J}_{LP}$ is given in appendix A.3.

#### Phase portrait

The further analysis focuses on the planar c:G:LP system as it has the same asymptotic behavior as the c:G:LATP system. In order to get a first impression of the dynamics Figure 5.7 shows the phase portrait for the default parameter values from Table 4.3. As there is no estimate of $w_L$ it has been set to zero, which means that wellbeing is simply given by per-capita consumption.

The phase portrait features three equilibria which are all located at the nullcline with $P = 0$. These correspond to the three equilibria of the c:G:LA system shown in Figure 5.2. While the desert state with $L = 0$ is still an attractor the forest state at $L \approx 0.72\, C^*_{\text{PI}}$ has become a saddle as it is unstable in the $P$-direction. This accords with the intuition that a small population on a planet with intact natural system will be growing exponentially and thus the state will veer away from the equilibrium. Another unstable equilibrium is located at $L \approx 0.54\, C^*_{\text{PI}}$.

The nullclines with $\dot{P} = 0$ and $P > 0$, given by equation (5.19) is given by a linear slope for $w_L = 0$. The nullcline with $\dot{L} = 0$ and $L > 0$, given by equation (5.19), has a unimodal shape. The maximum turning point of this curve corresponds to the carrying capacity $P_{\text{cc}}$ which is known from the previous section. As the nullclines for $P$ and $L$ do not intersect no steady coexistence is possible for the default parameter values. In fact all trajectories, independent of the initial state, will ultimately converge to the desert state. This means that the negative

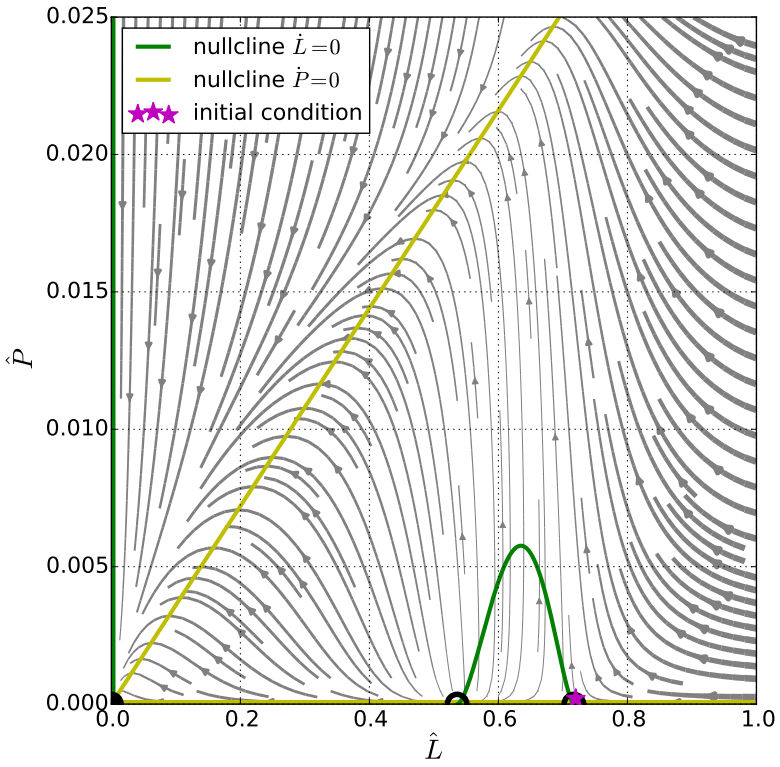


**Figure 5.7:** Phase portrait of the c:G:LP system in the collapse regime. Gray arrows show the direction of the flow, colored lines correspond to nullclines. At their intersections there are three equilibria with $P = 0$ of which only the desert state at $L = 0$ is asymptotically stable. There are no coexistence equilibria with $P > 0$ and $L > 0$. The star marker corresponds to the initial condition of the trajectory shown in Figure 5.13. Parameters are set to the default values from Table 4.3; $\hat{w_L} = 0$; $\hat{y_B} = 0.1$

feedback of population decline for scarce resource levels is not strong enough to enable a regeneration of the natural system. The subset of the parameter space which features this kind of asymptotic dynamics is denoted as **collapse regime**.

#### Bifurcations via $p$ and $b$

In the scenario with constant population a lower population level enabled a stable equilibrium with an intact natural system (see Figure 5.5). Similarly one might ask what effect a reduced reproduction rate $p$ might have on the dynamics. Therefore a one-dimensional bifurcation analysis for varying $p$ has been performed (Figure 5.8, top).

For relatively high reproduction rates such as the default value of $\hat{p} = 4$ the desert state is the only attractor of the system. Furthermore two unstable equilibria with $P = 0$ exist. If $\hat{p}$ is

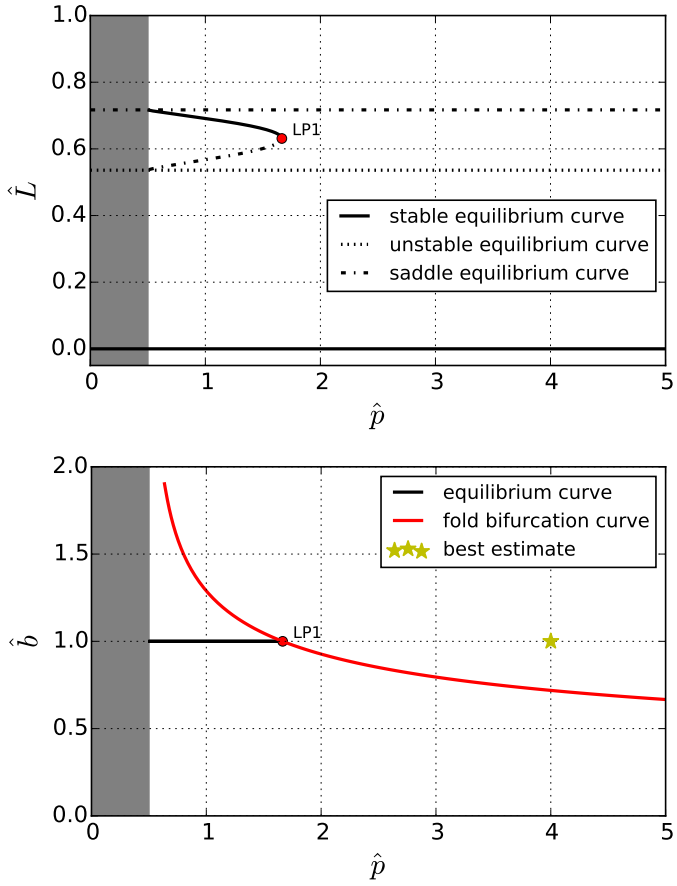


**Figure 5.8:** Bifurcation diagrams of the c:G:LP system in analogy to Figure 5.5 for constant $P$. Top: When the reproduction rate $p$ decreases a fold bifurcation of the coexistence equilibria (LP1) occurs. At $\hat{p} = 0.5$ the coexistence equilibria coalesce with the equilibria with $P = 0$ in a transcritical bifurcation. For $\hat{p} \leq 0.5$ (shaded gray) the inequality in equation (5.15) is violated and no coexistence equilibria can exist. $\hat{b} = 1$. Bottom: Two-dimensional bifurcation diagram of simultaneous variations of $p$ and the harvesting rate $b$. The fold bifurcation curve (red) divides the parameter space into two dynamical regimes. The star marker shows the location of the best parameter estimates. Remaining parameters are set to default values from Table 4.3.

decreased at some critical value a **fold bifurcation** occurs leading to two coexistence equilibria with $P > 0$ of which one is stable and one unstable. $\hat{p}$ can be further decreased to the point at which the inequality condition $2pW_p > q_0$ from equation (5.15) is violated ($\hat{p} = 0.5$). Exactly at this point the coexistence equilibria coalesce with the equilibria with $P = 0$ in a **transcritical bifurcation**. Note that for all potential coexistence equilibria the planetary boundary of the terrestrial carbon stock $\beta_L = 0.5\,C^*$ is not transgressed.

In analogy to the scenario with constant population the harvesting effort $b$ will affect the dynamics in a similar way. Thus the fold bifurcation point has been continued in the $b$-direction,

leading to the two-dimensional bifurcation diagram shown in the lower panel of Figure 5.8. Again the fold bifurcation boundary divides the parameter space into two dynamic regimes. For both low values of $p$ and $b$ the system features a stable coexistence state. If either $p$ or $b$ are increased, at some critical value a fold bifurcation will occur at which the coexistence equilibria vanish and the desert state is left as only attractor.

#### Topology of the managed system

In section 5.2.1 the topology of the c:G:LAP system with constant population was investigated under the assumption that the harvesting effort $b$ is manageable by the humans. For the case with dynamic population one might, motivated by the reasoning of Malthus (see section 2.2.3), regard the reproductivity $p$ as management option for the humans. Again the framework presented in section 2.1.6 can be applied.

The default dynamics is given by the governing equations of c:G:LP and the default parameter values from Table 4.3. The management option lies in the variation of the parameter $p$ between the default value $\hat{p}^+ = 4$ and the lower limit $\hat{p}^- = 1$. The desired region is simply given by the planetary boundary estimate for the terrestrial carbon stock from section 4.4, $\beta_L = 0.5\,C^*$. The resulting partition of the phase space is shown in Figure 5.9.

The default dynamics (with $\hat{p} = 4$) has not stable equilibrium within the desired region so that there is **no shelter** and consequently **no upstream** region. For the managed flow (with $\hat{p} = 1$) there are two coexistence equilibria within the sunny part of the phase space of which one in asymptotically stable. The basin of attraction of this equilibrium lies completely within the sunny region and therefore coincides with the **backwaters** $W$ in terms of the topological classification. From the remaining part of the sunny region the system will ultimately converge to the desert state in the dark, hence it is termed **sunny abyss** $\Upsilon^+$ as there is no chance for staying in the sun. From the dark region of the phase space it is not possible — with or without managing — to reach a sunny state so that it is completely classified as **trench** $\Theta$.

These findings indicate that the collapse which is the ultimate fate of all agricultural societies for the default parameters, can be prevented if the humans manage to adjust their reproduction to a lower level. Meanwhile lower birth rates imply a higher equilibrium wellbeing according to equation (5.15). These findings are in accordance with the hypothetical reasoning of Malthus [103, Ch. 4]. On the other hand the active management via an “unnatural” low birth rate is required forever as there is no state from which one can stay in the sun without management.

In a more general topological analysis one could account for several concurrent management options, for instance via the reproduction rate and the harvesting effort. In that case also a moderate adjustment of both parameters would lead to a coexistence state (see Figure 5.8).

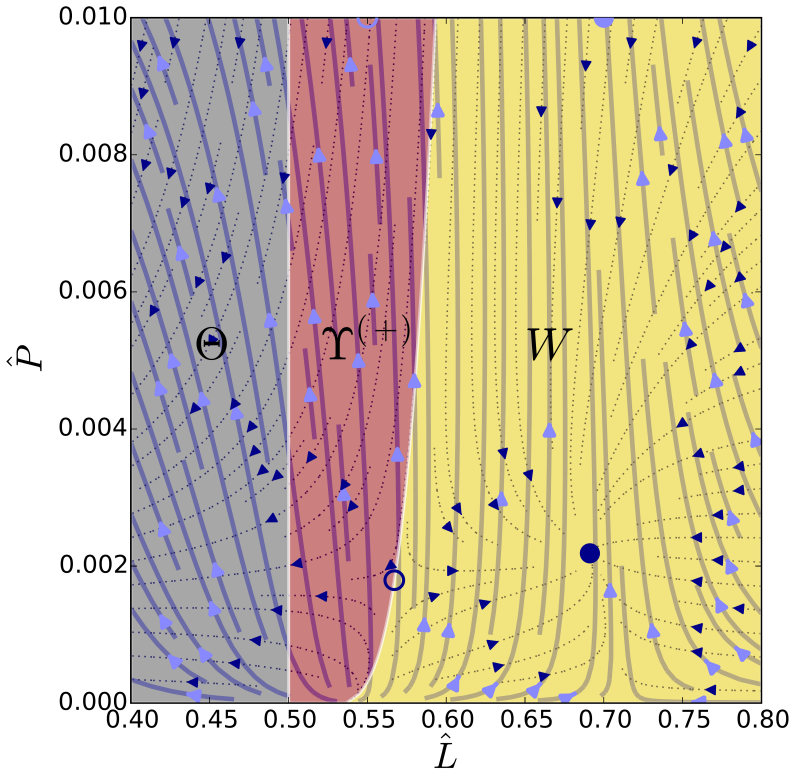


**Figure 5.9:** Partitioning of the phase space of the c:G:LP model, according to the topology classification introduced in section 2.1.6. While the default flow (pale blue arrows) with $\hat{p} = 4$ has only one equilibrium located at $L = 0$ the managed flow (dotted dark blue arrows) with $\hat{p} = 1$ has an additional stable coexistence equilibrium within the desired region. Its basin of attraction corresponds to the backwaters $W$. The remaining trajectories converge to the desert state. They form the sunny abyss $\Upsilon^+$ if the start inside the sunny part. The dark region coincides with the trench $\Theta$. Parameters are set to the default values from Table 4.3; $\hat{w_L} = 0$.

### Variation of the economic parameters $y_B$ and $w_L$

Apart from the parameters considered so far, the confidence in the estimate of the economic parameter $y_B$ which reflects the productivity of the economy, is relatively low. This is particularly true as it has been estimated from data of recent times which do not fit to the agricultural setting of the scenario. However, $y_B$ strongly affects the flow of the system as can be seen from equation (5.19) which shows that the slope of the nullcline is proportional to $y_B^{\frac{5}{2}}$. If all parameters are set to the default values but $y_B$ is halved, the phase portrait changes considerably (Figure 5.10).

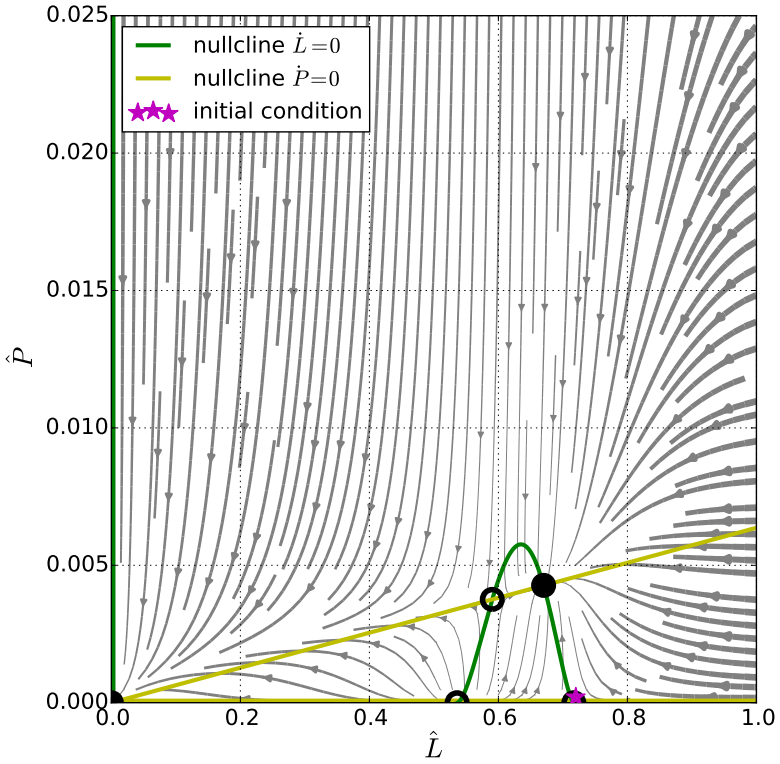


**Figure 5.10:** Phase portrait of the c:G:LP system in the sustainable regime. Gray arrows show the direction of the flow, colored lines correspond to nullclines. There are five equilibria of which the desert state and one coexistence state are asymptotically stable. The star marker corresponds to the initial condition of the trajectory shown in Figure 5.13. Except for $y_B$ the parameters set to the default values from Table 4.3; $\hat{w_L} = 0$; $\hat{y_B} = 0.05$.

Additionally to the three equilibria located at $P = 0$ the phase portrait features **two coexistence equilibria** at the intersections of the nullclines. Thus a reduction of the productivity $y_B$ has a comparable effect to the reduction of the reproduction rate $p$ or the harvesting effort $b$. However, $y_B$ does not affect the level of the carrying capacity $P_{\text{cc}}$ which $b$ does, according to

equation (5.14). The subset of the parameter space for which a stable coexistence equilibrium exists is denoted as **sustainable regime**.

The topology has also been classified for a default dynamics from the sustainable regime. The resulting partition of the phase space is shown in Figure B.8 in the appendix.

According to equation (3.56) the parameter $w_L$ which values the relative contribution of ecosystem services to wellbeing, influences the dynamics in a comparable manner as $y_B$. Therefore these two parameters have been varied during a bifurcation analysis in order to identify different regimes in the parameter space. The according bifurcation diagram is shown in Figure 5.11.

For the case $w_L = 0$ it was already clear from the previous considerations that a fold bifurcation of the coexistence equilibria occurs if one decreases $y_B$ below a certain threshold. The red curve in the bifurcation diagram shows the continuation of this bifurcation point in the $w_L$ direction. As $w_L$ increases the critical value for $y_B$ decreases, dividing the parameter space into a regime without coexistence equilibria for large values of $y_B$ and $w_L$ and a regime, in which coexistence of nature and humans is possible below the red curve. Figuratively spoken this means that higher utility which is gathered from consumption and ecosystem services, destabilizes the system.

Opposed to the two-dimensional bifurcation diagrams presented above (Figures 5.5 and 5.8) a **Bogdanov-Takens bifurcation** (BT) occurs on the fold bifurcation curve (see section 2.1.5). This points divides the fold curve into a branch at which a stable node and a saddle bifurcate, and a branch at which an unstable node and a saddle coalesce. Furthermore an **Andronov-Hopf bifurcation** (AH) curve is adjacent to the BT point. Crossing this curve from right to left (in decreasing $w_L$-direction) makes the node equilibrium change its stability from unstable to stable. Thus, below the AH curve and the upper branch of the fold curve an attracting coexistence state exists. This parameter region corresponds to the **sustainable regime** introduced above.

It is known from theory a **homoclinic bifurcation** curve is adjacent to the BT point.[1] Between the homoclinic bifurcation curve and the AH curve the phase portrait features a **limit cycle** trajectory. Since the first Lyapunov coefficient in the upper part of the AH curve is positive, the bifurcation is *sub-critical* and the limit cycle unstable. Therefore the asymptotic behavior in the parameter regime between the AH and homoclinic curve is the same as in the remaining sustainable regime.

In the lower part of the AH curve the system features a **Bautin bifurcation** (GH) point which

1 As the homoclinic bifurcation is of global type it cannot be detected by the software package used and is hence only shown schematically in the bifurcation diagram in Figure 5.11.

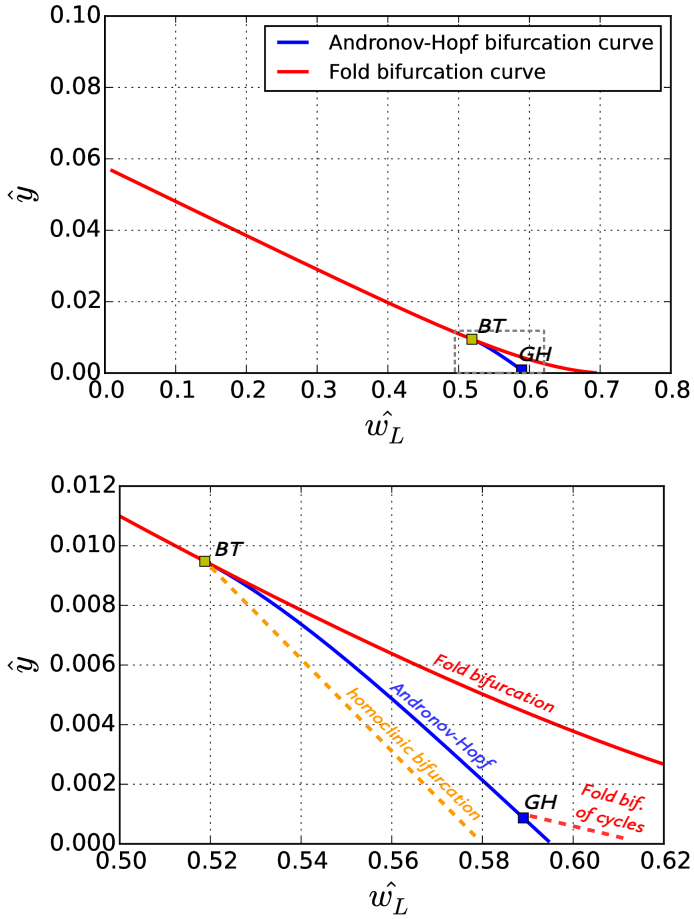


**Figure 5.11:** Codimension-two bifurcation diagram of the c:G:LP model for a simultaneous variation of the economic parameters $y_B$ and $w_L$. The lower panel shows a detail which is indicated in the upper panel. The bifurcation curves subdivide the parameter space into five topologically non-equivalent regimes. At their intersections a Bogdanov-Takens (BT) and a Bautin (GH) bifurcation occur which both have codimension two. For large values of either $y_B$ or $w_L$ the desert state is the only attractor, while for low values a stable coexistence equilibrium exists. The narrow parameter regime between the AH curve and the fold bifurcation of cycles curve features stable (attracting) limit cycles. Parameters are set to default values from Table 4.3.

also has codimension two. At this point the AH bifurcations change from sub- to super-critical. If the AH curve is crossed from the left to the right (increasing $w_L$-direction) **stable limit cycles** are born. These are possible asymptotic states in a narrow parameter regime which is bounded by the AH curve and a **fold bifurcation of cycles curve** which is also adjacent to the GH point. The unstable and stable limit cycles coalesce in the fold bifurcation of cycles, leaving an unstable

node to the right-hand side of the bifurcation curve.[1] The narrow parameter regime in which stable limit cycle trajectories are possible is referred to as **oscillatory regime**. An exemplary phase portrait for this regime is shown in Figure 5.12.

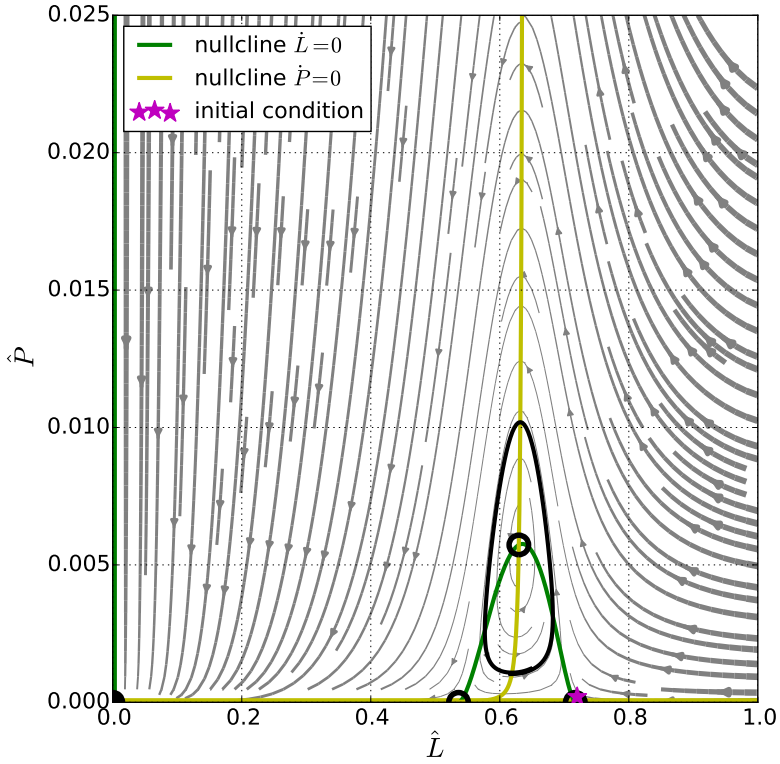


**Figure 5.12:** Phase portrait of the c:G:LP system in the oscillatory regime. Gray arrows show the direction of the flow, colored lines correspond to nullclines. There are five equilibria (two of them cannot be distinguished in this graphic) of which only the desert state is asymptotically stable. There is a stable limit cycle which constitutes another attractor of the system. The large contribution of ecosystem services to wellbeing creates a strong direct feedback loop between $L$ and $P$ and hence enables sustained oscillations in which the population changes by a factor of almost eight with a period of about 2000 years. The star marker corresponds to the initial condition of the trajectory shown in Figure 5.13. Except for $y_B$ parameters are set to the default values from Table 4.3; $\hat{w_L} = 0.59$; $\hat{y_B} = 0.001$.

1 As the fold bifurcation of cycles is of the global type, it cannot be detected with the software used and is hence indicated only schematically in the bifurcation diagram in Figure 5.11.

### Dynamic regimes and exemplary trajectories

Summing up, the bifurcation curves subdivide the $y_B$-$w_L$-parameter space into five topologically non-equivalent regions. However, there are only three different combinations of attractors which motivate the following classification of dynamic regimes:

1. Within the region below the upper branch of the fold bifurcation curve and the AH curve, there exists the *stable desert state* equilibrium and a *stable coexistence equilibrium*. This regime is called **sustainable regime** as it allows a sustained coexistence of nature and humans.
2. The comparatively small region between the super-critical branch of the AH curve and the curve of fold bifurcations of cycles is denoted **oscillatory regime**. Here the *stable desert state* and a *stable limit cycle* are the coexisting attractors.
3. In the remaining region of the parameter space the *stable desert state* is the only attractor of the system, in which all trajectories will terminate. It is termed **collapse regime** as it does not allow a steady coexistence of humans and nature.

Figure 5.13 shows exemplary trajectories from all dynamic regimes identified above. The initial conditions are marked in the corresponding phase portraits which are shown in Figures 5.7, 5.10 and 5.12. The initial conditions in each case are chosen such that the carbon cycle is in the forest state equilibrium and only a very small number of humans populates the planet.

The first scenario shows a trajectory from the sustainable regime ($\hat{y_B} = 0.05$, $\hat{w_L} = 0$). In the initial phase until $\hat{t} \approx 5 \equiv 500\,\mathrm{a}$ the population curve is S-shaped as it grows first slowly, then faster and finally again slower in absolute numbers. Simultaneously the terrestrial carbon stock is continuously decreased from its initial value towards its equilibrium value, due to the harvesting of biomass. The emissions of carbon into the atmosphere lead to an increase in atmospheric carbon which causes the temperature to rise as well. After $\hat{t} \approx 10$ there no change in the variables is visible, meaning that the steady coexistence state is reached.

The second plot shows an example trajectory from the oscillatory regime ($\hat{y_B} = 0.001$, $\hat{w_L} = 0.59$). In this case it takes longer for the population to grow because the initial wellbeing is mainly due to ecosystem services and hence much lower than in the previous scenario. After $\hat{t} \approx 15 \equiv 1500\,\mathrm{a}$ it reaches a peak value which lies above the equilibrium population of the previous case. As this peak is accompanied by a strong decline in terrestrial carbon $L$ the wellbeing $W$ drops below its equilibrium value $\hat{W}^* \approx 0.38$, leading to a fast decline of $P$. After $\hat{t} \approx 25$ $P$ reaches a minimum. This enables the natural systems to regenerate and $L$ increases relatively fast towards its forest state level. Due to the large contribution of ecosystem services to wellbeing, the high level of $L$ causes $P$ to grow again, giving the same situation as in the

initial phase. This leads to oscillations of all dynamic variables with a period of about $\Delta\hat{t} \approx 20$, corresponding to 2000 years. For similar parameter values which lie in the sustainable regime one would also observe oscillations but their amplitude would diminish over time and the system converge to the stable focus type equilibrium.

The last trajectory shown in Figure 5.13 is representative for the collapse regime ($\hat{y_B} = 0.1$, $\hat{w_L} = 0$). As in the sustainable scenario the initial phase is characterized by a high level of wellbeing and corresponding fast growth of the population. $P$ reaches a peak value after $\hat{t} \approx 6 \equiv 600\,\text{a}$ which lies far above the maximum population levels of the previous scenarios. In the following phase $P$ is moderately declining while $W$ is approximately constant, but below the equilibrium value $W^*$. In this phase of high population levels the harvesting of biomass puts large pressure onto the terrestrial systems as indicated by rapidly decreasing $L$ and increasing $T$. After $\hat{t} \approx 8$ the carbon cycle reaches a "tipping point" at which the decrease in $L$ accelerates while $A$, $M$ and $T$ rise, leading to a desert-like state after $\hat{t} \approx 12$. With a short delay the population dies out as well, since their livelihood vanishes with extinction of the terrestrial carbon stock such that after $\hat{t} \approx 15$ an unpopulated desert planet prevails.

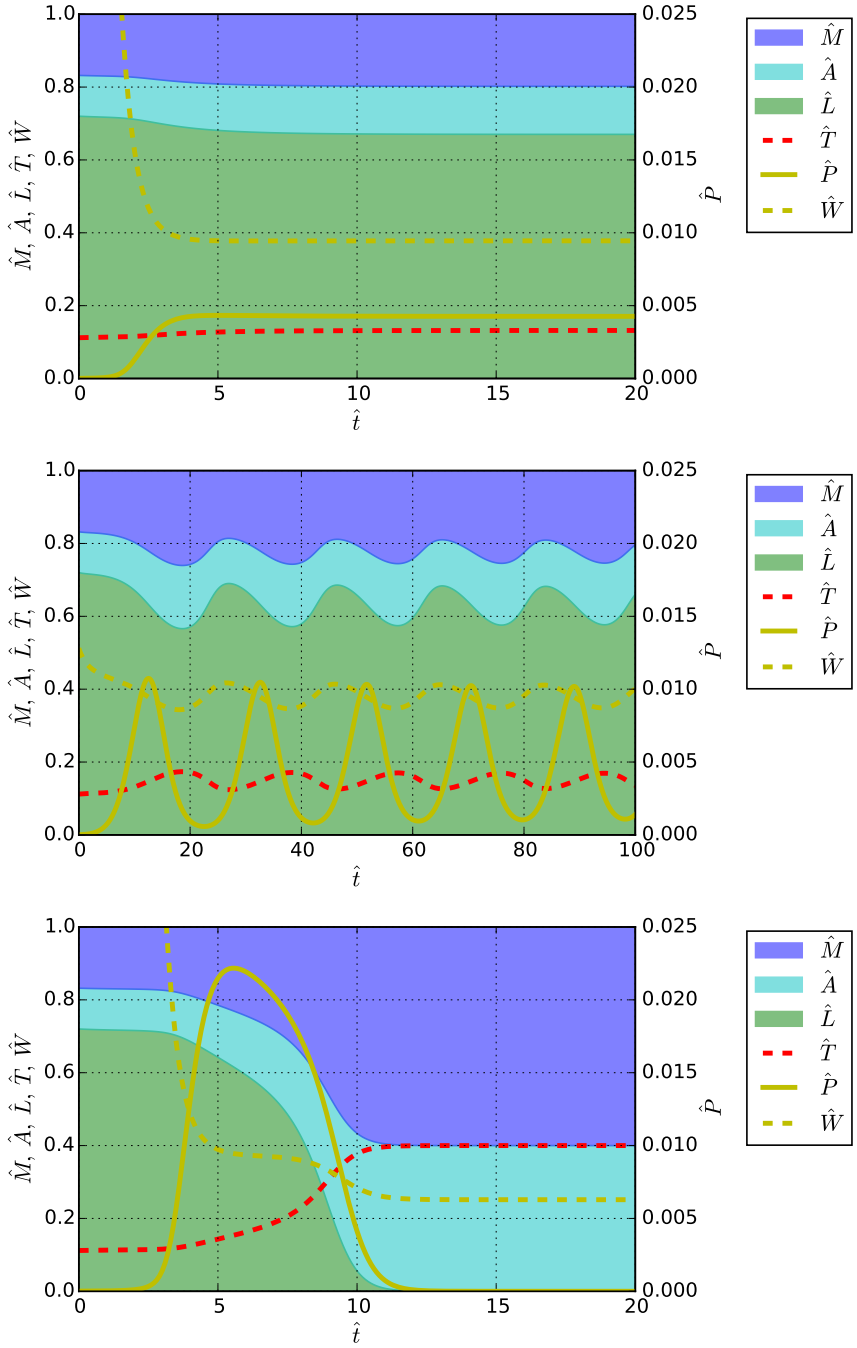


**Figure 5.13:** Exemplary trajectories of the c:G:LP model which are representative for all dynamic regimes introduced in the text. In the upper scenario ($\hat{y_B} = 0.05$, $\hat{w_L} = 0$) the asymptotic state is given by a steady coexistence of nature and humans. The second case from the oscillatory regime ($\hat{y_B} = 0.001$, $\hat{w_L} = 0.59$) features a coexistence which is characterized by oscillations in all variables with a period of $\Delta\hat{t} \approx 20 \equiv 2000\,\mathrm{a}$; interestingly, $W$ changes the least (Note the different scale of the time axis in the second plot). The lower scenario is representative for the collapse regime ($\hat{y_B} = 0.1$, $\hat{w_L} = 0$), in which humans and nature only coexist in a transient phase, but ultimately the system converges to an unpopulated desert state. The corresponding phase portraits are shown in Figures 5.7 (collapse), 5.10 (sustainable) and 5.12 (oscillatory).
Initial conditions: $\hat{L}_0 = 0.72$, $\hat{P}_0 = 10^{-5}$. Except for $y_B$ and $w_L$ the parameters are set to default values from Table 4.3.

## 5.3 Industrial societies

In this section the dynamics of the six-dimensional c:G:LAGTPK model which has been introduced in section 3.4 is analyzed. This version of the copan:GLOBAL model describes industrial societies and therefore introduces physical capital $K$ as a factor of production. Moreover it enables the use of fossil fuels which are extracted from a geological carbon stock $G$.

The first part of this section presents some general analytical findings on the asymptotic behavior of the system. These will motivate the following sections which focus on the phase space analysis of the model versions without (c:G:LPK) and with (c:G:LGPK) the use of fossil fuels.

### 5.3.1 Equilibria and Stabilities

The dynamics of the system is given by the six ordinary differential equations (3.78) to (3.83). Potential equilibria require all temporal derivatives to equal zero.

As the equation for the global mean temperature is unchanged, setting $\dot{T} = 0$ gives the same equilibrium condition as in the previous model versions:

$$T^* = \frac{1}{\Sigma} A^* \tag{5.23}$$

The dynamics of the atmospheric carbon stock is also affected by the geological carbon $G$ such that setting $\dot{A} = 0$ gives the following equilibrium condition:

$$A^* = \frac{C^* - L^* - G^*}{1+m} \tag{5.24}$$

Equations (5.23) and (5.24) hold true for every potential equilibrium state of the system. Independent of the parameter values, the remaining equations have the following trivial solution:

$$L_0^* = 0 \tag{5.25}$$

$$G_0^* = G_0 \tag{5.26}$$

$$P_0^* = 0 \tag{5.27}$$

$$K_0^* = 0 \tag{5.28}$$

where $0 \leq G_0 \leq C^*$ is an arbitrary value. Like in the previous scenarios this asymptotic state is referred to as **desert state** of the planet.

More interesting are possible **coexistence states** which require $L^* > 0$, $P^* > 0$ and $K^* > 0$.

The steady state of the geological carbon stock ($\dot{G} = 0$) requires the fossil fuel extraction to be zero ($F = 0$). If the fossil sector has a non-zero productivity ($a_F > 0$) a potential coexistence equilibrium, according to equation (3.86) thus requires:

$$G^*_{\text{coex}} = 0 \tag{5.29}$$

This means that the economy will use of fossil fuels as long as there are people and capital available, ultimately leading to a complete exploitation of the fossil resources. The time for this transient period will in general be infinite though, unless at parameter combinations for which the equilibrium is non-hyperbolic and the decay to zero is faster than exponential.

Solving the remaining equilibrium conditions for $L$, $P$ and $K$ is more involved as they depend on each other. As the asymptotic values of the remaining variables ($A^*$, $G^*$, $T^*$) are determined independently (see above), it is sufficient to consider the three-dimensional $L$-$P$-$K$-space. In this reduced phase space the nullclines at which one of the derivatives vanishes are two-dimensional surfaces. Setting $\dot{L}$ equal zero in equation (3.78) and solving for $P$ and $K$ under the condition $L > 0$ gives:

$$P(L,K|\dot{L} = 0) = \left(\frac{e_B}{a_B}\frac{f_{\text{net}}(L)}{L}\right)^{\frac{5}{2}} \frac{(a_B L^2 + a_F G^{*2})^2}{K} \tag{5.30}$$

$$K(L,P|\dot{L} = 0) = \left(\frac{e_B}{a_B}\frac{f_{\text{net}}(L)}{L}\right)^{\frac{5}{2}} \frac{(a_B L^2 + a_F G^{*2})^2}{P} \tag{5.31}$$

where $f_{\text{net}}(L) = (l_0 - l_T T^*(L))\sqrt{A^*(L)/\Sigma} - (a_0 + a_T T^*(L))$. The same can be done for $\dot{P} = 0$ in equation (3.82) under the condition $P > 0$:

$$P(L,K|\dot{P} = 0) = \left(\frac{(1-i)y_E}{W^* - \frac{w_L}{\Sigma}L}\right)^{\frac{5}{3}} \frac{P^{\frac{3}{2}}}{(a_B L^2 + a_F G^{*2})^{\frac{1}{2}}} \tag{5.32}$$

$$K(L,P|\dot{P} = 0) = \left(\frac{W^* - \frac{w_L}{\Sigma}L}{(1-i)y_E}\right)^{\frac{5}{2}} (a_B L^2 + a_F G^{*2})^{\frac{1}{3}} K^{\frac{2}{3}} \tag{5.33}$$

where $W^* = \sqrt{\frac{q_0}{2pW_p - q_0}}$. Finally, setting $\dot{K} = 0$ in equation (3.83) and demanding $K > 0$ gives:

$$P(L,K|\dot{K} = 0) = \left(\frac{k_0}{iy_E}\right)^{\frac{5}{2}} \frac{K^{\frac{3}{2}}}{(a_B L^2 + a_F G^{*2})^{\frac{1}{2}}} \tag{5.34}$$

$$K(L,P|\dot{K} = 0) = \left(\frac{iy_E}{k_0}\right)^{\frac{5}{3}} (a_B L^2 + a_F G^{*2})^{\frac{1}{3}} P^{\frac{2}{3}} \tag{5.35}$$

The next step is to use these expressions to compute the nullclines where two derivatives vanish. If (5.31) is substituted for $K$ in (5.34) one finds:

$$P(L|\dot{L}=0\wedge\dot{K}=0)=\frac{k_0 e_B^{\frac{3}{2}}}{i y_E a_B^{\frac{3}{2}}}\frac{f_{\text{net}}(L)^{\frac{3}{2}}(a_B L^2+a_F G^{*2})}{L^{\frac{3}{2}}} \tag{5.36}$$

Similarly, plugging (5.33) into (5.34) gives:

$$P(L|\dot{P}=0\wedge\dot{K}=0)=\frac{i^2(1-i)^3 y_E^5}{k_0^2}\frac{(a_B L^2+a_F G^{*2})}{(W^*-\frac{w_L}{\Sigma}L)^3} \tag{5.37}$$

Equations (5.36) and (5.37) define curves in the $P$-$L$-space at which two derivatives vanish. Setting them equal gives a conditional equation for $L^*_{\text{coex}}$, similar to equation (5.22) for the agricultural scenario. Writing out $f_{\text{net}}(L)$ using the expressions (5.23) and (5.24) gives:

$$\left[\left(l_0-l_T\frac{C^*-L-G^*}{\Sigma(1+m)}\right)\sqrt{\frac{C^*-L-G^*}{\Sigma(1+m)}}-\left(a_0+a_T\frac{C^*-L-G^*}{\Sigma(1+m)}\right)\right]^{\frac{3}{2}}\left(W^*-\frac{w_L}{\Sigma}L\right)^3 L^{-\frac{3}{2}}=\phi_{\text{ind}} \tag{5.38}$$

$$\text{where:}\qquad \phi_{\text{ind}}=\frac{i^3(1-i)^3 y_E^6 a_B^{\frac{3}{2}}}{k_0^3 e_B^{\frac{3}{2}}} \tag{5.39}$$

For $a_F>0$ $G^*=0$ holds while for $a_F=0$ the geological carbon stock is constant and $G^*=G_0$. The solutions of this equation can be determined numerically. Plugging a solution $L^*_{\text{coex}}$ into (5.36) or (5.37) gives a value for $P^*_{\text{coex}}$. Then $K^*_{\text{coex}}$ can determined by evaluating (5.31), (5.33) or (5.35) at the equilibrium values.

Equation (5.38) sets the number of possible coexistence equilibria. These lie at the intersections of the function which is defined by its left-hand side and the constant value on the right-hand side.

As for the agricultural scenario of the c:G:LATP model it can be shown that there is a maximum of **two coexistence equilibria** in the c:G:LAGTPK model (see Appendix A.4 for a graphical proof). It should be noted that besides these equilibria there might be other attractors in the system such as limit cycles for certain parameter values, whose existence has not been studied within the scope of this thesis.

The scalar $\phi_{\text{ind}}$ can be viewed as an effective parameter whose variation leads to a fold bifurcation of the coexistence equilibria at a critical value $\phi_{\text{ind, crit}}$. For values of $\phi_{\text{ind}}$ above this threshold no steady coexistence of nature and humans is possible. Thus large values of the productivities $y_E$ and $a_B$ destabilize the system while large depreciation rates $k_0$ and energy

densities $e_B$ stabilize it. The investment ratio $i$ has a non-monotonous influence as it appears in $\phi$ as $i^3(1-i)^3$. If $w_L = 0$, $W^*$ can be incorporated into the right-hand side of (5.38), giving a differently defined scalar:

$$\widetilde{\phi}_{\text{ind}} = \frac{i^3(1-i)^3 y_E^6 a_B^{\frac{3}{2}} (2pW_p - q_0)^{\frac{3}{2}}}{k_0^3 e_B^{\frac{3}{2}} q_0^{\frac{3}{2}}} \tag{5.40}$$

In analogy to the agricultural scenario this shows that large values of $p$ and $W_p$ might preclude coexistence equilibria while $q_0$ has a stabilizing effect.

It remains to determine the stabilities of the equilibria. As in the previous cases this can be done by computing the eigenvalues of the Jacobian of the system, evaluated at the equilibrium positions. Due to the costly analytical calculations this is not done within this thesis. However, it turns out that the additional dimensions compared to the c:G:LATP model do not affect the stabilities qualitatively. That is, the desert state is still a stable equilibrium, independent of the parameter choices. All other equilibria with $P = K = 0$ are linear unstable against simultaneous perturbations in both $P$ and $K$. The coexistence equilibrium with the lower value of $L$ is always an (unstable) saddle point. That with the higher value of $L$ is typically stable while it might become unstable in certain parameter regimes.

The analytical findings presented above show that the asymptotic behavior of the system is not depending on the dynamics of the geological carbon stock $G$. In the following two sections, two scenarios are considered, the first being without and the second with the use of fossil fuels.

### 5.3.2 Without fossil fuels

In the previous section all possible equilibrium states of the c:G:LAGTPK model were determined. In order to get a better impression of the actual dynamics, it is helpful to have a look at the phase portrait of the system. For now the use of fossil fuels is not considered which can be achieved by setting $a_F = 0$ as then $\dot{G} = 0$ and thus $G(t) = G(0) = G_0$. If furthermore the greenhouse effect and the diffusion are assumed to be instantaneous processes, the dynamics takes place in the three-dimensional $L$-$P$-$K$-phase-space (c:G:LPK).

#### Phase portrait

If all parameters are set to the default values from Table 4.3 and further $w_L = 0$, $\hat{a_B} = 60$ and $G_0 = 0.27\,C^*$ (as in Table 4.1) are assumed, there is a stable coexistence equilibrium which can be determined from equation (5.38):

$$\begin{aligned} L^*_{\text{coex}} &\approx 0.49\,C^* \\ P^*_{\text{coex}} &\approx 11.2 \cdot 10^9\,\text{H} \\ K^*_{\text{coex}} &\approx 28.3 \cdot 10^{12}\,\$ \end{aligned} \tag{5.41}$$

This means an average capital per person of $(\frac{K}{P})^*_{\text{coex}} \approx 2520\,\$\,\text{H}^{-1}$ in the coexistence state. These values seem to be of a realistic order of magnitude, even though the biomass productivity $\hat{a_B}$ was more or less arbitrarily chosen.

Figure 5.14 shows two-dimensional sections of the three-dimensional $L$-$P$-$K$-space at the coexistence equilibrium positions. All phase portraits feature the coexistence equilibrium at the intersections of the three nullclines derived in section 5.3.1. Furthermore in all cases the two nullclines of the considered variables have an intersection at the origin. These are, however, no equilibrium points as the derivative is non-zero in the direction perpendicular to the considered section.

The section of the $P$-$L$-space is qualitatively the same as that of the c:G:LATP model, shown in Figure 5.10, however, the $P$-nullcline has a slightly different shape. The section in the $K$-$L$-space looks very similar, which is due to the fact that $K$ and $P$ exhibit qualitatively similar dynamics. The section in the $P$-$K$ space reflects the population and capital dynamics at a the equilibrium value $L^*_{\text{coex}}$. For the fixed resource level only the coexistence state is attracting while the trajectories are repelled from the origin, at which two nullclines intersect.

The planar sections of the phase portrait only partly reflect the dynamics. Another possibility to visualize the dynamics is presented in Figure 5.15. It shows trajectories as thin lines in the

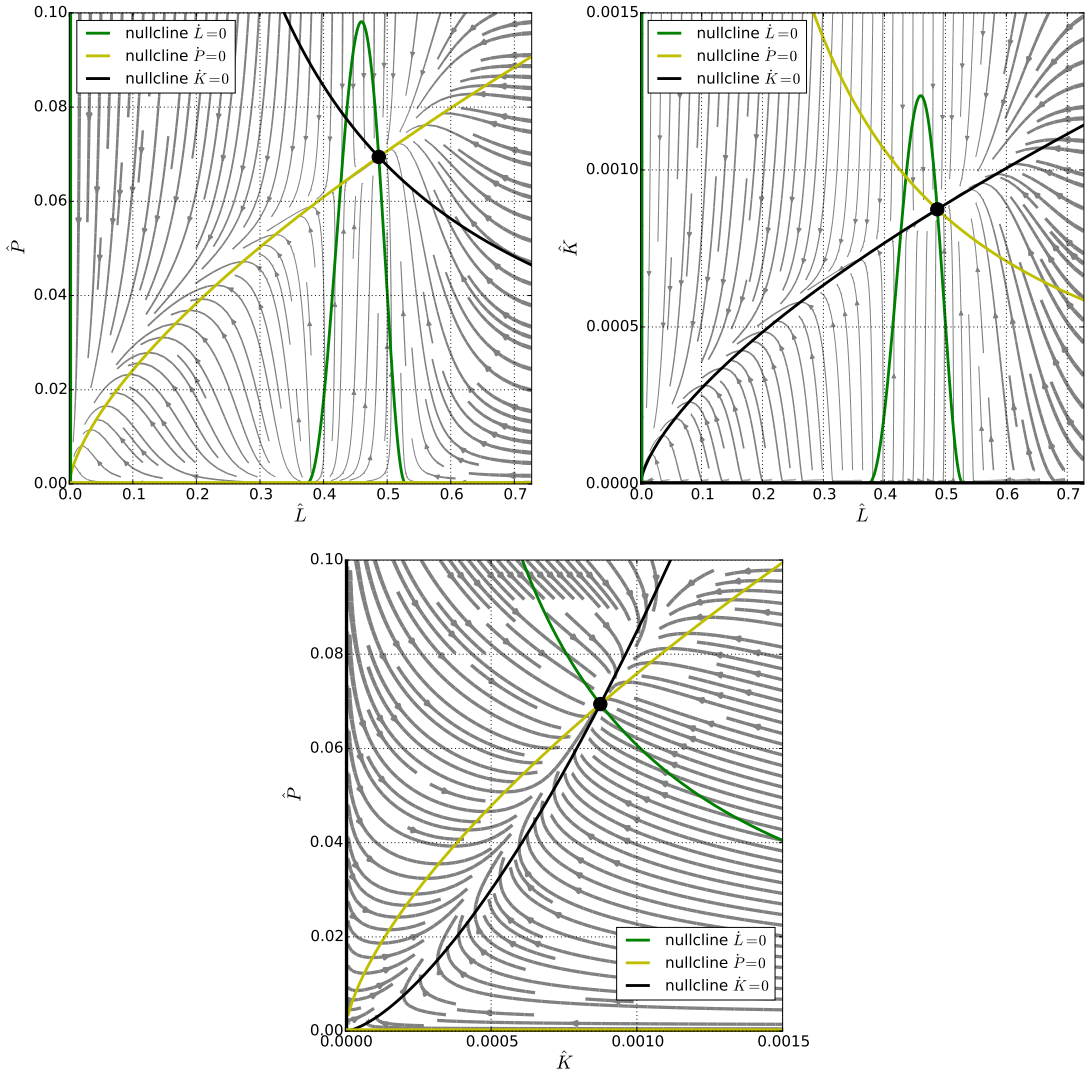


**Figure 5.14:** Two-dimensional sections of the phase portrait of the c:G:LPK model which describes capitalistic societies without the use of fossil fuels. The sections are shown at the position of the coexistence equilibrium given by equation (5.41). Gray arrows represent the flow whereby thicker lines correspond to faster flow. Colored lines indicate the nullclines according to equations (5.30) to (5.35). In the $P$-$L$-section and $K$-$L$-section (upper panels) the dynamics is qualitatively similar to that of the planar c:G:LP model shown in Figure 5.10. In both cases besides the attracting coexistence state the origin is attracting the flow. In the $P$-$K$-section (lower panel) the coexistence equilibrium is the only attractor. Note that the flow velocities in the $P$-$K$-section are scaled down by a factor of 10 compared to the upper plots. Thus, at high values of $L$ the dynamics in the $P$-$K$-direction is much faster than in the $L$-direction which can also be seen in the three-dimensional visualization in Figure 5.15. Parameters are set to default values from Table 4.3. $w_L = 0$, $\hat{a_B} = 60$, $\hat{a_F} = 0$.

$L$-$P$-$K$-space which start from randomly drawn initial conditions for the same parameter values as in Figure 5.14. In the upper panel (with $\hat{a_B} = 60$) the trajectories concentrate at the two stable equilibria, the desert state at $L_0^* = P_0^* = K_0^* = 0$, and the stable coexistence state. The coloring of the trajectories allows to roughly distinguish the basins of attraction of the two attractors. The saddle equilibrium which can be seen in the center of the indicated part of the phase space, lies at the boundary of the two basins of attraction.

As discussed in section 5.3.1 for parameter values which give $\phi > \phi_{\text{crit}}$, there are no coexistence equilibria. The lower panel of Figure 5.15 shows the three-dimensional phase portrait for a slightly larger biomass sector productivity of $\hat{a_B} = 80$. On the first look it is very similar to the plot in the upper panel as there are also two regions in which the trajectories concentrate. However, in this case the two regions are not separated but in fact connected via a thin "channel" through which all trajectories from the part of the phase space with large $L$ run into the part with low $L$ and ultimately converge to the desert state. This corresponds to the finding from Figure 5.14 that for large $L$ the dynamics in the $P$-$K$-section is much faster than that in the $L$-direction. Therefore at large $L$ the trajectories first approach the state where $\dot{P} = \dot{K} = 0$ and then the state changes in $L$-direction.

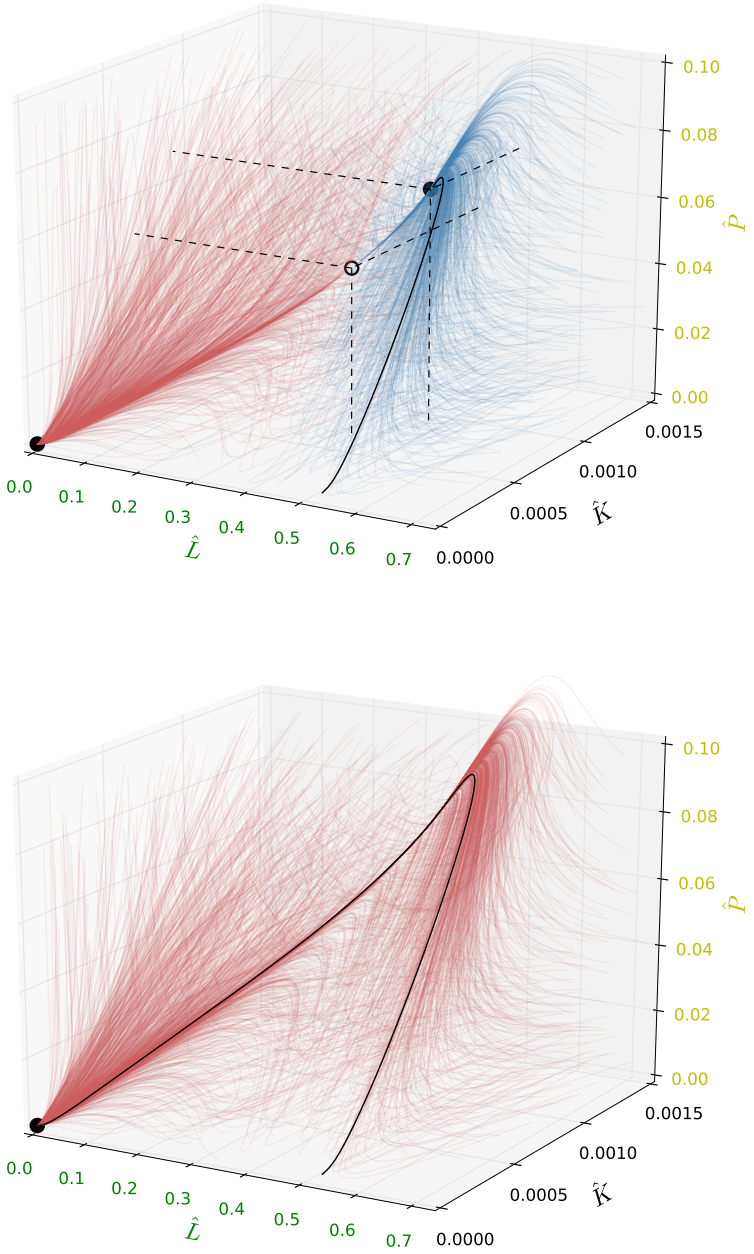


**Figure 5.15:** Three-dimensional visualization of the phase portrait of the c:G:LPK model via trajectories starting from randomly drawn initial conditions. In the upper plot ($\hat{a_B} = 60$) there are two attractors, the desert state at the origin and a coexistence equilibrium given by equation (5.41). The coloring of the trajectories helps to distinguish the two distinct basins of attraction. The general geometric structure of the flow in the lower plot ($\hat{a_B} = 80$) is very similar to the upper case. However, all trajectories converge to the desert state. Thereby trajectories starting at high $L$ values run through a channel-like structure which connects the distinct basins of attraction from the upper plot. The black colored trajectories correspond to those shown in Figure 5.16. Parameters are set to the default values from Table 4.3. $w_L = 0$, $\hat{a_F} = 0$.

### Exemplary trajectories

To complete the analysis of this section Figure 5.16 shows two exemplary trajectories for the same initial conditions but different values of $a_B$, corresponding to the phase portraits in Figure 5.15. As $a_F = 0$ the geological carbon stock is constant over time in both cases. The initial behavior of the trajectories in both cases is very similar. Both population $P$ and physical capital $K$ increase fast, reaching a maximum after $\hat{t} \approx 5$, corresponding to 500 years. In the first case (with $\hat{a_B} = 60$) $P$ and $K$ show a small overshoot but reach their equilibrium values after $\hat{t} \approx 10$. For larger $\hat{t}$ the system is in the stable coexistence state of the natural and the human spheres. In the second case (with $\hat{a_B} = 80$) $P$ and $K$ also start to decline after a small overshoot. However, they keep decreasing slowly over a transient period of $\Delta\hat{t} \approx 20$, in which also the terrestrial carbon stock diminishes. Over this transient period the wellbeing $W$ is approximately constant and lies slightly below its equilibrium value $W^*$. After $\hat{t} \approx 25$ the decreasing of $L$, $P$ and $K$ accelerates and the system collapses into the desert state which it exhibits from $\hat{t} \approx 35$ onwards.

Generally the trajectories of $P$, $K$ and $Y$ feature a very similar shape. There is no growth of capital when population declines or vice versa. Thus also the total economic output cannot grow decoupled from the population or capital dynamics. This can be explained due to the fact that only labor, physical capital and resources are considered as factors of production while there is no independent *technology* variable which would enable a decoupling of population dynamics and economic growth (see section 6.3 for a further discussion).

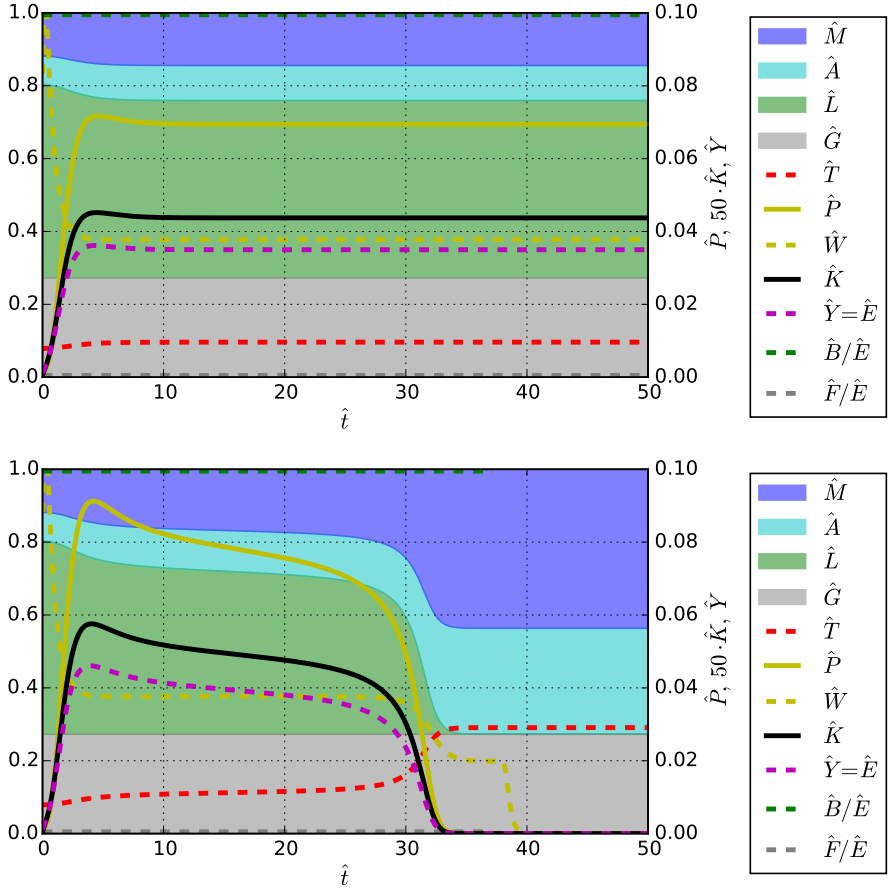


**Figure 5.16:** Exemplary trajectories of the c:G:LPK model for the same initial conditions but different biomass sector productivities $\hat{a_B}$. In the initial phase (until $\hat{t} \approx 5$) the system's state evolves very similar with $P$, $K$ and $Y$ increasing fast, overshooting a maximum and then decreasing slowly. In the upper case with lower productivity ($\hat{a_B} = 60$) the system reaches a steady coexistence state after $\hat{t} \approx 10 \equiv 1000$ a. For higher productivity ($\hat{a_B} = 80$) there is a transient period of $\Delta\hat{t} \approx 20 \equiv 2000$ a with slowly decreasing $L$, $P$, $K$ and $Y$ which is followed by a fast collapse into the final desert state with $L = P = K = 0$.
Initial conditions: $\hat{L}_0 = 0.53$, $\hat{G}_0 = 0.27$, $\hat{P}_0 = 10^{-3}$, $\hat{K}_0 = 10^{-5}$. Parameters are set to default values from Table 4.3. $w_L = 0$, $\hat{a_F} = 0$.

### 5.3.3 With fossil fuels

After having studied capitalistic societies which do not use fossil fuels in the previous section, for the following results the usage of both biomass and fossil resource is allowed. The scenario thus corresponds to the industrial era, the most recent phase in the human history. Technically this is achieved by choosing a fossil sector productivity $a_F > 0$ in the governing equations of the c:G:LAGTPK model.

As it was argued in section 5.3.1 the asymptotic state of the system in this case is characterized by $G^* = 0$ (equation (5.26)) because the people will exploit the geological carbon stock as long as there are fossil fuels available. The productivity parameter $a_F$ just determines the speed and hence the timescale of the process of fossil fuel extraction. It was further shown in section 5.3.1 that the existence of a coexistence equilibrium is independent of the fossil sector productivity $a_F$ as this parameter does not appear in equation (5.38). Thus the dynamics of the geological carbon stock does not affect the asymptotic behavior qualitatively and can rather be regarded as a side process whose speed is set by the other variables and the productivity parameter $a_F$.

The carbon which is extracted from the geological pool is emitted into the atmosphere from where it is being taken up by the ocean via diffusion and the vegetation via photosynthesis. Hence it is incorporated into the natural carbon cycle, thereby shifting its equilibrium state to higher absolute values of $L$, $A$ and $M$. This means that even though the carbon cycle might rest in a "forest state" with high $L$, the increasing amounts of maritime carbon (which is related to ocean acidification) and atmospheric carbon (which causes climate change) might push the earth system into an undesirable state.

#### Fixed total emissions

Even though the dynamic equations predict a complete exploitation of the geological carbon stock for large times, one might consider the hypothetical case in which the emissions due to fossil fuels are limited to an accumulated amount denoted by $E$. The remaining carbon in the ground $G_\mathrm{r}$ is then given by:

$$G_\mathrm{r} = G_0 - E \tag{5.42}$$

$G_r$ can be plugged into equation (5.38) to determine how the position of the potential coexistence equilibria changes due the emitted carbon amount $E$. Since the left-hand side of equation (5.38) is decreasing with $E$, also the critical right-hand side value $\phi_{\mathrm{ind,\,crit}}$ at which the coexistence equilibria bifurcate, is lowered. This means that while the existence of the equilibria is not affected by the use of fossil fuels, a release of geological carbon into the natural carbon cycle causes the sustainable parameter regime to shrink. This effect is shown for the

biomass sector productivity $a_B$ in the bifurcation diagram in Figure 5.17.

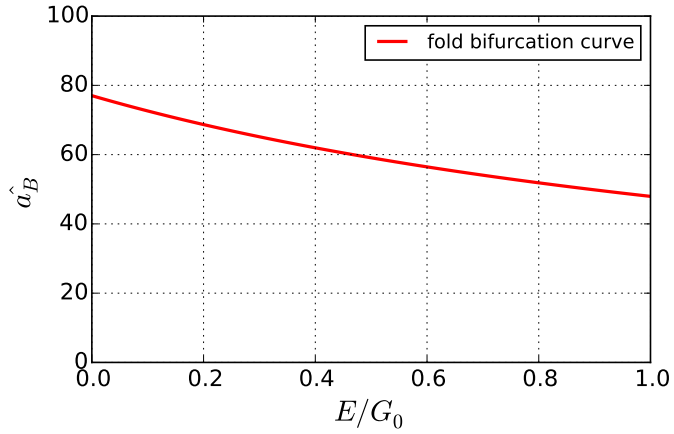


**Figure 5.17:** Bifurcation diagram of the c:G:LGPK system for a variation of the total emissions $E$ and the biomass sector productivity $a_B$. If no biomass is used ($a_B = 0$) coexistence equilibria exist independent of the total emissions $E$. The critical value for $a_B$ above which the system is in the collapse regime, however, decreases with the amount of emissions. When the use of fossil fuels is not prescribed but rather modeled dynamically, $E/G_0 = 1$ holds asymptotically.
Parameters are set to default values from Table 4.3; $\hat{w}_L = 0$; $\hat{G}_0 = 0.27$.

### Exemplary trajectories

From now on the dynamically determined fossil use is considered again. As the qualitative asymptotic behavior is unchanged compared to the c:G:LPK model (without use of fossil fuels), the phase portrait will look qualitatively similar as those shown in Figures 5.14 and 5.15, merely with shifted equilibria towards larger values of $L$. Therefore the following analysis focuses on specific trajectories which are observed for different values of the sectoral productivities $a_B$ and $a_F$.

The upper plot in Figure 5.18 shows the trajectory for a scenarios in which fossil fuels are the only energy form used by humans. This is achieved by setting $\hat{a_B} = 0$ and $\hat{a_F} = 80$ which is a more or less arbitrary choice. The initial conditions are chosen such that the natural system is in the forest state equilibrium and the levels of population and capital are very low. In an initial phase of high wellbeing $W$ the population $P$ and physical capital $K$ increase fast, reaching a maximum after $\hat{t} \approx 4 \equiv 400\,\mathrm{a}$. Meanwhile the geological carbon stock $G$ is steadily decreasing. After the peak $P$ and $K$ decrease slowly but monotonously, indicating that the wellbeing lies below the equilibrium value $W^*$. While $W$ stays at a constant level, $P$, $K$ and $G$ are further decreasing. The speed of this decrease is, however, diminishing; after $\hat{t} \approx 20$ the geological carbon stock is reduced by a factor of two and after $\hat{t} = 50$ there is still roughly a third of the initial resources available. Even after $\hat{t} = 200$ there is a visible amount of fossil fuels left,

indicating the very slow convergence towards the equilibrium. It is noteworthy that almost all of the emitted geological carbon is taken up by the terrestrial systems as the maritime and atmospheric stock only slightly increase. For this reason also the temperature increase due to the emission of fossil carbon is relatively small.

In the second scenario in Figure 5.18 both biomass and fossil fuels are used by humans with the biomass sector having a relatively low productivity ($\hat{a_B} = 20$, $\hat{a_F} = 80$). Due to the larger stock size of the terrestrial carbon pool $L$ compared to the geological pool $G$ ($L_0 > G_0$) the shares of both energy sectors are initially almost equal ($\hat{B}/\hat{E} \approx \hat{F}/\hat{E}$). In the initial phase, again, $P$ and $K$ are increasing fast, reaching a peak after $\hat{t} \approx 4 \equiv 400\,\mathrm{a}$ and then slowly start to decrease. Meanwhile $G$ declines and the emitted carbon is mainly taken up by the terrestrial systems such that $L$ grows. Due to the increasing availability of biomass the energy share of this sector outruns the fossil sector's share, after $\hat{t} \approx 20$ the $\hat{B}/\hat{E}$ lies above 80 %. After a period in which $P$ and $K$ were almost constant, these variables start to rise again at a very slow speed. After $\hat{t} = 200$ $P$ and $K$ have reached their equilibrium values which lie above their initial peak. The biomass share for large $\hat{t}$ is close to 100 % while the fossil carbon pool is almost completely exploited.

Finally, in the lower panel of Figure 5.18 a scenario with fossil fuels and relatively high biomass productivity is considered ($\hat{a_B} = 60$, $\hat{a_F} = 80$). As expected in this case the initial share of the biomass sector of about 75 % is much higher than that of the fossil sector. The collectively higher productivity of the energy sectors compared to the previous scenarios leads to a faster initial increase in $P$ and $K$. Like the total economic output $Y$ these variables reach a peak after $\hat{t} \approx 4$ and stabilize at a plateau around $\hat{t} \approx 10$. Also the terrestrial carbon stock $L$ stays at a constant level as the losses due to intensive harvesting are compensated by the uptake of emitted fossil carbon. As the geological carbon pool diminishes, additional pressure is put on the natural system, indicated by the increasing share of biomass in the energy use. The emission of carbon into the atmosphere cannot be compensated for by the terrestrial systems alone so that also the maritime and atmospheric stocks grow, accompanied by an increase in temperature. At some point (after $\hat{t} \approx 15$) the pressure on the carbon cycle becomes too large to sustain a coexistence of humans and nature. Over a short period of $\Delta\hat{t} \approx 5$ the natural system collapses into a desert state with $L = 0$ and high temperature. As the biomass production vanishes the economic output and wellbeing also drop, simultaneously with $P$ and $K$. After the collapse there are still fossil fuels available such that the remaining people can still exploit the geological carbon stock to cover their energy demand. From $\hat{t} \approx 25$ the trajectories of the socio-economic subsystem ($P$, $K$, $Y$ and $W$) evolve in a similar manner as in the upper scenario

with $a_B = 0$. However, the state of the natural subsystem is not human-friendly at all.[1] As the terrestrial systems are not able to recover the humans are solely dependent on fossil fuels and the population will die out with the complete exploitation of the geological carbon at large $\hat{t}$.

1 Note that accounting for climate impacts via the parameters $q_T$ and $k_T$ would cause $P$ and $K$ to decrease much faster in this case. For the trajectories presented here these effects are, however, neglected.

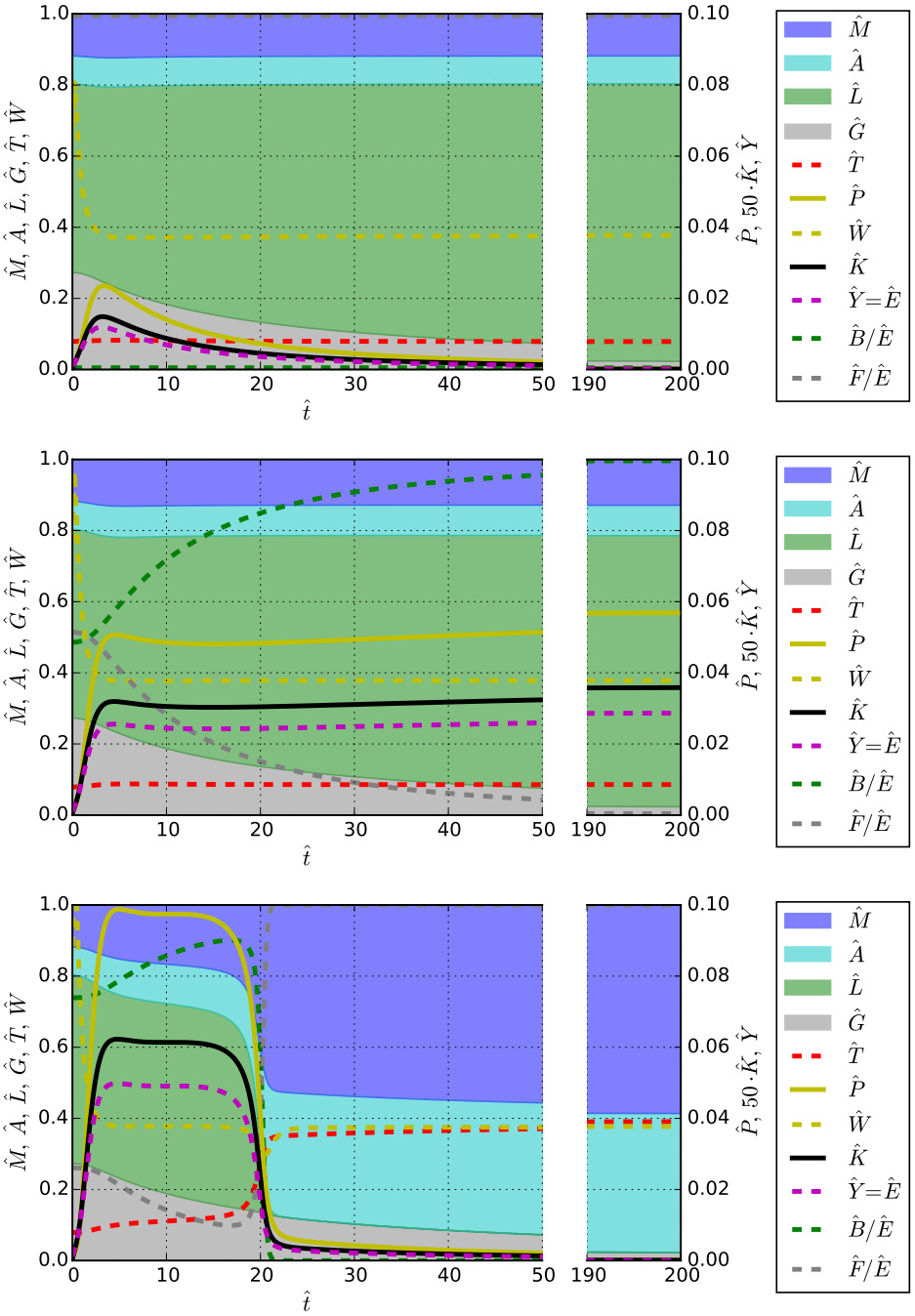


**Figure 5.18:** Exemplary trajectories of the c:G:LGPK model for the same initial conditions but different combinations of the sectoral productivities $a_B$ and $a_F$. In all scenarios fossil fuels are used ($\hat{a_F} = 80$), leading ultimately to a complete exploitation of the geological carbon stock, independent of the biomass sector productivity. If no biomass is used (upper panel, $\hat{a_B} = 0$) the final state is characterized by an intact nature but no humans surviving. In the second case (with $\hat{a_B} = 20$) the system reaches a stable coexistence state with intact nature and non-zero population. If the biomass productivity is too high (lower panel, $\hat{a_B} = 60$), after a transient period of coexistence the natural system will collapse into a desert state and ultimately neither nature nor humans will survive.
Initial conditions: $\hat{L}_0 = 0.53$, $\hat{G}_0 = 0.27$, $\hat{P}_0 = 10^{-3}$, $\hat{K}_0 = 10^{-5}$.
Parameters are set to default values from Table 4.3. $w_L = 0$, $\hat{a_F} = 0$.

# CHAPTER 6

## Discussion and Outlook

The scope of this thesis was to investigate the asymptotic dynamics of a co-evolutionary model of globally aggregated variable of the natural and socio-economic sub-systems of the planet. Furthermore, by the estimation of parameters from real world data, the relevant parameter regime has been curtailed in order to identify the most likely type of qualitative behavior of the earth system.

This chapter aims at summarizing and evaluating the main findings presented above and puts them into a broader context of other research performed so far. As a starting point the first section 6.1 gives an overview of the *key findings* achieved in this work. In the following sections 6.2, 6.3 and 6.4 these and other results are discussed and compared to findings from the respective disciplines. The final section 6.5 of this chapter discusses the methods used and gives an outlook on further directions of the model analysis regarding both model components and techniques.

## 6.1 Summary of the main results

The following list gives an overview of the most striking results which have been obtained in this thesis using the copan:GLOBAL model:

- The study of the carbon cycle model component (c:G:LAT) revealed the three qualitatively different, parameter-dependent **dynamic regimes** of which the **bistable topology** (with stable desert and forest states) was found to be the most probable. The significant human influence on global scale earth system dynamics which is missing in this submodel was however shown to lead to a behavior diametrically opposed to what this component alone would suggest, which thus necessitates a **coevolutionary** modeling approach. (Section 5.1)
- For hunter-gatherer and non-capitalistic agricultural societies (c:G:LATP) a **planetary carrying capacity** of roughly $300 \cdot 10^6$ humans was estimated in line with estimated numbers from medieval times. (Section 5.2)
- The capitalistic agricultural scenario (c:G:LATPK) features a state of stably coexisting humans and nature with a global population of roughly 11 billion humans and a per-capita capital of roughly 2500 $ for a reasonable parametrization. (Section 5.3.2)
- In the industrial scenarios all trajectories which start from rather low levels of population and capital feature an initial period of exponential growth (of population, capital and economic output) and which reaches its maximum after roughly 400 years.
- For both the agricultural and industrial scenarios a **sustainable** parameter regime with coexisting humans and nature as well as a **collapse** regime with eventual distinction of both humans and nature was found. (Sections 5.2.2 and 5.3.1) Those socio-economic parameters which facilitate sustainability (“stabilizing”) and those which push the system towards the collapse regime (“destabilizing”) are shown in Table 6.1 below. Most notably, an otherwise desirable reduction of mortality or increase in agricultural productivity may ultimately have the adverse effect of favoring a collapse due to overexploitation of the environment.
- For the agricultural scenario (c:G:LP) an **oscillatory** parameter regime which features stable limit cycles was identified. It is enabled by a dominant contribution of ecosystem services to wellbeing. (Section 5.2.2)
- The asymptotic (though of course not the transient) behavior of the system for the industrial scenario (c:G:LAGTPK) was found to be independent of the use of fossil fuels. The associated emissions of carbon were found to be mainly taken up be the terrestrial systems. (Section 5.3.3)

**Table 6.1:** Overview of the dynamic effect of the socio-economic parameters. The denotation of the parameters can be found in Tables 3.2 and 3.3.

| scenario | effect | parameter |
|---|---|---|
| agricultural | stabilizing | $q_0$ |
| | destabilizing | $p$, $W_p$, $b$, $y_B$, $w_L$ |
| industrial | stabilizing | $q_0$, $k_0$, $e_B$ |
| | destabilizing | $p$, $W_p$, $y_E$, $a_B$, $w_L$ |
| | bidirectional | $i$ |

## 6.2 Carbon cycle dynamics

The parametrization of the carbon cycle dynamics was chosen using recent IPCC data and hence matches both pre-industrial and present stock sizes of terrestrial, maritime and atmospheric carbon as well as the major flows between these. There are, however, no data available on photosynthesis, respiration or diffusion flows for other parts of the $L$-$A$-$M$-space (for instance for the upper left region of the phase space in Figure 5.2) as the carbon cycle in the past did not exhibit such "extreme" states. To make things worse, there is a high uncertainty associated with the IPCC data which is propagated onto the parameter estimates of the model. Putting all these aspects into consideration one should refrain from regarding the parametrized carbon cycle component as quantitatively accurate representation of earth system dynamics. These considerable uncertainties further justify the neglect of the albedo effect throughout the thesis as it would only alter the dynamics to an extent which is insignificant compared to the uncertainty which is there anyway.

Despite these issues, the three dynamic regimes (monostable desert, bistable, monostable forest) which have been identified constitute a common feature of simple ecological or climatological models [97, Ch. 11.3]. The carbon cycle model of Anderies et al. for instance which is of comparable complexity features the same dynamic regimes, depending on the choice of parameters [2]. However, the Anderies model has a topology with a globally stable forest state for the default parameter values. In contrast to this the parametrization according to the IPCC data suggests a bistable topology to be more probable. It should be emphasized that only the bistability of the natural sub-system enables the occurrence of the "collapse" regimes which were identified in the agricultural and industrial scenarios. Even though such collapses have been observed for several localized human civilizations such as the Mayas or the Polynesians on Easter Island [15, 25], it is not clear whether *global collapses* of both nature and human population are really possible or would be prevented by processes not included in the model. This point should be kept in mind when interpreting the results found for the coevolutionary scenarios.

The dynamics of the carbon cycle becomes more involved when the emissions due to fossil fuels are accounted for. For the default parametrization it was found that only the position of the forest state equilibrium is pushed to larger values of the terrestrial carbon stock while its stability is unaffected (see Figure 5.17 for $a_B = 0$). The altered position of the equilibrium further indicates that the terrestrial systems are the major sink for the additional carbon while the amounts in oceans and atmosphere only slightly increase. This feature of the carbon dynamics appears somewhat questionable if compared with findings that the airborne fraction of $CO_2$ amounts to about 40 to 60 % and that the ocean sink and the terrestrial sink play comparable roles [30, 56]. While these cited calculations focus on rather short timescales, also long-term simulations of EMICs indicate larger airborne fractions and corresponding temperature increases than those found for the copan:GLOBAL model [58]. On the one hand due to the conceptual and qualitative nature of the model this discrepancy to findings from climate science could be regarded as only little problematic. On the other hand it might pose a problem for further studies in which the effect of climate impacts (for instance in form of increased mortality and depreciation via the parameters $q_T$ and $k_T$) is investigated. Significant effects through climate damages are only to expect if there is a considerable temperature increase associated with the emission of fossil carbon. This could potentially be achieved via a different parametrization of the carbon cycle in which photosynthesis happens on a slower timescale. It could also be necessary to extend or modify the governing processes of the carbon cycle model, for instance by adding a *deep ocean* stock in which carbon from the upper ocean is accumulated on a relatively long timescale, thereby strengthening the ocean sink for atmospheric carbon. Yet another explanation for the lacking realism of the model might be the neglect of other limiting factors for vegetation growth like the availability of water and nitrogen. Including simplistic water and nitrogen cycle dynamics would potentially weaken the terrestrial carbon sink and hence favor the increase of atmospheric carbon and global mean temperatures.

## 6.3 Socio-economic dynamics

The socio-economic sub-system of the model is mainly represented by the population dynamics on the one hand and the Solow-Swan like growth model for the physical capital stock on the other hand. Population and capital stock feature a qualitatively similar dynamics as their increase is proportional to the economic output and decrease at a certain rate due to mortality and depreciation. On the other hand they contribute to the economic output as factors of production via a Cobb-Douglas production function. This structural similarity of the variables is reflected by the phase portraits in Figure 5.14 as well as the similar shapes of the trajectories in Figures 5.16 and 5.18. The dynamics of the agricultural societies (c:G:LP) and capitalistic societies without the use of fossil fuels (c:G:LPK) hence only differ quantitatively.

### 6.3.1 Comparison with real world observations and predictions

For the agricultural scenario a planetary *carrying capacity* of $P_{\text{cc}} \approx 300 \cdot 10^6$ humans was found which is in perfect agreement with actual estimates of the global population in medieval times which lies within the range of $200-500 \cdot 10^6$ humans [52, 75]. This accordance can be valued as a validation of the parameter estimates. The fact that the default parameter estimates lie within the collapse regime but no global collapse has been observed historically can be explained in different ways. As discussed above the parametrization of the carbon cycle which enables the collapse is subject to high uncertainties. Furthermore the data used to estimate the economic parameters ($y_B$ and $b$) are dated in the last century and thus from the industrial era. It can be expected that the productivity of biomass harvesting in former times was considerably lower, which would result in a higher carrying capacity and the occurrence of a stable coexistence of humans and nature. Finally another explanation for the absence of a collapse could be the onset of the industrial revolution and the concurrent use of fossil fuels. These took pressure from the terrestrial systems as they depict an alternative energy source to biomass. Ironically, if this explanation was indeed true, it would mean that fossil fuels have helped to prevent a collapse before leading into another dangerous state.

With the exception of the sectoral productivities ($a_B$ and $a_F$) a reasonable parametrization of the industrial scenario was less problematic since it corresponds to the recent era of human history for which economic and demographic data are available. For the scenario without use of fossil fuels a coexistence state with a population of 11.2 billion humans, a total capital stock of $28.3 \cdot 10^{12}$ \$ and a corresponding per-capita capital of 2520 \$ was found. The total capital stock value compares well with the estimates found in [10]. If one assumes a total accumulated emission of fossil carbon of 550 GtC$= 0.1\, C^*$ (from pre-industrial times until today about 375 GtC have been emitted; see Figure 2.13) and the same productivity of the biomass sector, one finds an equilibrium population of 15.2 billion people. Both mentioned

equilibrium population levels compare well with the UN projection of about 11.2 billion humans by 2100, when the population growth will be close to zero [108, "medium variant" of 2015 revision]. Moreover, in the industrial scenarios, population and economic output reach their maximum after $\hat{t} = 4 \equiv 400$ years which nicely matches the time from 1750 (roughly the onset of industrialization) until 2100 for which the UN project the global population to be maximal (Figures 5.16 and 5.18). This perfect accordance between modeled values and real world data underpins the validity of both the model and the parameter estimates.

While the temporal evolution and the quantities of many socio-economic variables fit well to actual data, some features of the social dynamics are less in line with real world observations. For both the agricultural and industrial scenario the per-capita consumption (which is in the model identical to wellbeing if ecosystem services are not regarded) is decreasing in those phases of population growth and ultimately approaches a steady-state value of $\hat{W}^* \approx 0.38 \equiv 760\,\$$ per person and year, which is solely determined by demographic parameters (Equation 5.15). This behavior reminds of Malthus' argument, discussed in section 2.2.3. This observation might hold true for the agricultural scenario since population and wellbeing levels were indeed found to be roughly constant from year 0 to 1750 [52, 75]. Also the equilibrium wellbeing lies in the same order of magnitude as the gross word product (GWP) per capita values of about $470 - 620\,\$$ which were estimated in [13, 63].[1] However, since the onset of the industrial revolution about 250 years ago, the real GWP per capita has *increased* substantially (particularly in the industrialized nations) up to about 7600 $ in 2008[63]. This value is already 10 times larger than the predicted equilibrium value of the model. The increasing levels of wellbeing in industrial scenarios is not captured by the model dynamics. This can be explained with the functional forms of the equations which govern the population dynamics as discussed in the subsequent section 6.3.2.

The equilibrium wellbeing level of $W^* \approx 760\,\$$ can be translated into a per-capita energy supply. For the parametrization of the agricultural societies ($y_B$, $e_B$) this yields a number of about 122 GJ per year, while for the industrial parametrization ($y_E$) a per-capita supply of about 5.2 GJ is calculated. As a comparison might serve the per-capita primary energy use in an agricultural country like Bangladesh which amounted to about 9 GJ in 2013 and an industrialized country like Germany which amounted to about 157 GJ in 2014 [27]. Seemingly, the numbers of the model scenario are interchanged. For the industrial setting the mismatch can be explained due to the low equilibrium income level as discussed above. For the agricultural setting in turn the low equilibrium income level is realistic, but there is a high uncertainty

1 The authors in [13, 63] use 1990 international $ (with purchasing power parities) while the model quantities are given in 2011 international $ which have a lower value due to inflation.

associated with the economic parameter $y_B$ which is used to translate the income into an energy supply. Moreover, one also needs to account for the very low conversion efficiencies from primary biomass energy to usable end energy within the agricultural scenario. These also lead to a comparably large demand of primary energy.

### 6.3.2 Demographic modeling approaches

Figure 6.1 shows different models for the dependencies of fertility and mortality on wellbeing which have been mentioned in the previous chapters (see Equations (2.46), (3.42) and (3.43), (4.13) and (4.14)). The Malthus model features a single stable equilibrium at low wellbeing. While it is an aid in explaining the constant levels of population and wellbeing until the industrialization, more recent data show a completely different dependence (see Figure 4.1). The fertility and mortality dependencies in copan:GLOBAL are in better agreement with the recent data for higher incomes. For very low levels of wellbeing no data are available, thus a similar dependence as in the Malthus model is assumed. This results in a single stable "Malthusian" equilibrium at low incomes. Equilibria at higher incomes can be excluded such that ultimately the society finds itself in the "Malthusian trap". A sustained growth of incomes, an escape from the trap, which took place in many countries since the onset of the industrialization, is therefore not observable in the copan:GLOBAL model. The "alternative" model with different exponents which has been proposed in chapter 4.2 to better capture recent data, potentially features another equilibrium at higher incomes as shown in the right panel of Figure 6.1. Since wellbeing is inversely proportional to population this is an unstable equilibrium. Therefore also the alternative functional forms do not solve this drawback of the model. Moreover it introduces additional parameters which increase the complexity of the model while the qualitative behavior remains similar. The functional forms used within this thesis make a compromise between the theory for low incomes (Malthus), the empirical findings for higher incomes and the striving for low model complexity.

From a dynamical perspective the stability of the Malthusian equilibrium in the model can be explained by the fact that wellbeing decreases with increasing population ($W \propto Y/P \propto P^{-\frac{3}{5}}$). Thus, a destabilization of the Malthusian equilibrium would require entities which contribute to wellbeing without needing to be divided amongst the population, hence being independent of $P$. The *ecosystem services* which have been considered at some points fulfill this property. Indeed Figure 5.11 shows that a stronger contribution of ecosystem services to wellbeing (large $w_L$ and small $y_B$) destabilizes the Malthusian equilibrium and enables an oscillatory coexistence for agricultural societies. Moreover the notions of *knowledge* and *technological progress* do not need to be divided since the same ideas can serve many individuals at the same time. It might also be argued that certain forms of physical capital, for instance infrastructure, contribute to

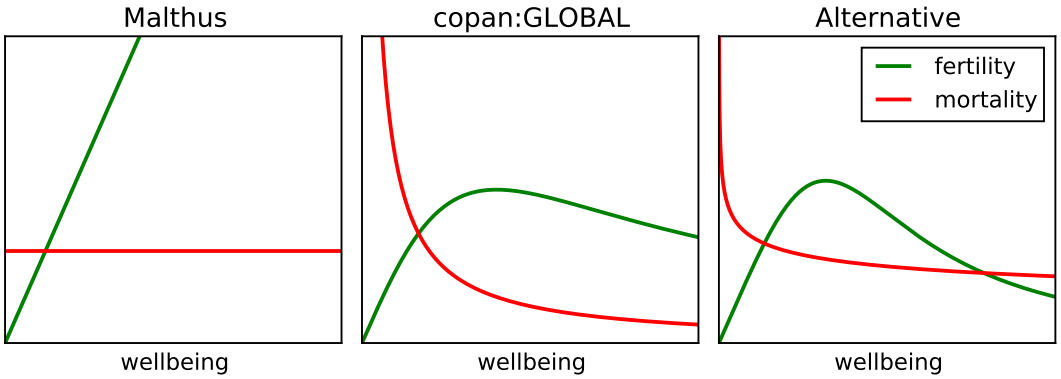


**Figure 6.1:** Comparison of the qualitative dependencies of fertility (green) and mortality (red) on wellbeing for different models which are discussed in the text. All model versions feature a stable "Malthusian" equilibrium at low levels of wellbeing. In contrast to the Malthus model the functions of copan:GLOBAL are in better agreement with data for high incomes from the industrial era. The more complex alternative model potentially features an additional equilibrium at higher levels of wellbeing which is, however, dynamically unstable.

wellbeing not only as a factor of production which fosters consumption [14]. Extending the model by a variable which reflects technological progress or modifying the functional form of the wellbeing variable might thus improve the realism of the socio-economic dynamics. A comparable extension would lie in the incorporation of the renewable technology knowledge stock $S$ which is part of the complete c:G model (see Figure 3.1).

Advanced theories of economic growth are able to explain the "breakout" from the Malthusian regime into a state of sustained growth [31]. This is indeed explained through *technological progress* as well as the accumulation of *human capital*, which are not explicitly included in the socio-economic sub-model of copan:GLOBAL. The available economic theories could aid in developing further versions of the model. Many questions regarding the qualitative effect of parameters or processes can, however, also be answered with the Solow-Swan like growth model used for this work.

### 6.3.3 Stabilizing and destabilizing processes and management options

For both the agricultural and the industrial scenario a parameter regime which enable an asymptotic coexistence of humans and nature and a collapse regime could be distinguished. From the derived conditional equations (5.20) and (5.38) for the existence of coexistence equilibria one can read which parameters push the system towards the collapse regime and which stabilize it.

Generally an increase in those parameters which positively contribute to economic or population growth may be beneficial in the short run but ultimately destabilizes the system. For the

agricultural scenario these are the biomass harvesting rate $b$, the economic productivity $y_B$ and the parameters $p$ and $W_p$ which set the fertility of the population. The mortality parameter $q_0$ on the other hand negatively influences the population growth and thus has a stabilizing effect on the overall dynamics.

For the industrial scenario it should be pointed out that only the biomass sector productivity $a_B$ but not the fossil sector productivity $a_F$ determine the asymptotic states of the system. The energy density $e_B$ is beneficial for sustainability. Similar to the mortality parameter $q_0$, the depreciation $k_0$ has a stabilizing effect as it harms the physical capital as factor of production. The parameters which account for climate impacts ($q_T$ and $k_T$ in equations (3.43) and (3.77)) essentially shift the baseline mortality and depreciation parameters depending on the temperature. The effective mortality and depreciation will increase with rising temperatures, thus having a stabilizing effect on the dynamics. Lower temperatures in turn would lead to lower death rates and depreciation, hence enabling a faster convergence to a potential coexistence state. Due to this twofold feedback the accounting for climate impacts might potentially result in the occurrence of periodicity, as observed in [48]. The investment ratio $i$ has a non-monotonous influence on the critical parameter $\phi$ which determines the dynamic regime. $\phi$ is maximized if the economic output is equally shared between the factors population and capital. Preferring either investments or consumption will in turn decrease $\phi$ and hence stabilize the dynamics. This can be explained due to the fact that the investment ratio of $i^* = 0.5$ maximizes the total economic output.

These findings become particularly momentous if the ability of humans to influence socio-economic parameters is considered. If the society for instance was to optimize the investment ratio in order to maximize the economic output, this could potentially cause the system to tip into a different dynamic regime, eventually leading to a collapse of both nature and society. On the other hand the ability to manage the socio-economic dynamics via parameters might facilitate the possibility to stay within a desired region, for example given by planetary boundaries. While some parameters such as death rate, depreciation rate or energy densities of fuels are rather natural constants, others might significantly be altered by human actions. An example for a politically implemented steering of birth rates constitutes the “One-child policy” of China which was in force from the late 1970s until 2015 [78]. While such measures are highly disputable for moral reasons and their success debatable [46], they reveal that humanity in principle has the ability to steer socio-economic development on large scales. Such scenarios have been studied by applying the topology framework introduced in [43] to the agricultural model version (Figures 5.6, 5.9, B.7 and B.8). The topology framework moreover provides a meaningful way to communicate subtle dynamical properties of complex systems in an understandable way to laymen.

## 6.4 Comparison to predator-prey dynamics

A remarkable feature of the dynamics of the agricultural scenario is the occurrence of periodic trajectories which are present for a small parameter regime in which ecosystem services dominantly determine wellbeing (Figures 5.11 and 5.13). Within this parameter regime the governing equations of the c:G:LP system are similar to common models of *predator-prey dynamics*. Here the biomass of the terrestrial systems plays the role of the prey which has a natural growth rate (due to photosynthesis) and is exploited by the predator (due to harvesting) which is depicted by the human population. The humans in turn reproduce proportional to the availability of biomass resources and are subject to a natural mortality. The large contribution of ecosystem services effectively makes the resources non-competitive (in contrast to per-capita consumption) which enables the appearance of periodicity as explained in section 5.2.2 and also observed in [15]. Structurally similar equations for predator-prey dynamics also feature periodic solutions. Most prominent of these is the Lotka-Volterra system for which the cyclic trajectories are, however, not isolated and hence they are no limit cycles [45]. Thus the Lotka-Volterra system is structurally unstable. There are modified versions of ecological population dynamics models though which feature limit cycles comparable to those found for c:G:LP.

## 6.5 Further directions

This section gives a condensed overview of possible further directions of research on the copan:GLOBAL model. As discussed above there are some features of both the natural and socio-economic dynamics which still require *fine-tuning* of the model equations or the parametrization in order to better agree with empirical findings. A more realistic representation of the climate system, for instance by introducing a deep ocean carbon stock or water an nitrogen cycles, would allow for the study of *climate impacts*. A more sophisticated growth model could potentially be achieved by incorporating some knowledge or technology variable into the dynamics, but on the other hand this would increase the complexity of the model. As long as the study aims primarily at qualitative understanding rather than quantitative predictions one might want to stick to the established model version.

So far the only energy sources considered are biomass and fossil fuels. The complete copan:GLOBAL model described in section 3.1 additionally accounts for the use of *renewable energies*, such as solar or wind. As their availability is not constrained by a limited or renewable resources they potentially introduce a qualitatively different dynamics. Moreover, as a “clean” energy source which neither causes emissions of carbon into the atmosphere nor puts pressure on the terrestrial systems, the use of renewables can be expected to facilitate a sustainable coexistence of nature and humans. The model with inclusion of renewable energies might hence be used to simulate a transition from the recent unsustainable era into an upcoming era

of sustainability.

Such a transition towards sustainability might possibly require other *social processes* than those (mainly purely economic) accounted for in the model so far. A potential candidate poses the *change of values* in the face of emerging threats which might lead to a decrease in fertility or the deliberate refraining from the use of certain (unsustainable) energy forms.

One assumption which underlies the copan:GLOBAL model is that dominant co-evolutionary feedbacks in the earth system can be described by globally accumulated variables. On the other hand several regions of the world differ substantially for instance regarding their climate or political situation. Such differences could lead to diverse regional evolutions which are not resolved in coarse grained global variables. A historic example constitutes the "Great Divergence" between industrial countries and development countries in which even in recent times agriculture is the predominant economic sector [105]. In a *regionalized version* of the model some natural and socio-economic variables (such as terrestrial carbon, population and physical capital) would be modeled regionally. Regionally varying parameter values and initial conditions would account for regional differences. The local dynamics would still be coupled via a common atmosphere which is characterized by a fast mixing of the carbon emissions. From a dynamical systems perspective this corresponds to a system of indirectly coupled "oscillators" via a common environment. These might exhibit typical phenomena such as *synchronization*. In a next step direct coupling mechanisms such as trade or migration could be integrated into the regionalized model. These processes could happen on an underlying *network topology* leading to other interesting phenomena and closing the gap to related models developed within the copan group [7, 107]. From an earth science perspective it would be of high interest which conditions and which parameters determine the "success" of certain regions compared to others.

The results presented in chapter 5 primarily focus on the asymptotic dynamics of the model. The discussion of several exemplary trajectories, however, revealed that also the *transient* behavior features interesting properties. For instance, the duration of a period of coexistence preceding a collapse is highly dependent on the parameter values. In particular, the assumptions of instantaneous greenhouse effect and diffusion were legitimated by the argument that they do not influence the asymptotic dynamics. The transient behavior might yet be considerably altered by regarding these processes as they introduce slower timescales which might delay some feedbacks. Thus, an complementary study of both transient and asymptotic dynamics would potentially yield more insights into the co-evolutionary earth system.

# CHAPTER 7

## Conclusion

The broader intent of the present thesis was to investigate the global coevolutionary dynamics of humans and nature on timescales of the Holocene epoch. For this purpose the model copan:GLOBAL was employed which constitutes a holistic Earth system model describing the evolution of key quantities of the planetary scale dynamics. Through the balanced representation of natural and anthropogenic components and the low dimensional complexity the model strives for bridging a gap in the broader landscape of Earth system models (see Figure 1.2). Thereby it also constitutes a contribution to the scientific challenge of modeling the Anthropocene which is characterized by highly interwoven and complex connections between the anthroposphere and the ecosphere [88].

The guiding principle within the design and setup of the model was to combine established modeling approaches from various disciplines of Earth and social sciences. Hence, the global economic system is described by a growth model in the style of Solow-Swan which is combined with the use of resources depicted by different forms of energy. The allocation of the factors of production to the multiple economic sectors is realized via a general equilibrium assumption. A demographic model which poses a trade-off between the desired dynamical properties and the accordance with empirical evidence completes the socio-economic model component. The representation of the natural Earth system via the global carbon cycle is beneficial as it features components which are incorporating various parts of the ecosphere such as the atmosphere, hydrosphere, lithosphere and biosphere. The representation of Earth's climate via the global mean surface temperature is sufficient for the purpose of the model since regionally varying impacts of climate change are not of interest. Altogether the state of the Earth system in the model is represented by a low number of global quantities and its temporal evolution prescribed by the dominant processes on a planetary scale which are expressed by simple

functional relationships. Notable processes *not* included in the current model version include non-economic social processes, like the evolution and imitation of values and traits, and natural processes that would constrain vegetation growth, such as a hydrological cycle.

The formulation of the model in terms of ordinary differential equations allows the application of mathematical methods from the broad field of dynamical systems theory. Thus, by emphasizing qualitative techniques such as bifurcation analysis the present work distinguishes itself from related efforts which rather focus on quantitative results. The design of the model allows flexibly including or excluding certain variables or processes in order to adapt it to actual or hypothetical scenarios which have been or might be undergone in the course of Earth's history.

As a first step of the model investigation appropriate sub-models of the complete model which correspond to different stages of the socio-cultural evolution of humans were derived. These comprise the sole natural dynamics of the carbon cycle without interference of humans, a scenario of hunter-gatherer and agricultural societies and a sub-model reflecting the coevolutionary dynamics in the industrial era. For each of these scenarios which involve the human factor a fundamental distinction between a sustainable regime and a collapse regime emerged. This dualism depicts a common feature of ecological, particularly social-ecological systems and hence constitutes a typical narrative in the broader field of sustainability science. The emergence of an oscillatory regime in the agricultural scenario is another common feature of ecological models and was explained by the structural similarity to predator-prey dynamics and the occurrence of an supercritical Andronov-Hopf bifurcation.

The various dynamic regimes which have been identified result from the existence of different attractors in dependence of the parameter values. By analytical reasoning and numerical bifurcation analyses those parameters and related processes could be identified which favor a collapse, oscillations or sustainability, respectively. Some of these reveal a potential conflict between goals of human development (reduction of mortality, improvement of productivity) on the one hand and ecological sustainability on the other hand. The analysis also allowed the identification of parameters which might potentially be relevant and suited in the context of deliberate control of Earth system dynamics through humans. In this regard the recently proposed concept of "topology of sustainable management of dynamical systems with desirable states" was applied to certain model scenarios which improved the qualitative understanding of the dynamics and generally allows for a better communicability of subtle system properties.

Beyond these rather qualitative findings a major concern of this thesis was the estimation of the model parameters based on available real-world data. Thus, the relevant parameter regime could be curtailed and the further analysis restricted to few parameters which could not or only unconfidently be estimated. Tying the model dynamics to actual data also facilitated the com-

parison of characteristic quantities of the model with estimates gained by other means. Most notably, the modeled planetary carrying capacity for purely agricultural societies and their level of wellbeing nicely compare to real-world estimates for medieval times. This accordance can be valued as a way of validation of the model. For the industrial scenario some characteristics like the duration of the period of fast population growth nicely agree with current observations and predictions while others like the evolution of per-capita consumption indicate a lack of quantitative accuracy.

Although the model primarily aims at qualitative insights, the quantitative discrepancies might aid in the further development of the model. A bunch of possible further directions of research on the model have been proposed which range from fine-tuning of parameters and governing equations of both the natural and the socio-economic components to the formulation of a regionalized version of the model which would potentially reveal additional dynamical phenomena, in particular many more oscillatory modes.

In summary the results of this thesis exemplary show that the coevolutionary modeling approach has the potential to significantly contribute to a more holistic and systemic understanding of the Earth system. Hence, it enables the identification (though not its precise localization) of a safe and just operating space for humanity which is an essential challenge for sustainability science. Through the outbalanced representation of both social and natural dynamics novel insights can be gained which cannot be found with the established models which rather focus on either of the mentioned components. In particular, the copan:GLOBAL model proved to be a flexible tool to qualitatively analyze the major global processes during different socio-cultural eras of human history and thus depicts a step forward towards a better understanding of the dynamics of the Earth system in the Holocene and the Anthropocene.

# Bibliography


1. *Agriculture, value added*. 2016. URL: http://data.worldbank.org/indicator/NV.AGR.TOTL.ZS (visited on Apr. 11, 2016) (cit. on p. 74).
2. ANDERIES, J. M., CARPENTER, S. R., STEFFEN, W., and ROCKSTRÖM, J.: 'The topology of non-linear global carbon dynamics: from tipping points to planetary boundaries'. *Environmental Research Letters* (2013), vol. 8(4): p. 044048 (cit. on pp. 5, 45, 66, 68, 76, 83, 123).
3. ARNOLD, V. I.: *Ordinary Differential Equations*. Springer, 1992 (cit. on p. 15).
4. AUBIN, J.-P.: *Viability Theory*. Springer Science & Business Media, 2009 (cit. on p. 29).
5. AUBIN, J.-P., BAYEN, A., and SAINT-PIERRE, P.: *Viability Theory: New Directions*. Springer Science & Business Media, 2011 (cit. on p. 29).
6. AUBIN, J.-P. and SAINT-PIERRE, P.: 'An Introduction to Viability Theory and Management of Renewable Resources'. *Advanced Methods for Decision Making and Risk Management in Sustainability Science*. Ed. by KROPP, J. and SCHEFFRAN, J. Nova Science Publishers, 2007 (cit. on p. 29).
7. AUER, S., HEITZIG, J., KORNEK, U., SCHÖLL, E., and KURTHS, J.: 'The Dynamics of Coalition Formation on Complex Networks'. 2015 (cit. on p. 131).
8. AYRES, R. U. and BERGH, J. C. van den: 'A theory of economic growth with material/energy resources and dematerialization: Interaction of three growth mechanisms'. *Ecological Economics* (2005-10), vol. 55(1): pp. 96–118 (cit. on p. 34).
9. BARENBLATT, G. I.: *Scaling*. Cambridge Texts in Applied Mathematics. Cambridge University Press, 2003 (cit. on p. 61).
10. BERLEMANN, M. and WESSELHÖFT, J.-E.: 'Estimating Aggregate Capital Stocks Using the Perpetual Inventory Method'. *Review of Economics* (2014), vol. 65(1) (cit. on p. 125).
11. *Birth rate, crude*. 2016. URL: http://data.worldbank.org/indicator/SP.DYN.CBRT.IN (visited on Apr. 18, 2016) (cit. on p. 69).

12. BOKANOWSKI, O., MARTIN, S., MUNOS, R., and ZIDANI, H.: 'An anti-diffusive scheme for viability problems'. *Applied Numerical Mathematics* (2006), vol. 56(9): pp. 1147–1162 (cit. on p. 29).

13. BOLT, J. and ZANDEN, J. L. van: 'The Maddison Project: collaborative research on historical national accounts'. *The Economic History Review* (2014), vol. (cit. on p. 126).

14. BOUMANS, R., COSTANZA, R., FARLEY, J., WILSON, M. A., PORTELA, R., ROTMANS, J., VILLA, F., and GRASSO, M.: 'Modeling the dynamics of the integrated earth system and the value of global ecosystem services using the GUMBO model'. *Ecological Economics* (2002), vol. 41(3): pp. 529–560 (cit. on pp. 5, 128).

15. BRANDER, J. A. and TAYLOR, M. S.: 'The Simple Economics of Easter Island: A Ricardo-Maltus Model to Renewable Resource Use'. *The american economic review* (1998), vol. 88(1): pp. 119–138 (cit. on pp. 5, 52, 123, 130).

16. BROVKIN, V., BENDTSEN, J., CLAUSSEN, M., GANAPOLSKI, A., KUBATZKI, C., PETHOUKOV, V., and ANDREEV, A.: 'Carbon cycle, vegetation and climate dynamics in the Holocene: Experiments with the CLIMBER-2 model'. *Global Biogeochemical Cycles* (2002), vol. 16(4): pp. 81–86 (cit. on p. 2).

17. CIAIS, P. et al.: 'Carbon and Other Biogeochemical Cycles'. *Climate Change 2013: The Physical Science Basis. Working Group I Contribution to the Fifth Assessment Report of the Intergovernmental Panel on Climate Change.* (2013), vol.: pp. 465–570 (cit. on pp. 39, 66).

18. CLAUSSEN, M. et al.: 'Earth system models of intermediate complexity: Closing the gap in the spectrum of climate system models'. *Climate Dynamics* (2002), vol. 18(7): pp. 579–586 (cit. on p. 2).

19. CLEWLEY, R. H., SHERWOOD, W. E., LAMAR, M. D., and GUCKENHEIMER, J. M.: *PyDSTool, a software environment for dynamical systems modeling*. 2007. URL: `http://pydstool.sourceforge.net` (cit. on p. 82).

20. CLEWLEY, R.: 'Hybrid Models and Biological Model Reduction with PyDSTool'. *PLoS Computational Biology* (2012), vol. 8(8): e1002628 (cit. on p. 82).

21. COX, P. M., BETTS, R. A., JONES, C. D., SPALL, S. A., and TOTTERDELL, I. J.: 'Acceleration of global warming due to carbon-cycle feedbacks in a coupled climate model.' *Nature* (2000), vol. 408(6809): pp. 184–187 (cit. on pp. 2, 40).

22. CRUCIFIX, M., LOUTRE, M. F., TULKENS, P., FICHEFET, T., and BERGER, A.: 'Climate evolution during the Holocene: A study with an Earth system model of intermediate complexity'. *Climate Dynamics* (2002), vol. 19(1): pp. 43–60 (cit. on p. 2).

23. CRUTZEN, P. J.: 'Geology of mankind'. *Nature* (2002), vol. 415(January): p. 23 (cit. on p. 1).

24. *Death rate, crude*. 2016. URL: http://data.worldbank.org/indicator/SP.DYN.CDRT.IN (visited on Apr. 18, 2016) (cit. on p. 69).

25. DIAMOND, J. M.: *Collapse: How Societies Choose To Fail Or Succeed*. Allen Lane science Teil 537. Viking Penguin, 2005 (cit. on pp. 1, 123).

26. *Energy intensity level of primary energy*. 2016. URL: http://data.worldbank.org/indicator/EG.EGY.PRIM.PP.KD (visited on Apr. 11, 2016) (cit. on p. 75).

27. *Energy use*. 2016. URL: http://data.worldbank.org/indicator/EG.USE.PCAP.KG.OE (visited on June 7, 2016) (cit. on p. 126).

28. FAGAN, B. M.: *The Long Summer: How Climate Changed Civilization*. Basic Books, 2004 (cit. on p. 1).

29. FAO: *FAO Global food price monitor*. Tech. rep. 2014 (cit. on p. 74).

30. FRIEDLINGSTEIN, P.: 'Carbon cycle feedbacks and future climate change'. *Philosophical Transactions of the Royal Society A: Mathematical, Physical and Engineering Sciences* (2015), vol.: pp. 1–22 (cit. on pp. 39, 40, 124).

31. GALOR, O.: 'From Stagnation to Growth: Unified Growth Theory'. *Handbook of Economic Growth* (2005), vol. 1: pp. 171–293 (cit. on p. 128).

32. GANOPOLSKI, A., PETOUKHOV, V., RAHMSTORF, S., BROVKIN, V., CLAUSSEN, M., ELISEEV, A., and KUBATZKI, C.: 'CLIMBER-2: a climate sysetm model of intermediate complexity. Part II: model sensitivity'. *Climate Dynamics* (2001), vol. 17: pp. 735–751 (cit. on p. 2).

33. *GDP per capita, PPP*. 2016. URL: http://data.worldbank.org/indicator/NY.GDP.PCAP.PP.KD (visited on Apr. 18, 2016) (cit. on p. 69).

34. *GDP, PPP*. 2016. URL: http://data.worldbank.org/indicator/NY.GDP.MKTP.PP.KD (visited on Apr. 11, 2016) (cit. on p. 74).

35. GINGRICH, S., NIEDERTSCHEIDER, M., KASTNER, T., HABERL, H., COSOR, G., KRAUSMANN, F., KUEMMERLE, T., MÜLLER, D., REITH-MUSEL, A., JEPSEN, M. R., VADINEANU, A., and ERB, K.-H.: 'Exploring long-term trends in land use change and aboveground human appropriation of net primary production in nine European countries'. *Land Use Policy* (2015), vol. 47: pp. 426–438 (cit. on p. 73).

36. GORDON, C., COOPER, C., SENIOR, C. A., BANKS, H., GREGORY, J. M., JOHNS, T. C., MITCHELL, J. F. B., and WOOD, R. A.: 'The simulation of SST, sea ice extents and ocean heat transports in a version of the Hadley Centre coupled model without flux adjustments'. *Climate Dynamics* (2000), vol. 16: pp. 147–168 (cit. on p. 2).

37. *Gross capital formation*. 2016. URL: `http://data.worldbank.org/indicator/NE.GDI.TOTL.ZS` (cit. on p. 75).

38. HABERL, H., ERB, K. H., KRAUSMANN, F., GAUBE, V., BONDEAU, A., PLUTZAR, C., GINGRICH, S., LUCHT, W., and FISCHER-KOWALSKI, M.: 'Quantifying and mapping the human appropriation of net primary production in earth's terrestrial ecosystems'. *Proceedings of the National Academy of Sciences* (2007), vol. 104(31): pp. 12942–12947 (cit. on p. 73).

39. HALE, J. K., BUTTANRI, H., and KOCAK, H.: *Dynamics and Bifurcations*. Texts in Applied Mathematics. Springer Science & Business Media, 2012 (cit. on p. 15).

40. HARVEY, D., GREGORY, J., HOFFERT, M., JAIN, A., LAL, M., LEEMANS, R., RAPER, S., WIGLEY, T., and WOLDE, J. de: *An Introduction to Simple Climate Models used in the IPCC Second Assessment Report*. Tech. rep. 1997 (cit. on p. 2).

41. HECK, V., DONGES, J. F., and LUCHT, W.: 'Collateral transgression of planetary boundaries due to climate engineering by terrestrial carbon dioxide removal'. *Earth System Dynamics Discussions* (2016), vol. 2016: pp. 1–24 (cit. on p. 76).

42. HECKBERT, S.: 'MayaSim: An Agent-Based Model of the Ancient Maya Social-Ecological System'. *Journal of Artificial Societies and Social Simulation* (2013), vol. 16(4): p. 11 (cit. on p. 5).

43. HEITZIG, J., KITTEL, T., DONGES, J. F., and MOLKENTHIN, N.: 'Topology of sustainable management of dynamical systems with desirable states: from defining planetary boundaries to safe operating spaces in the Earth system'. *Earth System Dynamics* (2016), vol. 7(1): pp. 21–50 (cit. on pp. 4, 5, 8, 29, 30, 76, 90, 129).

44. HEITZIG, J.: *copan:GLOBAL*. Tech. rep. PIK, 2015 (cit. on pp. 41, 42).

45. HOFBAUER, J. and SIGMUND, K.: *Evolutionary games and population dynamics*. Cambridge University Press, 1998 (cit. on p. 130).

46. HVISTENDAHL, M.: 'Has China outgrown the one-child policy?' *Science* (2010), vol. 329(5998): pp. 1458–1461 (cit. on p. 129).

47. JOHNS, T. C., GREGORY, J. M., JOHNSON, C. E., JONES, A., LOWE, J. A., and WOODAGE, M. J.: 'Anthropogenic climate change for 1860 to 2100 simulated with the HadCM3 model under updated emissions scenarios'. *Climate Dynamics* (2003), vol. 20(6): pp. 583–612 (cit. on p. 2).

48. KELLIE-SMITH, O. and COX, P. M.: 'Emergent dynamics of the climate-economy system in the Anthropocene'. *Philosophical Transactions of the Royal Society A: Mathematical, Physical and Engineering Sciences* (2011-03), vol. 369(1938): pp. 868–886 (cit. on pp. 6, 68, 129).

49. KRAUSMANN, F., ERB, K. H., GINGRICH, S., LAUK, C., and HABERL, H.: 'Global patterns of socioeconomic biomass flows in the year 2000: A comprehensive assessment of supply, consumption and constraints'. *Ecological Economics* (2008), vol. 65(3): pp. 471–487 (cit. on p. 73).

50. KRAUSMANN, F., ERB, K.-H., GINGRICH, S., HABERL, H., BONDEAU, A., GAUBE, V., LAUK, C., PLUTZAR, C., and SEARCHINGER, T. D.: 'Global human appropriation of net primary production doubled in the 20th century.' *Proceedings of the National Academy of Sciences* (2013), vol. 110(25): pp. 10324–9 (cit. on pp. 73, 74).

51. KRAUSMANN, F., ERB, K.-H., GINGRICH, S., HABERL, H., BONDEAU, A., GAUBE, V., LAUK, C., PLUTZAR, C., and SEARCHINGER, T. D.: *Human appropriation of net primary production (HANPP) 1910 to 2005: HANPP paramaters by world regions*. URL: `http://www.uni-klu.ac.at/socec/inhalt/5605.htm` (visited on Oct. 15, 2015) (cit. on p. 73).

52. KREMER, M.: *Population growth and technological change: One million B.C. to 1990*. 1993 (cit. on pp. 1, 90, 125, 126).

53. KUZNETSOV, Y. A.: *Elements of Applied Bifurcation Theory*. Springer, 1998 (cit. on pp. 9–17, 22–25, 27, 28).

54. LADE, S. J., NIIRANEN, S., HENTATI-SUNDBERG, J., BLENCKNER, T., BOONSTRA, W. J., ORACH, K., QUAAS, M. F., ÖSTERBLOM, H., and SCHLÜTER, M.: 'An empirical model of the Baltic Sea reveals the importance of social dynamics for ecological regime shifts.' *Proceedings of the National Academy of Sciences* (2015), vol. 112(35): pp. 11120–5 (cit. on p. 5).

55. LADE, S. J., TAVONI, A., LEVIN, S. A., and SCHLÜTER, M.: 'Regime shifts in a social-ecological system'. *Theoretical ecology* (2013), vol. 6(3): pp. 359–372 (cit. on p. 5).

56. LE QUÉRÉ, C., RAUPACH, M. R., CANADELL, J. G., and AL., G. M.: 'Trends in the sources and sinks of carbon dioxide'. *Nature Geoscience* (2009), vol. 2(12): pp. 831–836 (cit. on pp. 40, 124).

57. LEIMBACH, M., BAUER, N., BAUMSTARK, L., and EDENHOFER, O.: 'Mitigation costs in a globalized world: Climate policy analysis with REMIND-R'. *Environmental Modeling and Assessment* (2010), vol. 15(3): pp. 155–173 (cit. on p. 3).

58. LENTON, T. M.: 'Land and ocean carbon cycle feedback effects on global warming in a simple Earth system model'. *Tellus* (2000), vol. 52B: pp. 1159–1188 (cit. on pp. 2, 40, 68, 124).

59. LENTON, T. M., HELD, H., KRIEGLER, E., HALL, J. W., LUCHT, W., RAHMSTORF, S., and SCHELLNHUBER, H. J.: 'Tipping elements in the Earth's climate system.' *Proceedings of the National Academy of Sciences* (2008), vol. 105(6): pp. 1786–1793 (cit. on p. 2).

60. *Levelized Cost and Levelized Avoided Cost of New Generation Resources in the Annual Energy Outlook 2015*. 2015 (cit. on p. 75).

61. LEVERMANN, A.: *Heed the warnings in extreme weather – or risk losing Earth*. 2014. URL: https://www.theguardian.com/environment/blog/2014/jan/31/climate-change-extreme-weather-earth (cit. on p. 6).

62. LEWIS, S. L. and MASLIN, M. A.: 'Defining the Anthropocene'. *Nature* (2015), vol. 519(7542): pp. 171–180 (cit. on p. 1).

63. MADDISON, A.: *Statistics on World Population, GDP and Per Capita GDP, 1-2008 AD*. URL: http://www.ggdc.net/maddison/maddison-project/home.htm (visited on June 1, 2016) (cit. on p. 126).

64. MALM, A. and HORNBORG, A.: 'The geology of mankind? A critique of the Anthropocene narrative'. *The Anthropocene Review* (2014), vol. 1(1): pp. 62–69 (cit. on p. 1).

65. MALTHUS, T.: 'An essay on the principle of population, as it affects the future improvement of society'. *Contemporary Sociology* (1798), vol. 2(3): p. 340 (cit. on p. 35).

66. MCKENDRY, P.: 'Energy production from biomass (part 1): overview of biomass'. *Bioresource Technol* (2002), vol. 83(1): pp. 37–46 (cit. on p. 75).

67. MEADOWS, D. H., MEADOWS, D. L., RANDERS, J., and BEHRENS, W. W.: *The limits to growth*. Club of Rome, 1972 (cit. on p. 3).

68. MEADOWS, D. H., RANDERS, J., and MEADOWS, D. L.: *Limits to Growth: The 30-Year Update*. Chelsea Green Publishing, 2004 (cit. on p. 3).

69. MENCK, P. J., HEITZIG, J., MARWAN, N., and KURTHS, J.: 'How basin stability complements the linear-stability paradigm'. *Nature Physics* (2013), vol. 9(2): pp. 89–92 (cit. on p. 13).

70. MOTESHARREI, S., RIVAS, J., and KALNAY, E.: 'Human and nature dynamics (HANDY): Modeling inequality and use of resources in the collapse or sustainability of societies'. *Ecological Economics* (2014), vol. 101: pp. 90–102 (cit. on p. 6).

71. MÜLLER-HANSEN, F., HEGSELMANN, R., HEITZIG, J., LEVERMANN, A., MÄS, M., DONGES, J., SCHLÜTER, M., KOLB, J., THONICKE, K., and KURTHS, J.: 'Ways to Represent Human Behavior in Earth System Models'. *in preparation for Earth System Dynamics* (2016), vol. (cit. on p. 34).

72. NADIRI, M. I. and PRUCHA, I.: 'Estimation of the depreciation rate of physical and R&D capital in the US total manufacturing sector'. *Economic Inquiry* (1996), vol. 34: pp. 43–56 (cit. on p. 76).

73. NORDHAUS, W. D.: 'Rolling the 'DICE': an optimal transition path for controlling greenhouse gases'. *Resource and Energy Economics* (1993), vol. 15(1): pp. 27–50 (cit. on p. 3).

74. *Oil Statistics (Production Costs, Breakeven Price)*. 2014. URL: https://knoema.com/vhzbeig/oil-statistics-production-costs-breakeven-price (visited on Apr. 11, 2016) (cit. on p. 75).

75. ORTIZ-OSPINA, E. and ROSER, M.: *World Population Growth*. 2016. URL: https://ourworldindata.org/world-population-growth/ (visited on May 8, 2016) (cit. on pp. 37, 125, 126).

76. PAILLARD, D.: 'The timing of Pleistocene glaciations from a simple multiple-state climate model'. *Nature* (1998), vol. 391(January): pp. 916–918 (cit. on p. 2).

77. PETOUKHOV, V., GANOPOLSKI, A., BROVKIN, V., CLAUSSEN, M., ELISEEV, A., KUBATZKI, C., and RAHMSTORF, S.: 'CLIMBER-2: a climate system model of intermediate complexity. Part I: model description and performance for present climate'. *Climate Dynamics* (2000), vol. 16: pp. 1–17 (cit. on p. 2).

78. PHILLIPS, T.: *China ends one-child policy after 35 years*. 2015. URL: https://www.theguardian.com/world/2015/oct/29/china-abandons-one-child-policy (cit. on p. 129).

79. *Population, total*. 2016. URL: http://data.worldbank.org/indicator/SP.POP.TOTL (visited on Apr. 18, 2016) (cit. on p. 69).

80. RANDERS, J.: *2052: A Global Forecast for the Next Forty Years*. Chelsea Green Publishing, 2012 (cit. on p. 3).

81. RAWORTH, K.: 'A Safe and Just Space For Humanity: Can we live within the Doughnut?' *Oxfam Discussion Papers* (2012), vol. 8(1): pp. 1–26 (cit. on pp. 4, 77).

82. RIND, D.: 'Complexity and Climate'. *Science* (1999), vol. 284(1999): pp. 105–107 (cit. on p. 2).

83. ROCKSTRÖM, A. et al.: 'Planetary Boundaries: Exploring the Safe Operating Space for Humanity'. *Ecology And Society* (2009), vol. 14(2) (cit. on pp. 4, 76).

84. ROCKSTRÖM, J.: 'A safe operating space for humanity'. *Nature* (2009), vol. 461(September) (cit. on p. 4).

85. ROMER, D.: *Advanced Macroeconomics*. 3rd ed. McGraw-Hill, 2005 (cit. on p. 34).

86. RYABININ, V., KHARECHA, P., REYNOLDS, J., HISLOP, L., ROCKSTRÖM, J., GITHEKO, A., DUBE, P., FRANTZESKAKI, N., LOORBACH, D., ROTMANS, J., ALEKSEEV, G., GADDIS, B., YE, J., and FELLOW, G. E. O.: 'An Earth System Perspective'. *Global Environment Outlook 5 (GEO 5)*. United Nations Environment Programme, 2012: pp. 193–214 (cit. on p. 3).

87. SAINT-PIERRE, P.: 'Approximation of the viability kernel'. *Applied Mathematics & Optimization* (1994), vol. 29(2): pp. 187–209 (cit. on p. 29).

88. SCHELLNHUBER, H. J.: 'Earth System Science and the second Copernican revolution'. *Nature* (1999), vol. 402 (cit. on pp. 4, 5, 133).

89. SCHELLNHUBER, H. J.: 'Discourse: Earth System Analysis - The Scope of the Challenge'. *Earth System Analysis: Integrating Science for Sustainability* (1998), vol.: pp. 3–195 (cit. on pp. 4, 5).

90. SCHLÜTER, M., MCALLISTER, R. R. L., ARLINGHAUS, R., BUNNEFELD, N., EISENACK, K., HÖLKER, F., and MILNER-GULLAND, E. J.: 'New horizons for managing the environment: A review of coupled social-ecological systems modeling'. *Natural Resource Modeling* (2012), vol. 25(1): pp. 219–272 (cit. on p. 5).

91. SOLOMON, S., QIN, D., MANNING, M., MARQUIS, M., AVERYT, K., TIGNOR, M. M., LEROY MILLER, H., CHEN, Z., and (EDS.): *Climate Change 2007: The Physical Science Basis. Contribution of Working Group I to the Fourth Assessment Report of the Intergovernmental Panel on Climate Change*. 2007 (cit. on p. 3).

92. STEFFEN, W., BROADGATE, W., DEUTSCH, L., GAFFNEY, O., and LUDWIG, C.: 'The trajectory of the Anthropocene : The Great Acceleration'. *The Anthropocene Review* (2015), vol. (cit. on p. 1).

93. STEFFEN, W. et al.: 'Planetary boundaries: Guiding human development on a changing planet'. *Science* (2015), vol. 347(6223): pp. 1259855– (cit. on pp. 4, 76).

94. STOCKER, T. F., QIN, D., PLATTNER, G.-K., TIGNOR, M. M., ALLEN, S. K., BOSCHUNG, J., NAUELS, A., XIA, Y., MIDGLEY, P. M., and BEX, V.: *Climate Change 2013: The Physical Science Basis. Contribution of Working Group I to the Fifth Assessment Report of the Intergovernmental Panel on Climate Change*. 2013 (cit. on p. 3).

95. STOMMEL, H.: 'Thermohaline Convection with Two Stable Regimes of Flow'. *Tellus* (1961), vol. 13(2): pp. 224–230 (cit. on p. 2).

96. STROGATZ, S. H.: *Nonlinear Dynamics and Chaos: With Applications to Physics, Biology, Chemistry, and Engineering*. Perseus Books, 2014: p. 500 (cit. on pp. 12, 13, 18, 21, 23, 24).

97. TAYLOR, F.: *Elementary Climate Physics*. Oxford University Press, 2005 (cit. on pp. 2, 123).

98. TAYLOR, M. P.: 'Purchasing Power Parity'. *Review of Interntional Economics* (2003), vol. 11(3): pp. 436–452 (cit. on p. 69).

99. *Turn Down the Heat: Why a 4°C Warmer World must be Avoided*. Tech. rep. The World Bank, 2012: p. 106 (cit. on p. 3).

100. VERBURG, P. H., DEARING, J. A., DYKE, J. G., LEEUW, S. V. D., SEITZINGER, S., STEFFEN, W., and SYVITSKI, J.: 'Methods and approaches to modelling the Anthropocene'. *Global Environmental Change* (2015), vol. (cit. on pp. 1, 3).

101. VUUREN, D. P. van, LUCAS, P. L., HÄYHÄ, T., CORNELL, S. E., and STAFFORD-SMITH, M.: 'Horses for courses: analytical tools to explore planetary boundaries'. *Earth System Dynamics* (2016), vol. 7: pp. 267–279 (cit. on p. 1).

102. WATERS, C. N. et al.: 'The Anthropocene is functionally and stratigraphically distinct from the Holocene'. *Science* (2016), vol. 351(6269): pages (cit. on p. 1).

103. WEIL, D. N.: *Economic Growth*. 3rd ed. Pearson Addison-Wesley, 2012 (cit. on pp. 31, 32, 37, 97).

104. WERNER, K.: *Wachstum und Entwicklung. Kapitalakkumulation*. 2016 (cit. on p. 31).

105. *What was the Great Divergence?* 2013-09. URL: `http://www.economist.com/blogs/freeexchange/2013/08/economic-history-1` (cit. on p. 131).

106. WIEDERMANN, M.: 'Opinion formation and imitation on complex networks driven by local nonlinear resource dynamics'. PhD thesis. Humboldt-Universität zu Berlin, 2014 (cit. on p. 7).

107. WIEDERMANN, M., DONGES, J. F., HEITZIG, J., LUCHT, W., and KURTHS, J.: 'Macroscopic description of complex adaptive networks coevolving with dynamic node states'. *Physical Review E* (2015), vol. 91(5): p. 052801 (cit. on pp. 6, 131).

108. *World Population Prospects*. 2015. URL: `http://esa.un.org/unpd/wpp/` (visited on June 1, 2016) (cit. on p. 126).

109. ZALASIEWICZ, J., WILLIAMS, M., HAYWOOD, A., and ELLIS, M.: 'The Anthropocene: a new epoch of geological time?' *Philosophical transactions. Series A, Mathematical, physical, and engineering sciences* (2011), vol. 369(1938): pp. 835–41 (cit. on p. 1).

# List of Figures


1.1 Coevolution space and coevolutionary pathways . . . . . 5
1.2 Landscape of Earth System Models . . . . . 7

2.1 Topological equivalence. . . . . 14
2.2 Topological classification scheme for hyperbolic equilibria in planar system. . . . 16
2.3 Generic bifurcation diagram of a fold bifurcation. . . . . 20
2.4 Generic bifurcation diagram of a transcritical bifurcation. . . . . 20
2.5 Generic super-critical and sub-critical Andronov-Hopf bifurcations. . . . . 22
2.6 Fold bifurcation of cycles. . . . . 24
2.7 Homoclinic bifurcations in planar systems. . . . . 25
2.8 Generic bifurcation diagram of a Bogdanov-Takens bifurcation. . . . . 27
2.9 Generic bifurcation diagram of a Bautin bifurcation. . . . . 28
2.10 Topological partition of manageable dynamical systems with desirable states . . 30
2.11 Solow-Swan growth model . . . . . 33
2.12 Demographic transition model . . . . . 37
2.13 Global carbon cycle . . . . . 39

3.1 Schematic overview of the complete c:G model . . . . . 42
3.2 Schematic overview of c:G:LAT and c:G:L . . . . . 44
3.3 Schematic overview of c:G:LATP . . . . . 51
3.4 Fertility and mortality curves . . . . . 54
3.5 Schematic overview of c:G:LAGTPK . . . . . 57

4.1 Birth and death rate data and regression curves . . . . . 70

5.1 Bifurcation diagrams c:G:LAT for varying $a_T$ and $l_T$ . . . . . 82
5.2 Phase portrait c:G:LA in the bistable regime . . . . . 84
5.3 Exemplary trajectories c:G:LA . . . . . 86

5.4 Dynamics of terrestrial carbon stock in c:G:LAP for different population sizes . . 88
5.5 Bifurcation diagrams c:G:LAP with constant population size for varying $P$ and $b$ 89
5.6 Topological classification of c:G:LAP with high constant population . . . . . 90
5.7 Phase portrait c:G:LP in the collapse regime . . . . . 95
5.8 Bifurcation diagrams c:G:LP for varying $p$ and $b$ . . . . . 96
5.9 Topological classification of c:G:LP for default $y_B$ . . . . . 98
5.10 Phase portrait c:G:LP in the sustainable regime . . . . . 99
5.11 Bifurcation diagram c:G:LP for varying $y_B$ and $w_L$ . . . . . 101
5.12 Phase portrait c:G:LP in the oscillatory regime . . . . . 102
5.13 Exemplary trajectories c:G:LP from all dynamic regimes . . . . . 105
5.14 Two-dimensiional sections of the phase portrait of c:G:LPK . . . . . 111
5.15 Three-dimensional visualization of the phase portrait of c:G:LPK . . . . . 113
5.16 Exemplary trajectories c:G:LPK . . . . . 115
5.17 Bifurcation diagram c:G:LGPK for varying $a_B$ and $E$ . . . . . 117
5.18 Exemplary trajectories c:G:LGPK . . . . . 120

6.1 Comparison of demographic models . . . . . 128

A.1 Conditional equation for the coexistence equilibria . . . . . 159

B.1 Estimates of the parameter $b$ . . . . . 161
B.2 Estimates of the parameter $y_B$ . . . . . 162
B.3 Estimates of the parameter $y_E$ . . . . . 162
B.4 Estimates of the parameter $i$ . . . . . 163
B.5 Bifurcation diagram c:G:LAT for varying $a_0$ . . . . . 164
B.6 Bifurcation diagram c:G:LAT for varying $l_0$ . . . . . 164
B.7 Topological classification of c:G:LAP with low constant population . . . . . 165
B.8 Topological classification of c:G:LP for low $y_B$ . . . . . 166

## List of Tables

3.1 Variables and parameters of c:G:LAT . . . . . 47
3.2 Variables and parameters of c:G:LATP . . . . . 56
3.3 Variables and parameters of c:G:LAGTPK . . . . . 61

4.1 Pre-industrial and present carbon stocks and flows . . . . . 66
4.2 Regression values of the demographic parameters . . . . . 71
4.3 Overview of all estimated parameters and default values . . . . . 78

6.1 Overview of the dynamic effect of socio-economic parameters . . . . . 123

# APPENDIX A

## Supplementary Calculations

### A.1 Dimensionless formulation of c:G:LATP

The following dimensionless formulation is used for the analysis of the c:G:LATP model given by equations (3.50) to (3.53). The physical quantities of the model variables involve five independent physical dimensions (GtC, km, a, H, \$). Therefore the number of free parameters can be reduced by five according to the Buckingham Π-Theorem. The parameters $C^*_{\mathrm{PI}}$, $\Sigma$, $\delta$, $W_p$ and $b$ are chosen as reference parameters which are set to 1. Using these the following dimensionless variables are defined:

$$\hat{t} = \delta t \tag{A.1}$$

$$\hat{L} = \frac{L}{C^*_{\mathrm{PI}}} \tag{A.2}$$

$$\hat{A} = \frac{A}{C^*_{\mathrm{PI}}} \tag{A.3}$$

$$\hat{G} = \frac{G}{C^*_{\mathrm{PI}}} \tag{A.4}$$

$$\hat{T} = \frac{T\Sigma}{C^*_{\mathrm{PI}}} \tag{A.5}$$

$$\hat{P} = \frac{P b^{\frac{5}{3}}}{C^*_{\mathrm{PI}} \delta^{\frac{5}{3}}} \tag{A.6}$$

$$\hat{M} = \frac{M}{C^*_{\mathrm{PI}}} \tag{A.7}$$

$$\hat{B} = \frac{B}{C^*_{\mathrm{PI}} \delta} \tag{A.8}$$

$$\hat{W} = \frac{W}{W_p} \tag{A.9}$$

Plugging these into the dimensional equations (3.50) to 3.53 leads to the following **dimensionless equations**:

**c:G:LATP dimensionless**

$$\dot{\hat{L}} = \hat{L}\left((\hat{l_0} - \hat{l_T}\hat{T})\sqrt{\hat{A}} - (\hat{a_0} + \hat{a_T}\hat{T})\right) - \hat{B} \tag{A.10}$$

$$\dot{\hat{A}} = -\dot{\hat{L}} + \left(\hat{M} - m\hat{A}\right) \tag{A.11}$$

$$\dot{\hat{T}} = \hat{g}\left(\hat{A} - \hat{T}\right) \tag{A.12}$$

$$\dot{\hat{P}} = \hat{P}\left(\frac{2\hat{p}\hat{W}}{1+\hat{W}^2} - \frac{\hat{q_0} + \hat{q_T}\hat{T}}{\hat{W}} - \hat{q_P}\hat{P}\right) \tag{A.13}$$

where:

$$\hat{M} = 1 - \hat{L} - \hat{A} - \hat{G} \tag{A.14}$$

$$\hat{B} = \hat{L}^{\frac{2}{5}}\hat{P}^{\frac{3}{5}} \tag{A.15}$$

$$\hat{W} = \hat{y_B}\frac{\hat{B}}{\hat{P}} + \hat{w_L}\hat{L} \tag{A.16}$$

These have now eleven dimensionless instead of sixteen dimensional (except for $m$) free parameters. These are defined as follows:

$$\hat{a_0} = a_0 \frac{1}{\delta} \tag{A.17}$$

$$\hat{a_T} = a_T \frac{C^*_{\mathrm{PI}}}{\delta \Sigma} \tag{A.18}$$

$$\hat{l_0} = l_0 \frac{C^{*\frac{1}{2}}}{\delta \Sigma^{\frac{1}{2}}} \tag{A.19}$$

$$\hat{l_T} = l_T \frac{C^{*\frac{3}{2}}}{\delta \Sigma^{\frac{3}{2}}} \tag{A.20}$$

$$\hat{g} = g \frac{1}{\delta} \tag{A.21}$$

$$\hat{p} = p \frac{1}{\delta} \tag{A.22}$$

$$\hat{q_0} = q_0 \frac{1}{\delta W_p} \tag{A.23}$$

$$\hat{q_T} = q_T \frac{C^*_{\mathrm{PI}}}{\delta \Sigma W_p} \tag{A.24}$$

$$\hat{q_P} = q_P \frac{C^*_{\mathrm{PI}} \delta^{\frac{2}{3}}}{\Sigma b^{\frac{5}{3}}} \tag{A.25}$$

$$\hat{y_B} = y_B \frac{b^{\frac{5}{3}}}{W_p \delta^{\frac{2}{3}}} \tag{A.26}$$

$$\hat{w_L} = w_L \frac{C^*_{\mathrm{PI}}}{\Sigma W_p} \tag{A.27}$$

## A.2 Analytical equilibria of c:G:LAT

The existence of other equilibria of the c:G:LAT model than $L_0^* = 0$ depends on the specific values of the parameters $a_0$, $a_T$, $l_0$ and $l_T$. As explained in section 5.1 it is sufficient to solve the one-dimensional equation (3.24) which has no general analytical solution. Therefore in the following several special cases are regarded for which analytical expressions for the equilibria can be found.

**Case 1: $\mathbf{a_T = 0, l_T = 0}$**

There is one additional equilibrium located at:

$$L_2^* = C^* - \frac{a_0^2 \Sigma (1+m)}{l_0^2}, \qquad A_2^* = \frac{a_0^2 \Sigma}{l_0^2} \tag{A.28}$$

on the additional condition that $a_0\sqrt{1+m} < l_0\sqrt{C^*/\Sigma}$.

**Case 2: $\mathbf{a_0 = 0, l_T = 0}$**

There is always one additional equilibrium located at:

$$L_2^* = C^*, \qquad A_2^* = 0 \tag{A.29}$$

Another potential equilibrium is located at:

$$L_3^* = C^* - \frac{l_0^2 \Sigma (1+m)}{a_T^2}, \qquad A_3^* = \frac{l_0^2 \Sigma}{a_T^2} \tag{A.30}$$

This additional a equilibrium exists if $l_0\sqrt{1+m} < a_T\sqrt{C^*/\Sigma}$.

**Case 3: $\mathbf{a_T > 0, l_T = 0}$**

There are potentially two additional equilibria located at:

$$L_\pm^* = C^* - \frac{l_0^2 \Sigma (1+m)}{a_T^2}\left[\frac{1}{2} - \varepsilon \pm \sqrt{\frac{1}{4} - \varepsilon}\right] \qquad \text{where: } \varepsilon = \frac{a_0 a_T}{l_0^2} \tag{A.31}$$

$$A_\pm^* = \frac{l_0^2 \Sigma}{a_T^2}\left[\frac{1}{2} - \varepsilon \pm \sqrt{\frac{1}{4} - \varepsilon}\right] \tag{A.32}$$

$L_+$ and $L_-$ are present if the following conditions hold:

$$4a_0a_T < l_0^2 \qquad \wedge \qquad l_0\sqrt{1+m} < 2a_T\sqrt{C^*/\Sigma} \tag{A.33}$$

If the first term comes to equality and the second still holds, $L_+$ and $L_-$ coalesce to one equilibrium.

Only $L_+$ but not $L_-$ is present under the following conditions:

$$4a_0a_T < l_0^2 \qquad \wedge \qquad a_0(1+m) + a_TC^*/\Sigma < l_0\sqrt{C^*(1+m)/\Sigma} \tag{A.34}$$

**Case 4:** $\mathbf{l_T > 0, a_0 = 0}$

As for case 2 there is one additional equilibrium located at:

$$L_2^* = C^*, \qquad A_2^* = 0 \tag{A.35}$$

There is another potential equilibrium located at:

$$L_3^* = C^* - \frac{a_T^2\Sigma(1+m)}{l_T^2}\left[\frac{1}{2} + \kappa - \sqrt{\frac{1}{4}+\kappa}\right] \qquad \text{where: } \kappa = \frac{l_0l_T}{a_T^2} \tag{A.36}$$

$$A_3^* = \frac{a_T^2\Sigma}{l_T^2}\left[\frac{1}{2} + \kappa - \sqrt{\frac{1}{4}+\kappa}\right] \tag{A.37}$$

This equilibrium exists if the inequality $l_0(1+m) - l_TC^*/\Sigma < a_T\sqrt{C^*(1+m)/\Sigma}$ holds.

## A.3 Linear stability analysis of c:G:LAT and c:G:LP

### Jacobian of the c:G:LAT system

The Jacobian $\mathbf{J}_{LAT}$ of the three-dimensional c:G:LAT system given by equations (3.11), (3.12) and (3.13) is defined as

$$\mathbf{J}_{LA} = \begin{pmatrix} \frac{\partial \dot{L}}{\partial L} & \frac{\partial \dot{L}}{\partial A} & \frac{\partial \dot{L}}{\partial T} \\ \frac{\partial \dot{A}}{\partial L} & \frac{\partial \dot{A}}{\partial A} & \frac{\partial \dot{A}}{\partial T} \\ \frac{\partial \dot{T}}{\partial L} & \frac{\partial \dot{T}}{\partial A} & \frac{\partial \dot{T}}{\partial T} \end{pmatrix} \tag{A.38}$$

where the derivatives are given as follows:

$$\frac{\partial \dot{L}}{\partial L} = l_0 \Sigma^{-\frac{1}{2}} A^{\frac{1}{2}} - l_T \Sigma^{-\frac{1}{2}} A^{\frac{1}{2}} T - a_0 - a_T T \tag{A.39}$$

$$\frac{\partial \dot{L}}{\partial A} = \frac{1}{2} l_0 \Sigma^{-\frac{1}{2}} L A^{-\frac{1}{2}} - \frac{1}{2} l_T \Sigma^{-\frac{1}{2}} L A^{-\frac{1}{2}} T \tag{A.40}$$

$$\frac{\partial \dot{L}}{\partial T} = -l_T \Sigma^{-\frac{1}{2}} L A^{\frac{1}{2}} \tag{A.41}$$

$$\frac{\partial \dot{A}}{\partial L} = -\frac{\partial \dot{L}}{\partial L} - \delta \tag{A.42}$$

$$\frac{\partial \dot{A}}{\partial A} = -\frac{\partial \dot{L}}{\partial A} - \delta(1+m) \tag{A.43}$$

$$\frac{\partial \dot{A}}{\partial T} = -\frac{\partial \dot{L}}{\partial T} \tag{A.44}$$

$$\frac{\partial \dot{T}}{\partial L} = 0 \tag{A.45}$$

$$\frac{\partial \dot{T}}{\partial A} = g \Sigma^{-1} \tag{A.46}$$

$$\frac{\partial \dot{T}}{\partial T} = -g \tag{A.47}$$

**Jacobian of the c:G:LP system**

The Jacobian $\mathbf{J}_{LP}$ of the two-dimensional c:G:LP system given by equations (3.50) and (3.53) and the algebraic equations (3.23) and (3.16) is defined as

$$\mathbf{J}_{LP} = \begin{pmatrix} \frac{\partial \dot{L}}{\partial L} & \frac{\partial \dot{L}}{\partial P} \\ \frac{\partial \dot{P}}{\partial L} & \frac{\partial \dot{P}}{\partial P} \end{pmatrix} \tag{A.48}$$

where the derivatives are given as follows ($q_P = 0$):

$$\begin{aligned} \frac{\partial \dot{L}}{\partial L} =& -\frac{2}{5} b L^{-\frac{3}{5}} P^{\frac{3}{5}} - \frac{L}{2} \sqrt{\frac{1}{\Sigma(1+m)(C^*-L)}} \left( l_0 - \frac{l_T (C^*-L)}{\Sigma(1+m)} \right) \\ & - a_0 + \sqrt{\frac{C^*-L}{\Sigma(1+m)}} \left( l_0 - \frac{l_T (C^*-2L)}{\Sigma(1+m)} \right) - \frac{a_T (C^*-2L)}{\Sigma(1+m)} \end{aligned} \tag{A.49}$$

$$\frac{\partial \dot{L}}{\partial P} = -\frac{3}{5} b L^{\frac{2}{5}} P^{-\frac{2}{5}} \tag{A.50}$$

$$\begin{aligned} \frac{\partial \dot{P}}{\partial L} =& \frac{p W_p P \left( \frac{4}{5} b y_B L^{-\frac{3}{5}} P^{-\frac{2}{5}} + \frac{2 w_L}{\Sigma} \right)}{W_p^2 + W^2} - \frac{p W_p P \left( \frac{8}{5} b y_B W^2 L^{-\frac{3}{5}} P^{-\frac{2}{5}} + \frac{4 w_L}{\Sigma} \right)}{\left( W_p^2 + W^2 \right)^2} \\ & + \frac{q_0 P \left( \frac{2}{5} b y_B L^{-\frac{3}{5}} P^{-\frac{2}{5}} + \frac{w_L}{\Sigma} \right)}{W^2} \end{aligned} \tag{A.51}$$

$$\frac{\partial \dot{P}}{\partial P} = -\frac{4 p W_p b y_B L^{\frac{2}{5}}}{5 P^{\frac{2}{5}} \left( W_p^2 + W^2 \right)} + \frac{8 p W_p b y_B W^2 L^{\frac{2}{5}}}{5 P^{\frac{2}{5}} \left( W_p^2 + W^2 \right)^2} - \frac{2 q_0 b y_B L^{\frac{2}{5}}}{5 P^{\frac{2}{5}} W^2} + \frac{2 p W_p W}{W_p^2 + W^2} - \frac{q_0}{W} \tag{A.52}$$

## A.4 Graphical proof of the number of coexistence equilibria

Equations (5.20) and (5.38) determine the existence and number of coexistence equilibria of the c:G:LATP and c:G:LAGTPK model versions, respectively. The subsequent considerations show that there is a maximum of two solutions to these equations. The argumentation is analog for both equations.

Due to the fractional exponent the left-hand side of (5.20) and (5.38) is only well-defined if $f_{\text{phot}}(L) - f_{\text{resp}}(L) \geq 0$. This condition is met between the forest type equilibrium $L^*_{\text{high}}$ and the saddle equilibrium $L^*_{\text{low}}$ of the c:G:LAT model.[1]

For the case $w_L = 0$ the left-hand side of the conditional equations only has the roots $L^*_{\text{low}}$ and $L^*_{\text{high}}$ and is positive in between. The right-hand side is a positive scalar denoted $\phi$. If $\phi$ lies above the curve defined by the left-hand side, then there are no coexistence equilibria. Alternatively there are two intersections for smaller $\phi$ which correspond to the coexistence equilibria $L^*_{\text{coex}\,1/2}$ (see the green curve in Figure A.1).

For the case $w_L > 0$ the left-hand side features one additional root if $L^*_{\text{low}} < \frac{W^*}{w_L} < L^*_{\text{high}}$. As the right-hand side is positive there is again a maximum of two intersections which correspond to coexistence equilibria $L^*_{\text{coex}\,1/2}$ (see the blue curve in Figure A.1).

1 Depending on the carbon cycle parameters the saddle equilibrium $L^*_{\text{low}}$ can either lie between 0 and $L^*_{\text{high}}$, or be exactly zero (see Figure 5.1). For the parameter regime where only the desert state is stable the condition $f_{\text{phot}}(L) - f_{\text{resp}}(L) \geq 0$ does not hold for any $L$. Thus no coexistence equilibria are possible.

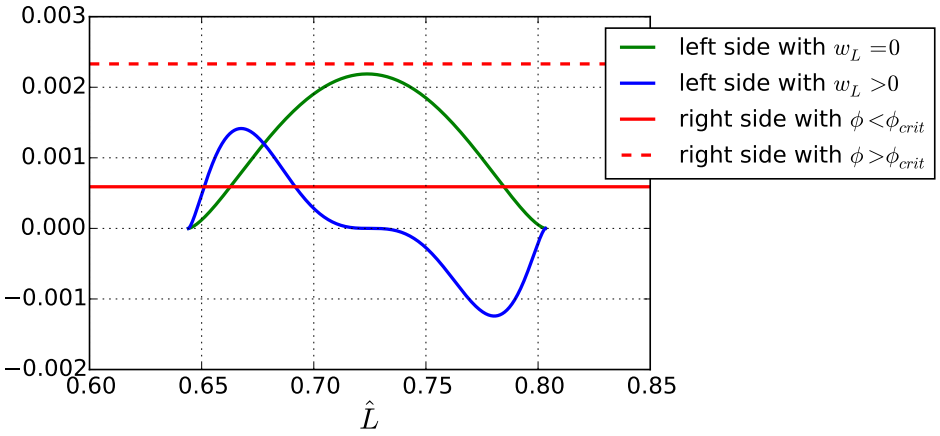


**Figure A.1:** The left-hand side of the conditional equation (5.38) for the determination of coexistence equilibria $L^*_{\text{coex}}$ is shown as green curve ($w_L = 0$) and blue curve ($w_L > 0$), respectively. The constant right-hand side is shown for two different values of $\phi$. For $\phi < \phi_{\text{crit}}$ there are two intersections, corresponding to two coexistence equilibria. For $\phi > \phi_{\text{crit}}$ there is no coexistence solution. The qualitative picture is the same for equation (5.20).
Parameters: $G^* = 0$; green curve: $w_L = 0$; blue curve: $\hat{W}^* = 5.8$, $\hat{w_L} = 8.0$; red continuous curve: $\hat{a_B} = 20$; red dashed curve: $\hat{a_B} = 50$; remaining parameters are set to the default values from Table 4.3.

# APPENDIX B

## Supplementary Figures

### B.1 Time series of the economic parameter estimates

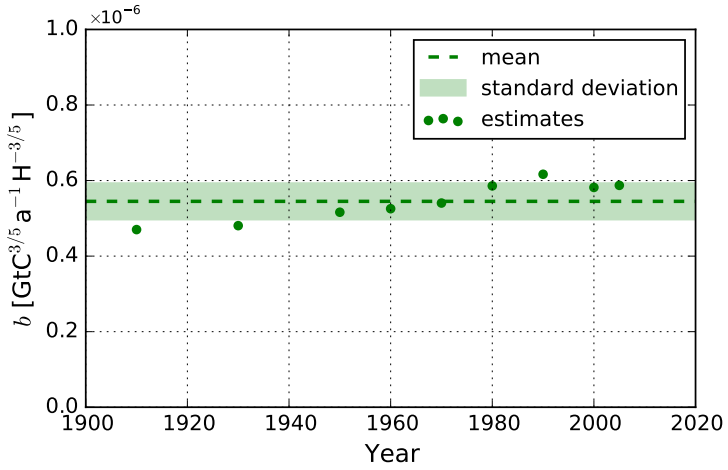


**Figure B.1:** Estimates of the biomass harvesting rate $b$ according to equation (4.18) for different years. The mean and standard deviation are used as best estimate, listed in Table 4.3.

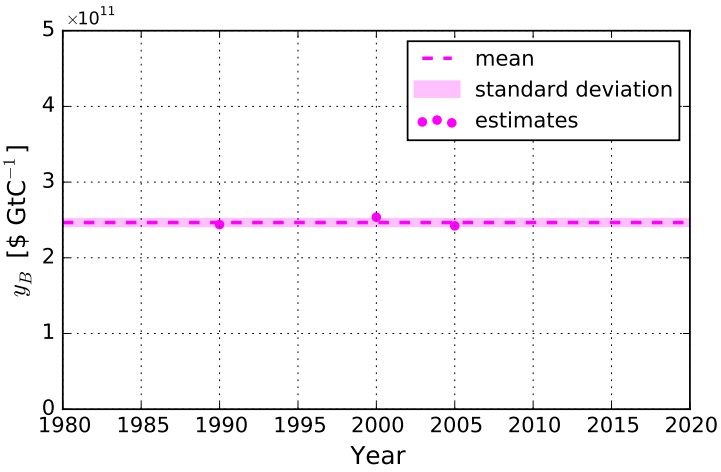


**Figure B.2:** Estimates of the parameter $y_B$ which relates biomass to monetary units, according to equation (4.20) for different years. The mean and standard deviation are used as best estimate, listed in Table 4.3.

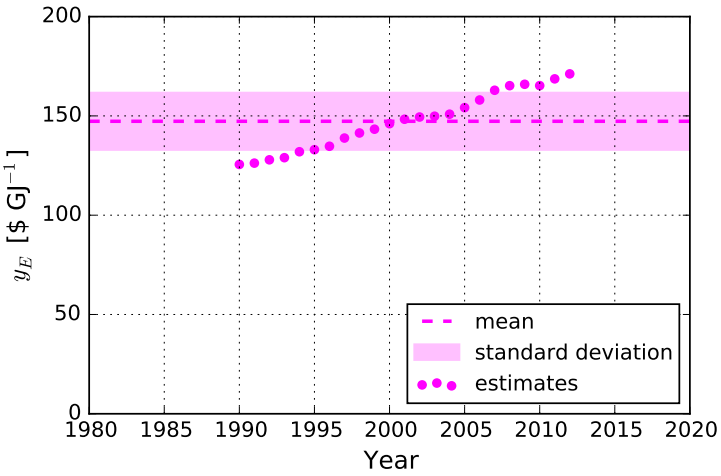


**Figure B.3:** Estimates of the parameter $y_E$ which relates energy to monetary units for different years. The mean and standard deviation are used as best estimate, listed in Table 4.3.

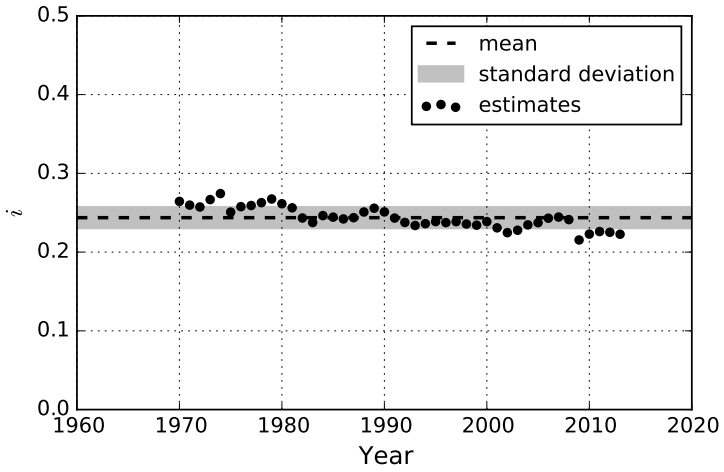


**Figure B.4:** Estimates of the investment ratio $i$ for different years. The mean and standard deviation are used as best estimate, listed in Table 4.3.

## B.2 Bifurcation diagrams of c:G:LAT for varying $a_0$ and $l_0$

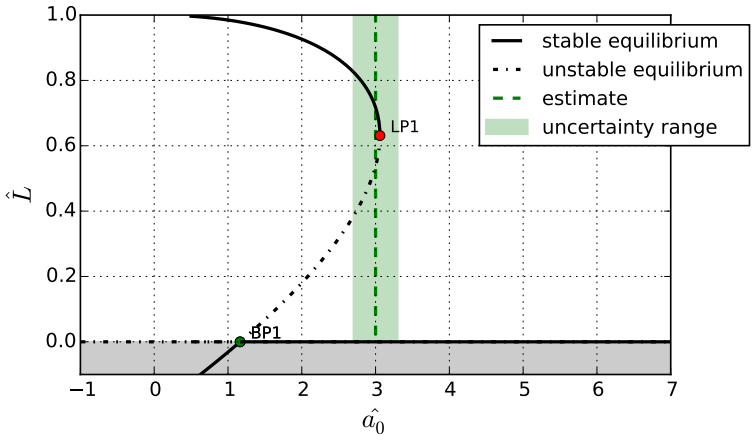


**Figure B.5:** Bifurcation diagram of the c:G:LAT system for a variation in $a_0$. Except for $a_0$ the parameters are chosen as in Table 4.3.

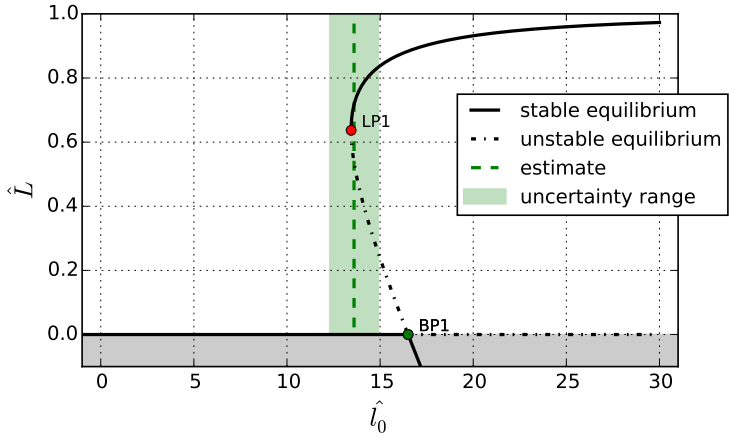


**Figure B.6:** Bifurcation diagram of the c:G:LAT system for a variation in $l_0$. Except for $l_0$ the parameters are chosen as in Table 4.3.

## B.3 Topological classifications for different parameter values

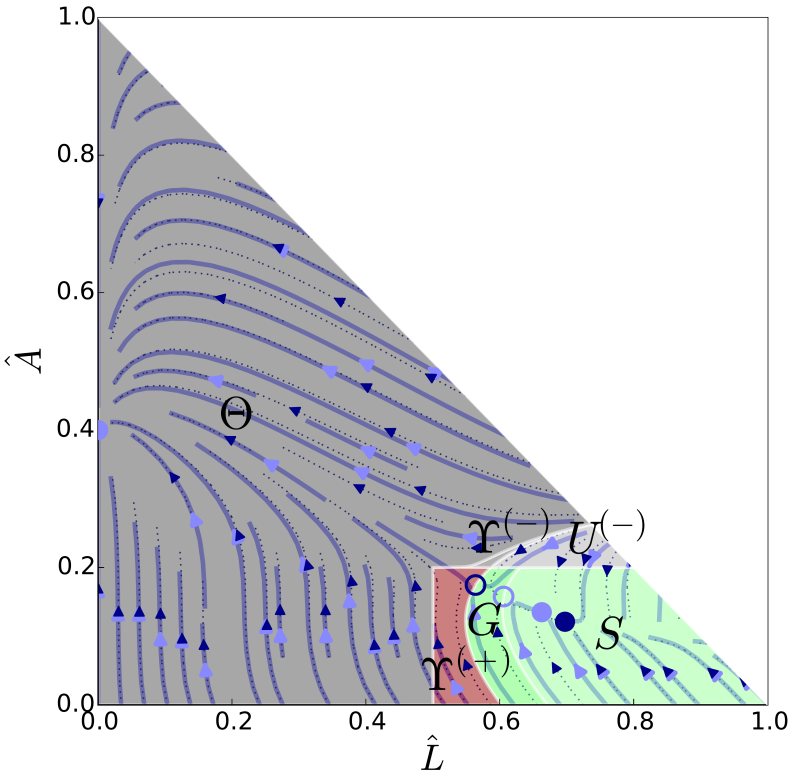


**Figure B.7:** Partitioning of the phase space of the c:G:LAP model with constant population, according to the topology classification introduced in section 2.1.6. In contrast to Figure 5.6 the population is set to $P = 250 \cdot 10^6$ H. In this case both the default and managed dynamics have an attractor within the desired region. Thus there is an **upstream region** which is subdivided into a **shelter** $S$ in which no management is necessary, a **glade** $G$ from which one can reach the shelter through managing and the **dark upstream** $U^{(-)}$ which is the part of the undesired region from which one can reach the shelter. The remaining topological regimes are the same as in Figure 5.6 for a higher population level. Parameters are set to the default values from Table 4.3.

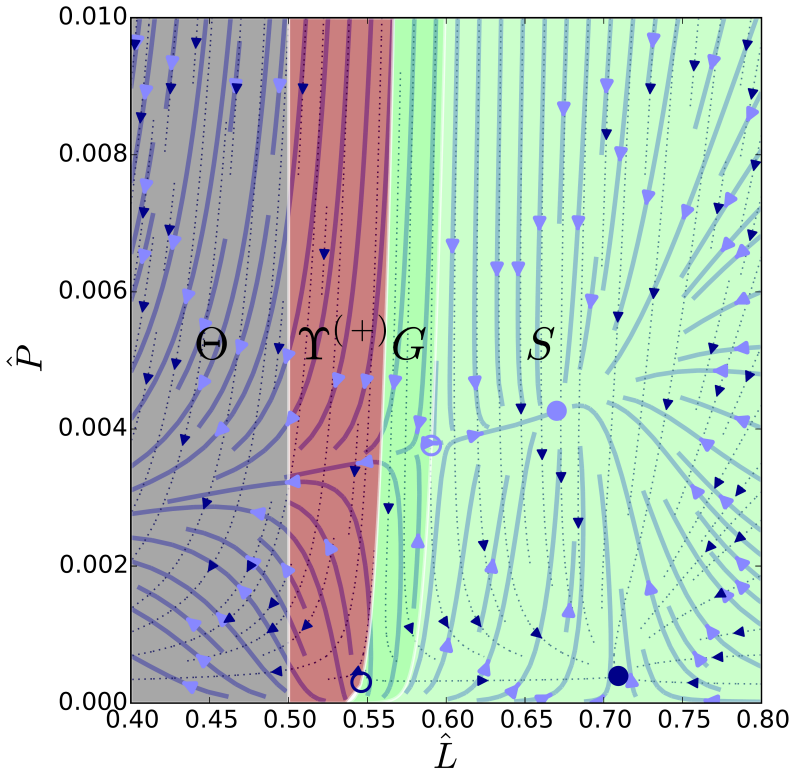


**Figure B.8:** Partitioning of the phase space of the c:G:LP model, according to the topology classification introduced in section 2.1.6. In contrast to Figure 5.9 the economic productivity parameter is set to $\hat{y_B} = 0.05$. In this case both the default and managed dynamics have an attractor within the desired region. Thus there is an **upstream region** which is subdivided into a **shelter** $S$ in which no management is necessary and a **glade** $G$ from which one can reach the shelter through managing. The remaining topological parts are the same as in Figure 5.9 for a value of $y_B$. Parameters are set to the default values from Table 4.3.

## Acknowledgments

First of all I would like to thank Jobst Heitzig who gave me the opportunity to write my master thesis on such an interesting and interdisciplinary topic. He was an outstanding supervisor who allowed me to pursue my own ideas but assisted and guided my work whenever that was needed. I thank Prof. Ulrich Parlitz who immediately agreed on supervising the thesis as a representative of the University of Göttingen. The opportunity to give a talk in his working group in December 2015 and the fruitful discussions in this context were a valuable contribution, especially to the second half of my thesis. I also thank Prof. Jürgen Kurths for the possibility to write a thesis at PIK at the intersection point between climate science and the physics of complex systems. Moreover, I would like to thank the whole copan team for the enjoyable times during countless Jour Fixes and manifold inspiring discussions which contributed to this work. Great thanks goes to Patrick Stoll, Fabian Geier and Tim Kittel for their helpful corrections and suggestions on different parts of the manuscript at different stages. I also want to say 'Thank you' to my friends and my family for supporting me in manifold ways during the last year which had its ups and downs. Finally, I want to thank my girlfriend Elisa for her moral support and enduring of my moods, especially during the last weeks of writing the manuscript. Thank you all!